ENZYME DEGRADABLE NETWORKS PREPARED FROM A POLY(TRIMETHYLENE CARBONATE)-PEPTIDE BIOHYBRID

by

Shadi Taghavi

A thesis submitted to the Department of Chemical Engineering

In conformity with the requirements for

the degree of Doctor of Philosophy

Queen's University

Kingston, Ontario, Canada

(May, 2018)

Abstract

The main objective of this thesis was to develop a biohybrid network with appropriate mechanical properties for a range of soft connective tissue engineering applications that could be degraded solely by the action of the target enzymes. An α-vinyl sulfone (VS), ω-methacrylate (MA) heterobifunctional poly(trimethylene carbonate) (PTMC)/ poly(ethylene glycol) (PEG)-PTMC was prepared and conjugated to a di-cysteine containing matrix metalloproteinase (MMP)-sensitive peptide to form a curable prepolymer. These biohybrid formulations were designed to be cured via a simplified one-step cross-linking process by having both the synthetic polymer and the MMP-sensitive peptide components in a single prepolymer. The degradation behavior and the change in moduli were assessed for the biohybrid networks *in vitro* using a proteinase-containing medium and *in vivo* using a Wistar rat model. Both studies confirmed the enzyme degradation of the biohybrid networks via the cleavage of the peptide component and the hydrolytic resistance of the synthetic polymer backbone and the thio-ether linkage over the experimental time frame. The new formulation may be able to support the lost or damaged soft connective tissue mechanically, with identical mechanical features, until the healing process is completed. In addition, a moderate tissue response was observed to the implanted biohybrid networks which was comparable to that observed towards a Vicryl™ suture. This observation suggested that these new materials can be considered biocompatible for tissue engineering applications. Overall, the developed biohybrid formulation has shown promising *in vitro* and *in vivo* degradation and mechanical properties that would be suitable for soft connective tissue engineering.

Co-Authorship

This dissertation is presented in a manuscript format. Each manuscript chapter is based on the following to be submitted journal articles:

Chapter 4, Shadi Taghavi, Brian Amsden, "Enzyme-degradable poly(trimethylene carbonate)-peptide biohybrid networks"

Chapter 5, Shadi Taghavi, Brian Amsden, " *In vivo* degradation and tissue response to the enzyme-degradable biohybrid poly(trimethylene carbonate) (PTMC)-based networks "

Acknowledgements

I would like to express my truthful gratitude to my supervisor Dr. Brian Amsden for the support and patience he has provided throughout my Ph.D. A special thank you goes out to Sara Mohajeri, Fei Chen, Dale Marecak, Stuart Young, Julian Chesterman, Amanda Brissenden, Nathan Holwell, and all the Amsden's lab members for making my time here extra special. I would also like to thank Deborah Harrington for her help and support with the animal study at the Animal Care Services. I would like to thank my thesis committee members Dr. Kimberly Woodhouse from the Chemical Engineering department and Dr. Timothy Bryant from the Mechanical and Materials Engineering department for their support and advice along my thesis project.

I feel so lucky to have such amazing family and friends who always supported me. I would like to express my deep love to my wonderful grandmothers Alieh and Nargess, my amazing aunts and uncles Afsar Vaziri, Noushin Taghavi, Ali Taghavi, and Arya Vaziri, my wonderful cousins Nadia Iannino and Lidia Iannino, and my incredible friends Nasim Bakhshizadeh, Mojdeh Houri, and Azadeh Goudarzi. Thank you all for being there for me through my ups and downs.

I would like to dedicate my thesis to the memory of my mother Ashraf Vaziri, my father Reza Taghavi and my brother Ashkan Taghavi. They are the true inspiration of my life. Maman! Thank you for believing in me and thanks for all the love that you gave me over 20 years that is always enough to make me feel alive. You taught me how to look at the challenges of my life from a different angle. Baba! Thank you for all your encouragements and all the lessons that you taught me with your exceptional patience and love. Ashkan! Thank you for being the coolest, the kindest, the most handsome, the funniest, and the most lovable brother in the world.

Table of Contents

Abstract ... ii

Co-Authorship ... iii

Acknowledgements ... iv

List of Figures ... viii

List of Tables ... x

List of Abbreviations ... xi

Chapter 1 Introduction ... 1

Chapter 2 Literature Review: Enzyme-degradable polymer biohybrid materials for tissue engineering and regenerative medicine ... 3

2.1 Abstract ... 3

2.2 Introduction ... 4

2.3 Design criteria in tissue engineering and regenerative medicine ... 8

2.3.1 Mimicking the biomechanics of the ECM ... 8

2.3.2 Mimicking the remodeling of ECM ... 12

2.4 Enzyme-degradation of biohybrid polymers ... 12

2.5 Enzyme-degradable biohybrid polymers ... 14

2.5.1 Biohybrid polymer composites of naturally-derived and synthetic polymers ... 16

2.5.2 Biohybrid single polymers ... 18

2.5.2.1 Grafting ... 19

2.5.2.2 Crosslinking through end group modification ... 21

2.5.2.3 Backbone incorporation ... 23

2.6 Host tissue interaction with implanted biomaterial ... 24

2.7 Conclusion and perspectives ... 25

Chapter 3 Scope ... 26

3.1 Proposed approach ... 26

3.2 Objectives ... 27

Chapter 4 Enzyme-degradable poly(trimethylene carbonate)-peptide biohybrid networks ... 29

4.1 Introduction ... 30

4.2 Materials and methods ... 33

4.2.1 Materials ... 33

4.2.2 Initiator and PTMC synthesis ... 34

4.2.3 Synthesis of heterobifunctional PEG-PTMC ... 36

4.2.4 Fractionation 38
4.2.5 Peptide conjugation 39
4.2.6 Prepolymer characterization 39
4.2.7 Network fabrication 40
4.2.8 Network characterization 40
4.2.9 *In vitro* degradation 41
4.2.10 Statistical analysis 42
4.3 Results 43
4.3.1 Peptide-(PTMC-MA)$_2$ prepolymer preparation and characterization 43
4.3.2 Peptide-(PTMC-PEG-MA)$_2$ prepolymer preparation and characterization 45
4.3.3 Network characterization 48
4.3.4 *In vitro* Degradation 50
4.4 Discussion 56
4.5 Conclusion 60
Chapter 5 *In vivo* degradation and tissue response to the enzyme-degradable biohybrid poly(trimethylene carbonate) (PTMC)-based networks 61
5.1 Abstract 61
5.2 Introduction 62
5.3 Materials and methods 64
5.3.1 Materials 64
5.3.2 Network preparation 65
5.3.3 *In vivo* degradation 66
5.3.4 Tissue response 68
5.3.4.1 Masson's Trichrome 68
5.3.4.2 CD68 staining 68
5.3.5 Statistical analysis 69
5.4 Results 70
5.4.1 Polymer characterization 70
5.4.2 *In vivo* degradation 70
5.4.2.1 Macroscopic examination of tissue response 70
5.4.2.2 Network property changes with time 72
5.4.2.3 Histology 75
5.5 Discussion 82
5.6 Conclusion 85

Chapter 6 Aqueous crosslinking of the poly(trimethylene carbonate)-poly(ethylene glycol) biohybrid networks 86
6.1 Abstract 86
6.2 Introduction 87
6.3 Materials and methods 88
6.3.1 Materials 88
6.3.2 Synthesis of Heterobifunctional PEG-PTMC, MMP-sensitive peptide conjugation, and characterization 88
6.3.3 Peptide-$(PTMC\text{-}PEG\text{-}MA)_2$ prepolymer characterization 88
6.3.4 Network formation in aqueous condition 89
6.3.5 Network characterization 90
6.3.6 Statistical analysis 90
6.4 Results 91
6.4.1 Prepolymer characterization 91
6.4.2 The characterization of the crosslinked networks in aqueous suspension 93
6.5 Discussion 94
6.6 Conclusion 96
Chapter 7 Conclusion and Recommendations 97
7.1 Conclusion 97
7.2 Recommendations for future work 98
References 100

List of Figures

Figure 2.1. A schematic of a biohybrid polymer structure configurations. ... 7
Figure 2.2. Mechanotransduction at the nucleus and at the focal adhesion ... 10
Figure 2.3. Post-injection and photo-cross-linking morphology of scaffolds stained with trypan blue ... 18
Figure 2.4. Incorporation of natural and synthetic macromolecules ... 19
Figure 2.5. Schematic of CS grafting onto PNIPAAm. ... 21
Figure 2.6. Michael type addition reaction ... 22
Figure 2.7. Schematic of PEG hydrogel system made of heterobifunctional PEG ... 24
Figure 4.1. Schematic of the Michael-type addition reaction to yield the prepolymer. ... 33
Figure 4.2. (a) Initiator synthesis; 4 molar equivalents of divinyl sulfone reacted with mercaptoethanol, (b) TMC polymerization; using 2-((2-(vinyl sulfonyl)ethyl)thio)ethanol as the initiator and stannous 2-ethylhexanoate as the catalyst, and (c) VS-PTMC-OH methacrylation ... 36
Figure 4.3. (a) TMC polymerization in presence of methacrylate-PEG as the initiator, and (b) vinyl sulfone functionalization of the hydroxyl end group of the MA-PEG-PTMC molecule. ... 37
Figure 4.4. A schematic of the syringe mold used to prepare crosslinked samples. ... 40
Figure 4.5. ^{1}H NMR spectra of (a) 2-((2-(vinylsulfonyl)ethyl)thio)ethanol initiator, (b) VS-PTMC-OH, (c) VS-PTMC-MA and (d) peptide-(PTMC-MA)$_2$ ... 44
Figure 4.6. ^{1}H NMR spectra of (a) PEG-MA initiator, (b) MA-PEG-PTMC-OH, (c) MA-PEG-PTMC-VS, and (d) peptide-(PTMC-PEG-MA)$_2$ ... 47
Figure 4.7. (a) Initial sol content, (b) water content and (c) compressive modulus of the networks prepared with peptide-(PTMC-MA)$_2$ ... 49
Figure 4.8. (a) Mass loss, (b) water content, and (c) compressive modulus of the networks prepared with peptide-(PTMC-MA)$_2$ ... 51
Figure 4.9. (a) Mass loss, and change in (b) water content and (c) compressive modulus of the networks prepared with peptide-(PTMC-PEG-MA)$_2$ ... 53
Figure 4.10. A comparison of the (a) mass loss, (b) water content, and (c) compressive modulus of the networks prepared with peptide-(PTMC-MA)$_2$ and peptide-(PTMC-PEG-MA)$_2$ ... 55
Figure 4.11. Schematic of surface erosion. ... 58
Figure 5.1. Chemical structure of the heterobifunctional (a) VS-PTMC-MA and (b) VS-PTMC-PEG-MA ... 65
Figure 5.2. Location of samples implantation; a) peptide-(PTMC-MA)$_2$ network, b) peptide-(PTMC-PEG-MA)$_2$ network, c) Vicryl^{TM} suture, and d) PEG-(PTMC-MA)$_2$ network ... 67

Figure 5.3. Physical appearance of the implants and tissue from PEG-(PTMC-MA)$_2$, peptide-(PTMC-PEG-MA)$_2$, peptide-(PTMC-MA)$_2$ and Vicryl^{TM} suture, after 1, 3, and 6 weeks of implantation. The implant area is shown by the arrow at week 6 for the Vicryl^{TM} suture. 71
Figure 5.4. (a) Mass loss, (b) sol content, and (c) compressive moduli of the peptide-(PTMC-MA)$_2$, peptide-(PTMC-PEG-MA)$_2$, and PEG-(PTMC-MA)$_2$ implants over 6 weeks (n=2). 73
Figure 5.5. Thermographs of the networks prepared from (a) peptide-(PTMC-MA)$_2$ and (b) peptide-(PTMC-PEG-MA)$_2$ after 4 weeks of degradation *in vivo* and *in vitro*........ 74
Figure 5.6. Masson's trichrome stained sections of the tissue surrounding implants at week 1, 3 and 6. The implant area (M) is on the right side of each image. The extent of the inflammatory zone (I) and the fibrous capsule area (F) are indicated by the black line. The scale bar is 50 µm........ 76
Figure 5.7. (a) The inflammatory zone thickness, (b) cell density, (c) the thickness of the fibrous capsule around the implanted area (n=2). 78
Figure 5.8. Fluorescent CD68 staining of the tissues surrounding implants at week 1, 3 and 6. The implanted area is indicated by (M) on the right side of each image. The white line indicates the extent of the inflammatory zone at the boundary of the implant. The scale bar is 50 µm. Macrophages are stained green while all cell nuclei are blue (n=2)........ 79
Figure 5.9. (a) The macrophage density, and (b) the ratio of macrophage to total cell number, in the inflammatory zone (n=2). 81
Figure 6.1. Thermal gelation of peptide-(PTMC-PEG-MA)$_2$ aqueous suspension, PEG-PTMC 1.7 kDa and PEG/PTMC weight fraction of 30%. 92

List of Tables

Table 2.1. Compressive and Young's moduli of human soft connective 5

Table 2.2. Some biohybrid polymers investigated *in vivo* for tissue engineering applications and their Young's moduli in comparison to the target tissue... 15

Table 4.1. Number average molecular weight (M_n), glass transition temperature (T_g), water solubility (WS) and molar mass dispersity (ĐM) of fractionated VS-PTMC-MA samples. 45

Table 5.1. T_g values (°C) of hydrated peptide-(PTMC-MA)2 and peptide-(PTMC-PEG-MA)2 networks over 4 weeks 75

Table 6.1. Number average molecular weights (M_n), glass transition temperature (T_g), and water solubility of different fractions of PEG-PTMC. PEG/PTMC ratio is the molecular weight ratio of the PEG block to the PEG-PTMC block. 91

List of Abbreviations

^1H NMR	Proton nuclear magnetic resonance
Acryl-PEG-SVA	Acrylate-PEG-succinimidyl valerate
ANOVA	Analysis of variance
APS	Ammonium persulfate
BSA	Bovine serum albumin
CS	Chondroitin sulfate
Da	Dalton
DAPI	4',6-diamidino-2-phenylindole
DCM	Dichloromethane
ĐM	Molar mass dispersity
DMAP	4-dimethylaminopyridine
DMF	Dimethylformamide
DMPA	2,2-dimethoxy-2-phenylacetophenone
DMSO	Dimethyl sufoxide
DSC	Differential scanning calorimetry
DVS	Divinyl sulfone
ECM	Extracellular matrix
EPCs	Endothelial progenitor cells
FA	Focal adhesion
FX	Focal Complex
GAGs	Glycosaminoglycans
GPC	Gel permeation chromatography
HA	Hyaluronic acid
HEPES	4-(2-hydroxyethyl)-1-piperazineethanesulfonic acid
kPa	Kilo Pascal
MA	Methacrylate

MGC	N-methacrylaye glycol chitosan
Mit.	Mitochondria
MMP	Matrix metalloproteinase
M_n	Number average molecular weight
MPa	Mega Pascal
MSC	Mesenchymal stem cells
NA	nascent adhesion
NaH	Sodium hydride
Nesprins	Nuclear envelope spectrin repeat protein
NP	Nucleus Pulposus
PBS	Phosphate buffered saline
PCL	Poly(e-caprolactone)
PEG	Poly(ethylene glycol)
PGA	Poly(glycolic acid)
PHAs	Polyhydroxyalkanoates
PHBs	Polyhydroxydroxybutyrates
PLA	Poly(lactic acid)
PLAL	Poly(lactic acid-co-lysine)
PLGA	Poly(lactic-co-glycolic acid)
PLLA	Poly(L-lactic acid)
PNIPAM	Poly(N-isopropylacrylamide)
ppm	Parts per milion
PTMC	Poly(trimethylene carbonate)
rER	Rough endoplasmicretculum
RGD	Arginine glycine aspartic
RhoA	Ras homolog gene member A
RM	Regenerative medicine
rpm	Rotation per minute

sER	Smooth endoplasmicretculum
TBS	Tris-buffered saline
TE	Tissue engineering
TEA	Trimethylamine
TEMED	N,N,N',N'-tetrametylethylenediamine
T_g	Glass transition temperature
TG	Transglutaminase
THF	Tetrahydrofuran
TIMPs	Tissue inhibitors of metalloproteinases
TMC	trimethylene carbonate
UV	Ultraviolet
VS	Vinyl sulfone
w/v	Weight per volume

Chapter 1

Introduction

The conventional treatment strategies for lost or damaged tissues attempt to reduce pain and restore tissue functionality. These strategies include surgical restoration, tissue transplantation, medical devices and permanent prostheses [1]. Transplantation is the most accepted treatment strategy for the lost or damaged tissues and organs. However, there are several complications associated with autologous and allograft tissue and organ transplantation. These complications include the morbidity of the donor site, infection, pain, limited source of donor tissue and host immunogenic responses [2]. Tissue engineering and regenerative medicine have emerged as alternative approaches to tissue reconstruction to overcome the limitation associated with conventional tissue transplantation.

Despite the advances in regenerative medicine and tissue engineering in tissue reconstruction, these fields have not yet been fully successful. This is due to the natural complexities of the living organs and tissues such as the existence of functional units, internal vascularization and reconnection to the main vascular system [3]. Nevertheless, the ultimate goal of regenerative medicine and tissue engineering is to be able to mimic the natural features of the extracellular matrix (ECM) with all its complexities.

Producing biomaterials that exhibit the key mechanical features of the target tissue ECM, is one of the great challenges in tissue engineering and regenerative medicine applications. The implanted biomaterial must have enough mechanical integrity to function from implantation time to completion of the remodeling process. Host biocompatibility, an appropriate degradation profile, permeability by nutrients and metabolites and well-defined interaction with the target cells are the other key factors of the designed biomaterial for such applications.

Degradable polymeric biomaterials for biomedical applications have gained significant attention during the past two decades [4]. There are several limitations associated with the long-term presence of implants and devices in the body. The first limitation is the loss of functionality over time that happens due to the homeostatic responses to the implantation injury or the interaction between the implant surface and blood or surrounding tissue [5]. Health complications and/or implant failure are potential negative outcomes. Host reactions following implantation of biomaterials include blood-material interactions, inflammation, foreign body reaction and fibrous capsule development [6].

The successful development of biomaterials for tissue engineering and regenerative medicine will require a combination of different characteristics and functionalities in order to mimic the complexity of the native structures. The advantages of natural and synthetic polymers can be combined by creating a new biohybrid material containing peptides in the synthetic polymer structure. The degradation of these peptides will be controlled by cell-secreted enzymes. This degradation behavior will mimic the ECM remodeling process, and thereby enable migration and proliferation of target cells in the implanted material. On the other hand, the synthetic polymer will provide the mechanical strength of the biohybrid material. The combination of the natural and synthetic polymer will make it possible to create structures that possess enhanced bioactivity and improved mechanical strength.

Chapter 2

Literature Review: Enzyme-degradable polymer biohybrid materials for tissue engineering and regenerative medicine

2.1 Abstract

The complications associated with the permanent existence of biomaterials in the living body emphasize the need to use of biodegradable implants in biomedical applications. Moreover, a well-controlled degradation of implants being used for tissue engineering applications is needed. This control can be achieved by utilizing the catalytic effect of enzymes secreted from target cell types. In fact, using an enzyme degradable system is essential for such applications to avoid the uncontrolled mechanical failure of commonly used hydrolytically degradable biomaterials. Biohybrid polymeric materials consist of naturally derived polymeric components and synthetic polymers. This group of polymeric biomaterials contains the advantages of synthetic polymers and enzyme-sensitive molecules and as such are promising candidates for tissue engineering applications. The synthetic polymer provides mechanical support to the tissue during the healing process, while the enzyme-sensitive phase provides the degradability which is controlled by the rate of cell growth, migration, and deposition of extracellular matrix (ECM) components. In the present review the design criteria of biohybrid polymers for tissue engineering and regenerative medicine applications are discussed. In addition, different strategies and recent advances in this area are presented.

2.2 Introduction

To overcome the limitations associated with conventional tissue transplantation such as morbidity of the donor site, infection, pain, limited sources of donor tissue and host immunogenic responses, tissue engineering (TE) and regenerative medicine (RM) have emerged as alternative approaches [2]. The term tissue engineering was proposed by Langer and Vacanti over two decades ago to describe a multidisciplinary research field with a focus on the development of biological scaffolds to improve, restore or maintain tissue function [7], [8]. By the beginning of the twenty-first century, the term regenerative medicine started to be used in parallel to TE to address the biological limitations associated with TE such as lack of functional microvasculature systems and cell binding motifs in respect to scaffold materials [3], [9]–[11].

A general strategy in TE and RM is to replace the lost or damaged tissue with an engineered construct that allows for cell attachment, proliferation and differentiation [12]. Scaffolding materials are used in TE and RM approaches to deliver cells and biomolecules, to maintain their bioactivities, and to provide mechanical support during tissue reconstruction [13]. Providing an environment that allows the cells to function as they do in the native tissue has emerged as a key factor in TE and RM [14]. As such, the materials used to form the scaffolds must mimic different aspects of the extracellular matrix (ECM) in order to provoke specific cellular responses and redirect new tissue formation [2], [15]. These aspects include the mechanical properties, cell-scaffold interactions, and degradation behavior of the innate ECM [4], [16]–[21]. In addition, an appropriate cell type must be populated in the scaffold that is determined by the tissue being replaced.

Despite the advances in TE and RM towards tissue reconstruction, these fields have not yet been fully successful. This lack of success is mostly due to the complexities of the native tissues that cannot be effectively mimicked by current strategies [3]. One of these complexities is the stiffness of the ECM that has essential effects on cell behavior [22]. The stiffness is mainly expressed by the Young's modulus which is a measure of the elasticity of the tissues or biomaterials being used in TE applications [23]. For load-bearing soft connective tissue engineering the compression characterization of the biomaterial must be considered due to the dominant compressive stresses in these tissues. Compressive modulus is theoretically equal to the Young's modulus that is a better representative for load-bearing soft connective tissues [23]. Cells in soft connective tissues are normally exposed to tensile and compressive stresses [24]. The moduli and the function of selected human soft tissues are listed in Table 2.1.

Table 2.1. Compressive and Young's moduli of human soft connective

Tissue	Compressive modulus (MPa)	Young's modulus (MPa)	Function	Reference
Articular cartilage	7-10	1-10	Lubrication, shock absorbance	[25]
Intervertebral discs	0.12-29	0.12-17	Lubrication, shock absorbance	[26]
Fat	0.002-0.012	0.001-0.012	Heat insulation, mechanical protection and padding, endocrine tissue	[27], [28]
Ligament	-	1.2-1.8	Withstanding tensile load to stabilize joints	[25]

To date, a wide range of natural and synthetic scaffolding materials have been designed and investigated for TE and RM applications. Natural polymers used in such applications include those extracted from the native ECM, such as collagen, fibrin, elastin, and hyaluronic acid. Other natural polymers used include those obtained from non-physiological sources, such as alginate, chitosan, silk, and hydrophobic polymers such as poly(hydroxyalkanoates) (PHAs) [29].

The major problem with most of the naturally derived materials is that their mechanical moduli do not match that of most soft connective tissues, and the batch-to-batch variability. On the other hand, hydrophobic natural polymers such as PHAs have mechanical moduli on the order of MPa and so may be suitable for some soft connective tissue engineering applications, but have uncontrolled degradation rates [30]. PHAs are degraded by a slow hydrolytic chain scission process in the amorphous regions which is continued by the action of non-specific lipases and serine esterases *in vivo* [31], [32].

Various synthetic polymers have been investigated as scaffolds for tissue engineering applications. Synthetic polymers are more readily processed into structures with a well-defined geometry. Their composition and molecular weight can be readily manipulated and the rate of their biodegradation can be tuned by modulation of the polymer composition [33]. Poor cell-scaffold interaction, due to the lack of cell-recognition sites, is the biggest disadvantage of synthetic polymers. Such cell-recognition capability of naturally-derived macromolecules is due to the existence of functional biological residues in key positions to interact with the target proteins and cells [34].

The successful development of polymeric biomaterials for tissue engineering and regenerative medicine will require a combination of different characteristics and functionalities in order to create scaffolds that mimic the complexity of native structures [35]. The advantages of natural and synthetic polymers can be combined by creating biohybrid materials containing naturally-derived molecules in the synthetic polymer structure [36]. The term biohybrid polymers was first introduced by B.K.G. Theng in 1970 to define an emerging group of materials consisting of the combination of naturally derived polymers and inorganic materials [37]. Nowadays, the term biohybrid polymer is used to define a polymeric structure that is composed of both natural and synthetic polymers [38]. Figure 2.1 shows schematic illustration of different biohybrid polymer configurations.

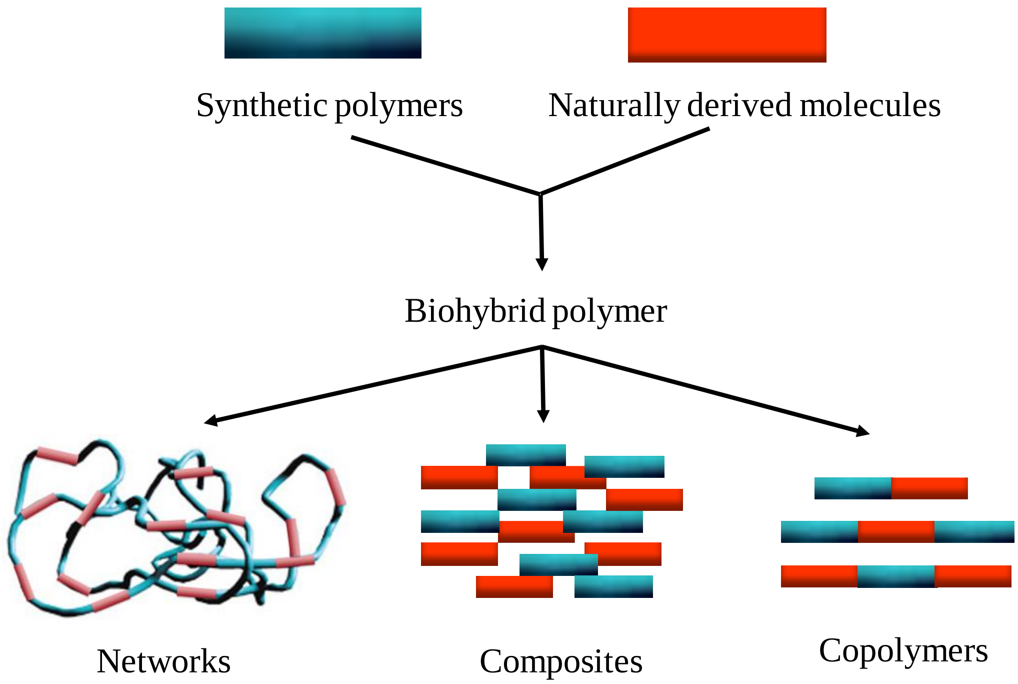

Figure 2.1. A schematic of a biohybrid polymer structure configurations.

The degradation of enzyme-degradable biohybrid polymers is designed to be controlled by cell-secreted enzymes that catalyze the hydrolysis of the naturally-derived molecules along their backbone. This degradation behavior is designed to mimic the natural ECM remodeling process, and thereby enable migration and proliferation of target cells in the implanted material and deposition of the native ECM. The synthetic polymer, on the other hand, provides the necessary mechanical strength as well as processability. Thus, the combination of natural and synthetic polymers makes it possible to create structures that possess both enhanced bioactivity and appropriate mechanical properties.

In this chapter, different strategies to make polymer biohybrid materials are reviewed. Previously studied approaches to achieve the design criteria discussed above are discussed to summarize the current state of such biomaterials. Finally, the underexplored aspects of the enzyme degradation process have been emphasized for future attention.

2.3 Design criteria in tissue engineering and regenerative medicine

There are several requirements to be considered in biohybrid polymer design for tissue engineering and regenerative medicine applications. The engineered biomaterial must mimic different aspects of the target ECM in order to provoke specific cellular responses and direct new tissue formation [2]. One of these aspects is the mechanical properties of the native ECM [17]. Mimicking the mechanical properties of the target ECM not only affects stem cell differentiation and ECM production but also controls cell behavior to avoid initiation of a number of diseases such as cancer [15]. Other aspects to consider are material degradation behavior, cell-biomaterial interactions, and whether a minimally invasive strategy to implant the biomaterials is necessary. Herein, two main design criteria, mimicking the biomechanics and the remodeling of the ECM, have been briefly reviewed.

2.3.1 Mimicking the biomechanics of the ECM

The extracellular matrix (ECM) is the interstitial environment between cells, which provides mechanical and biochemical support to the surrounding cells. The ability of various tissues to withstand physiological forces depends on the composition and structural integrity of their ECM [39]. ECM biomechanics regulate a number of cellular behaviors such as proliferation, migration, and morphogenesis. The cellular synthesis and remodeling of the macromolecules of the tissue are also affected by ECM biomechanics [40]. Cells can sense and respond to the mechanical stimulation of the surrounding microenvironment and transduce the mechanical signals into biochemical and molecular responses. This process is referred to as mechanotransduction (Figure

2.2) [41]. The biomechanical properties of the ECM determine the external forces that a cell experiences. Cells feel these forces via mechanosensors in the actomyosin cytoskeleton that link with the ECM [42]. The transmembrane receptors, integrins, are important mechanoreceptors that can be activated under a variety of intracellular signal cascades and which also facilitate the attachment of the cells to the surrounding microenvironment [43]. Integrin clustering develops nascent adhesions (NA) that can mature to focal complexes (FX) and focal adhesions (FA) via actomyosin contractility. Actomysin contractility in turn is controlled by ECM stiffness, cell shape, or external application of force. Integrin clustering can induce Ras homolog gene family, member A (RhoA) signaling by increasing myosin contractility, which leads to unfolding of proteins and the regulation of the cell shape [41]. RhoA is a small protein in the Rho family which is associated with cytoskeleton regulation. Nesprins or nuclear envelope spectrin-repeat proteins (N) are tied to the actomysin cytoskeleton and transmit the mechanical signal to the nucleus [44]. The nucleus and surrounding organelles including Golgi apparatus (Golgi), mitochondria (Mit.), and rough and smooth endoplasmicreticulum (rER/sER) are interconnected by filaments and microtubules [41]. Changing cell shape or contractility by nesprins can alter the spatial localization of organelles and induce conformational changes on nuclear pores which regulate the transportation of molecules between the nucleus and the cytoplasm [41].

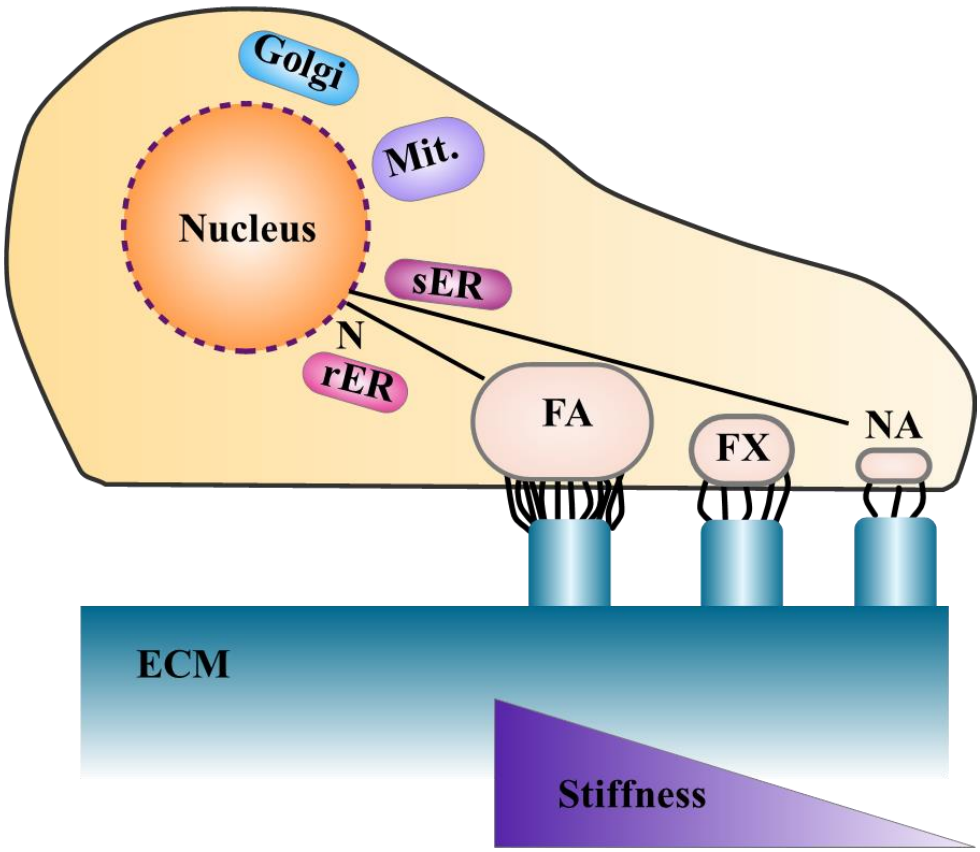

Figure 2.2. Mechanotransduction at the nucleus and at the focal adhesion; black lines indicate the integrin clustering that can be modified by stiffness, cell shape, or external forces. This process forms nascent adhesions (NA) and mature to focal complexes (FXs) and focal adhesions (FA). The nucleus is interconnected with Golgi apparatus, Mitochondria (Mit), rough and smooth endoplasmicreticulum (rER/sER), intermediate filaments and microtubules. Nesprins (N) maintain the cellular architecture by linking nucleus and subcellular domains, Figure adapted from [41].

There are rapid and long-term responses to mechanical stimulation that can occur within seconds and over months, respectively. The rapid responses are based on intracellular signaling pathways, such as changes in intracellular calcium concentration or regulation of membrane ion channels that happens in a short time and leads to flow changes in the membrane [43]. Long-term responses that are crucial in tissue remodeling include changes in cell orientation and shape and changes in ECM production and composition [43]. The mechanical load that is applied to the tissue will be distributed and absorbed differently based on the nature of the tissue and its ECM component distribution. The composition of the ECM is also dependent on the previous mechanical loads that the cells have been exposed to [43]. For example, in regions in articular cartilage that are exposed to more loading, the ECM is thicker and has a higher proteoglycan content [45]. ECM stiffness is another important parameter in controlling cell fate and stem cell fate [46]. Gobaa *et al.*, has demonstrated that the osteogenic differentiation index of human mesenchymal stem cells (MSCs) increased by increasing the crosslink density and stiffness of a poly(ethylene glycol) (PEG)-based substrate [46]. Furthermore, it has been shown by Navaro *et al.* that a lower matrix stiffness induced nucleus pulposus (NP)-derived stem cells differentiation toward a chondreogenic lineage, while a higher stiffness induced differentiation toward a osteogenic lineage [47].

Producing biomaterials that exhibit the key mechanical features of the target tissue ECM is one of the great challenges in tissue engineering and regenerative medicine. The implanted biomaterial must have enough mechanical integrity to function from implantation time to completion of the remodeling process. A successful approach in such applications requires a thorough understanding of the native tissue mechanics.

2.3.2 Mimicking the remodeling of ECM

Reorganization or renovation of existing tissues is called remodeling, which happens due to the secretion of certain ECM proteins by activated cells. Matrix metalloproteinases (MMPs) are proteolytic proteins that play a key role in hydrolysis of ECM components and affect the cellular activities and remodeling of the tissue [48]. The level of MMP activity can be controlled by secretion of tissue inhibitors of metalloproteinases (TIMPs). The extent of tissue remodeling is modulated by the balance between MMPs and TIMPs [49]. It is desirable that the implanted polymeric scaffold is replaced with functional ECM that is representative in composition to native ECM during the reconstruction process. For this aim, the implanted scaffold should be degraded via the natural degradation mechanism of ECM. In tissue engineering and regenerative medicine the cells that are seeded in the scaffold play an essential role in degradation of the biomaterial and deposition of the newly generated ECM components. The native remodeling process can be mimicked in such scaffolds by the cell's ability to balance the formation of the new tissue and the degradation of the biomaterial.

2.4 Enzyme-degradation of biohybrid polymers

Uncontrolled degradation of the polymer used to form the scaffold is not favorable for TE applications since it affects the mechanical stability of the implanted scaffold and causes scaffold mechanical deterioration before the completion of the tissue regeneration. A polymeric biomaterial is called biodegradable when it starts to break down gradually due to biological activities after a temporary period of function. Afterwards, the degradation products should be safely eliminated from body [50]. The degradation process can affect a range of events such as cell growth and host response. Thus, this process must be well understood for selecting and designing materials for specific applications.

There are a number of physical and chemical polymeric biomaterial degradation mechanisms such as dissolution, stress/fatigue cracking, hydrolysis, oxidation, and enzymatic degradation [51]. Among all these mechanisms enzyme-degradation has been extensively investigated over the last two decades as a promising strategy to have well-controlled degradation of polymeric biomaterials for biomedical applications [52]. Collagen [53], [54], elastin [55], elastin-like peptide [56], [57], natural and synthetic poly(amino acids), albumin, fibrin [58] and polysaccharides such as hyaluronic acid [59]–[61], chondroitin sulfate [62], chitin and chitosan [63] are the most studied enzyme-degradable naturally derived polymers in biomedical applications. Within these polymers, the amide bonds of proteins and glycoside bonds of polysaccharides are the main cleavable sites [64]. These sites are cleaved via hydrolysis catalyzed by enzymes known as hydrolases [65]. This class of enzymes includes glycosidases, proteases, and esterases.

The best strategy in TE applications is to utilize a degradation mechanism that is controlled by cell-secreted factors. In this way, the degradation rate of the scaffold would match the formation rate of the tissue [66]. Cell-secreted enzyme catalyzed degradation of the scaffold can ensure that mechanical support to the damaged tissue is maintained during the healing process. The enzyme-mediated degradation rate depends on the number of cells and their enzyme secretion rate. The target tissue cells also secrete ECM components to replace the implanted material while the degradation is happening. The regenerated tissue will then provide the mechanical support that was temporarily provided by the implanted biomaterial.

Enzyme-catalyzed degradation of polymeric biomaterials under *in vivo* conditions is a very complicated process. This is due to the complex chemistry of body fluids and the inflammatory response around the implanted site. Enzyme-catalyzed hydrolysis of polymeric biomaterials involves four steps. First, the enzyme must diffuse through the solution to the polymer surface. Second, the enzyme adsorbs to the polymer surface. Third, the enzyme acts as the catalyst for the hydrolysis reaction. Finally, the soluble products of the degradation diffuse from the polymeric substrate to the surrounding solution. Among the four steps, the slowest process determines the hydrolysis rate [50]. Therefore, this rate is affected by the physiochemical characteristics of the polymeric substrate as well as the enzyme characteristics. The other factors that affect both substrate and enzyme properties include the medium conditions, and the presence of stabilizers, activators or inhibitors. Chemical modification of the polymer can also affect the enzyme adsorption (for elastomers)/absorption (for hydrogels) and degradation rate including crosslinking, and removal or addition of chemical groups in the polymer chain [50]. For example, higher degrees of deacetylation or higher crosslink density can decrease the enzymatic degradation of chitosan due to the lower activity of lysozyme which is responsible for the *in vivo* degradation of peptidoglycans and chitin materials [50].

2.5 Enzyme-degradable biohybrid polymers

Enzyme-degradable biohybrid polymers for soft connective tissue engineering applications can be formed by combining the degradability features of naturally derived components with the well-defined mechanical characteristics of synthetic polymers [67]. There are two main fabrication strategies to fabricate biohybrid polymeric materials. A naturally derived polymer can be blended with a synthetic polymer to form a composite structure or to form a network by crosslinking, ionic bonding, hydrogen bonding, and/or hydrophobic interactions [68]. Alternatively, naturally derived molecules can be directly attached to synthetic polymer molecules to form a single hybrid macromolecule that can be crosslinked or self-assembled after conjugation to form a biohybrid network. The attachment of the natural component can be achieved via grafting, end group attachment, or backbone incorporation [69]. The advantage of biohybrid blends over biohybrid single macromolecules is a simplified fabrication process with no need for multiple addition of side/end reactive groups. However, for this group of biohybrid polymers differently functionalized polymers must first be prepared, which require mixing to achieve effective crosslinking. On the other hand, the main obstacle to the use of the single biohybrid macromolecules is the complication associated with the addition of reactive side/end groups. However, networks can be formed of this group of biohybrid polymers via a simplified one or two-step crosslinking process.

Poly(ethylene glycol) (PEG) [70]–[79], poly(ε-caprolactone) (PCL) [80], poly(lactic acid) (PLA) and related polymers such as poly(L-lactic acid) (PLLA) [81]–[84], poly(glycolic acid) (PGA) [85]–[87], poly(trimethylene carbonate) (PTMC) [88], and poly(N-isopropylacrylamide) (PNIPAM) [89]–[92] are the most studied synthetic polymers in the field of TE and RM to form biohybrid systems by being combined with enzyme degradable natural polymers. Table 2.2 contains a list of recent biohybrid approaches investigated *in vivo* for tissue engineering and regenerative medicine applications, their Young's moduli in comparison to those of the native target tissue, and the reported degradation time.

Table 2.2. Some biohybrid polymers investigated *in vivo* for tissue engineering applications and their Young's moduli in comparison to the target tissue.

Strategy	Hybrid polymer	E (MPa)	Target tissue	Native E (MPa)	Ref.
Blend	**PLGA/gelatin**	0.02	Articular Cartilage	7-10	[93]
	PLGA/collagen	-	Articular cartilage	7-10	[94]
	Poly(ester urethane)urea (PEUU)/dermal ECM	0.04-0.19	Abdominal Wall	0.008-8.3	[95]
	PCL/alginate	-	Cartilage	7-10	[96]
End group	**PEG/MMP-sensitive peptide**	0.005-0.02	Liver	0.001-0.01	[72]–[75]

2.5.1 Biohybrid polymer composites of naturally-derived and synthetic polymers

In this method the naturally derived and synthetic polymers are combined into one versatile material. For this aim, the different components are mixed alone or in a common solvent. If a common solvent is being used, the solubility of different components in water or organic solvents can be modified by forming a soluble derivative or by shortening the length by degradation [68]. This group of biohybrid polymers can be divided into two subgroups: non-crosslinked composites and crosslinked networks.

The biohybrid composites consist of non-covalently crosslinked natural and synthetic polymer blends. As an example, a collagen solution in 1% acetic acid was freeze-dried and mixed with PCL dissolved in dichloromethane (DCM) to form a hybrid composite film of collagen and PCL after solvent evaporation [97]. Fibroblasts attached and proliferated on the composite films suggesting that can be used as tissue engineered skin substrates [97]. As another example, a gelatin-PLGA composite scaffold was developed for tissue engineering of articular cartilage [93]. For this purpose, a gelatin solution was prepared in distilled water at 60 °C and then mortared with PLGA at 35 °C until a homogeneous gelatin-PLGA suspension was prepared. The suspension of 2.5 g gelatin and 0.5 g PLGA in 50 mL water was freeze dried following solidification in a silicone mold then seeded by porcine chondrocytes by mixing with 2 mL of the cell suspension (1×10^6 cells ml^{-1}). Sulfated glycosaminoglycans (sGAGs) content and type-II collagen amount increased over 2 weeks, which both verified the deposition of cartilage specific ECM in the seeded scaffold. The Young's modulus of the gelatin-PLGA composite scaffolds decreased from 22.7 kPa to 5.1 kPa over 42 days of degradation. These moduli values are much lower than the one of native articular cartilage. However, the simultaneous deposition of cartilage ECM can take up some of the necessary load.

The natural and synthetic polymer blends can also be separately crosslinked to form co-continuous networks. As an example, terminally acrylated star copolymers of poly(ε-caprolactone-co-D,L-lactide) P(CL-co-LA) and poly(ε-caprolactone-co-trimethylene carbonate) (PCL-co-PTMC) (8-11 kDa) were blended with N-methacrylate glycol chitosan in aqueous solution that also contained the photo initiator Irgacure 2959 [98]. Chondrocytes were suspended in the N-methacrylate glycol chitosan (MGC) solution and then mechanically mixed with the viscous liquid acrylated star-copolymers to form a homogenous and injectable mixture that was crosslinked by exposure to long-wave UV light to form a co-continuous network consisting of an interconnected hydrogel within an interconnected elastomer. The chondrocytes stayed viable and were able to produce cartilaginous ECM components in the hydrogel-elastomer scaffolds. The equilibrium moduli of the interconnected hydrogel was reported to be 1-2 MPa, which is suitable for articular cartilage and intervertebral disc replacement (Table 2.1). The morphology of the stained scaffolds is illustrated in Figure 2.3. However, the ester linkages along the polymer backbone are susceptible to uncontrolled hydrolytic degradation. The other potential disadvantage of the use of PLA and PCL is the formation of acidic degradation products that may decrease the cellularity as a function of time.

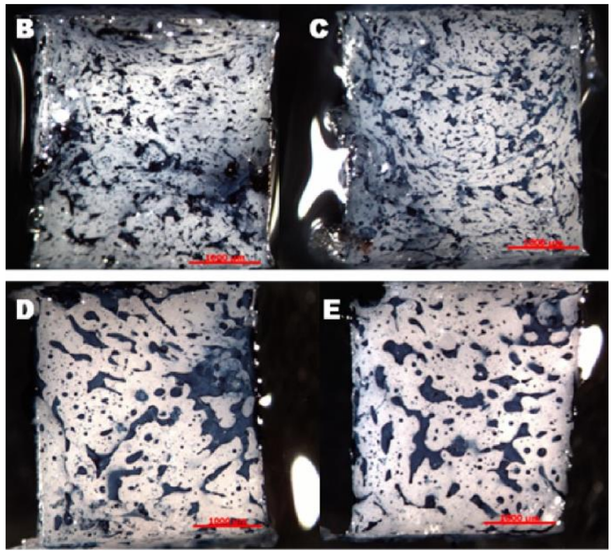

Figure 2.3. Post-injection and photo-cross-linking morphology of scaffolds stained with trypan blue to highlight the MGC phase in: (B, C) PCL-co-PLA, (D, E) PCL-co-PTMC. Scale bar 1000 µm [98].

2.5.2 Biohybrid single polymers

The other strategy to make biohybrid polymers is to covalently bind the natural and synthetic macromolecules together. The methods used include grafting, crosslinking through end group modification, and backbone incorporation of natural and synthetic polymers [69]. A schema of the covalent incorporation of synthetic and natural macromolecules is shown in Figure 2.4.

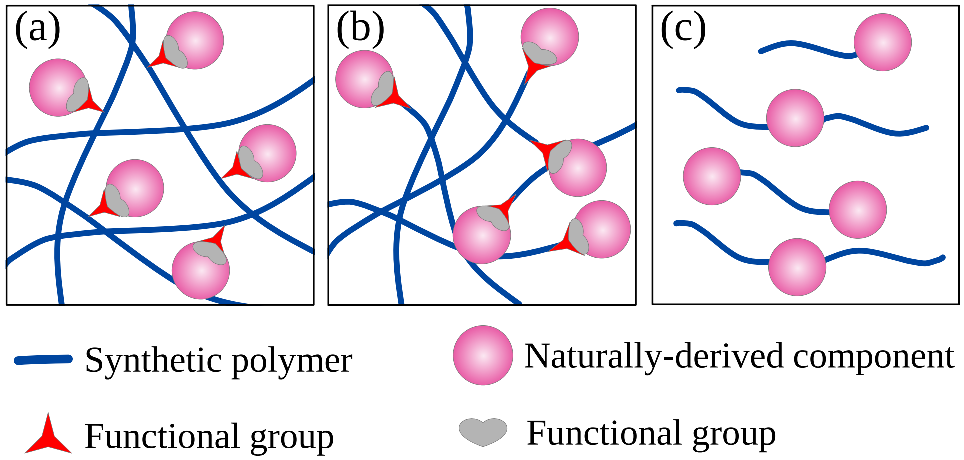

Figure 2.4. Incorporation of natural and synthetic macromolecules by grafting (a), crosslinking through end group (b), and backbone incorporation (c).

2.5.2.1 Grafting

Naturally derived and synthetic polymers can be covalently bound together via side-chain attachment or grafting. The functional side-chain groups either on the backbone of the synthetic polymer or the natural molecule can be designed to react to the other group of molecules after activation. For example, an MMP-sensitive transglutaminase (TG)-PEG was synthesized by mixing eight arm PEG containing factor XIIIa substrate peptides with either a glutamine acceptor or a lysine donor with an additional MMP-sensitive linker to mimic the mesenchymal stem cell (MSC) perivascular niche [99]. Growth factors were immobilized in this PEG-based perivascular niche model and, due to the structural transparency, cellular behaviors such as proliferation, spreading, and migration could be monitored throughout the experiment duration. This approach provides a promising platform for studying stem cells in their niches. Cook *et al.* demonstrated that using an arginine-glycine-aspartic acid (RGD) peptide-modified poly(lactic acid-co-lysine)

(PLAL) substrate resulted in better ECM production and proliferation of bovine aortic endothelial (BAE) cells compared to the unmodified PLAL [100]. The objective of their study was to provide an initial mechanical support for viable cells consisting of a degradable substrate until the cells could proliferate and generate ECM similar to that of the native tissue. They showed that the mean spread cell area increased 5.2 times on the peptide modified surface compared to 1.1 times on the unmodified PLAL surface after 4 h of incubation [100]. The disadvantage of this strategy is that PLAL undergoes hydrolysis via degradation of the ester bond in the polymer backbone, which may result in an uncontrolled mechanical failure.

Wiltsey *et al.* fabricated a thermogelling bioadhesive scaffold for intervertebral disk tissue engineering by covalently grafting poly(N-isopropylacrylamide) (PNIPAAm) to chondroitin sulfate (CS) (PNIPAAm-g-CS) [101], [102]. A schema of the CS grafting is illustrated in Figure 2.5. To accomplish this objective, redux polymerization of NIPAAm monomer was performed in the presence of methacrylated CS and a lightly crosslinked network was formed in which the propagating NIPAAm groups reacted across the MA groups. The stiffness of the hydrogels increased with increasing molar ratio of NIPAAm units to CS chains and was in the range of 5–6.7 kPa. The reported stiffness of this hydrogel is not high enough to withstand the natural forces of some load-bearing soft tissues such as articular cartilage. However, this value is suitable for NP tissue engineering (Table 2.1). The potential cytotoxicity of the degradation products is another issue with this group of networks that needs to be investigated [103].

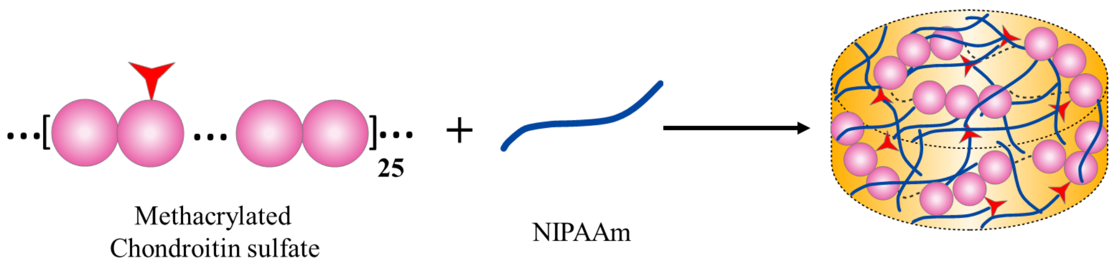

Figure 2.5. Schematic of CS grafting onto PNIPAAm. The molar ratio of the PNIPAAm units to the CS chains was between 600:1 and 4000:1. Figure adapted from [102].

2.5.2.2 Crosslinking through end group modification

Naturally derived polymers and synthetic polymers can be crosslinked to form a biohybrid network. For this aim, the end groups of the polymer chains or the pendant groups are functionalized to react to the other group of polymers. PEG-based hybrid polymers prepared by this method have been widely used in tissue engineering and regenerative medicine [104]. PEG-albumin [67], PEG-hyaluronic acid [68], and oligo(PEG-fumarate) crosslinked by cell-binding peptides [73]–[75] are some examples of this group of hybrid polymers. End-functionalized multi-arm PEG has been reacted to a cysteine-containing MMP-sensitive peptide to form a biohybrid network in a number of publications [72], [73], [75], [105]–[108]. The common functional groups that are used in such strategies are maleimide, acrylate, methacrylate, and vinyl sulfone which can react to a thiol group via Michael-type addition reaction [109]. Generally, the PEG-based hydrogels have low moduli in the order of tens to hundreds of kPa. For example, Lutolf *et al.* developed a cell-adhesive MMP-sensitive hydrogel by crosslinking through end group modification [107]. A schema of the biohybrid hydrogel formation is presented in Figure 2.6. The mechanical features of the final network were not investigated in this study. However, they have shown in another study that the networks prepared with 8-arm PEG had higher elastic moduli compared to the ones prepared with 4-arm PEG due to a higher crosslink density in 8-arm PEG hydrogels [79]. The elastic moduli of such networks was reported to be in the range of 4–14 kPa which is weaker than those of many soft connective tissues. This range of moduli can be used in the skeletal muscles or fat tissue engineering.

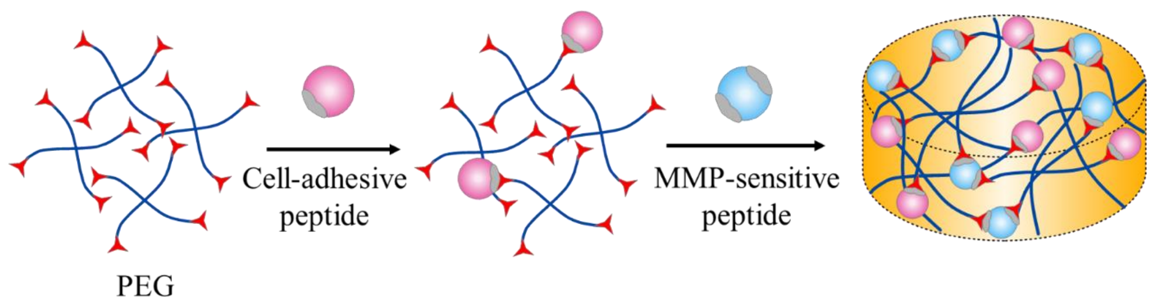

Figure 2.6. Michael type addition reaction between vinyl sulfone functionalized 4-arm PEG and mono-cysteine adhesion peptides or bis-cysteine MMP-sensitive peptides. Figure adapted from [107].

To improve the mechanical properties of the PEG-based hydrogels for connective soft tissue engineering, PEG can be copolymerized with other polymers such as poly(trimethylene carbonate) (PTMC). 4-arm PEG was used as an initiator to polymerize PTMC and form a block copolymer that was crosslinked by using MMP-sensitive peptide as a cross linker to form a tough and enzyme-degradable structure [88]. PTMC was chosen for this purpose because it undergoes very slow hydrolysis in biological environments [110] and so the degradation of the biohybrid hydrogels are controlled by the enzyme actions and cleavage of the MMP-sensitive peptide. The compressive moduli of the hydrogels made with different molecular weights of PTMC block was reported from 0.17 ± 0.04 MPa to 3.75 ± 0.54 MPa. The incorporation of PTMC block possessing 4 repeating unit to the 4-arm PEG increased the modulus of the hydrogel by 6 times.

2.5.2.3 Backbone incorporation

The formation of block copolymers of natural and synthetic polymers is the other strategy of biohybrid polymers fabrication. As an example, Peters *et al.*, investigated the ability of EPCs to form vessels within an engineered cell-adhesive and enzyme degradable PEG-based hydrogel [74]. An acrylated diblock copolymer of PEG and an RGD peptide plus an acrylated triblock copolymer of PEG and an MMP-sensitive peptide along with endothelial progenitor cells (EPCs) were mixed and crosslinked via a mild process [74]. Acrylate-PEG-succinimidyl valerate (Acryl-PEG-SVA) was reacted to RGD in a basic solution to form an Acryl-PEG-RGD. Similarly, MMP-sensitive peptide, (abbreviated as PQ) was reacted to Acryl-PEG-SVA at the C-and N-termini to form Acryl-PEG-PQ-PEG-Acryl. The schematic illustration of the resulting network is presented in Figure 2.7. The cells were encapsulated in a solution of the prepolymer dissolved in X and mixed with a photo initiator solution (0.11 M triethanolamine with 0.02 mM eosin Y, and 9.4 M 1-vinyl-2 pyrolidinone) and then photo-cured by exposure to white light 120 mW/cm^2 for 40 s. In this study the ability of EPCs to form a vessel in a tissue engineered PEG hydrogels with a compressive modulus of 18 ± 5 kPa was investigated. The MMP-sensitive peptide was incorporated to the backbone to confer a cell-responsive degradation. They demonstrated that the EPCs formed a 3D stable microvessel network in the absence of angiogenic growth factors. The cell viability following crosslinking and the change in mechanical properties over degradation were not reported. The initial stiffness of these networks is suitable for some connective tissue engineering such as fat tissue. However, this value was much lower than those of load-bearing soft connective tissues, which would limit the application of such biohybrid material.

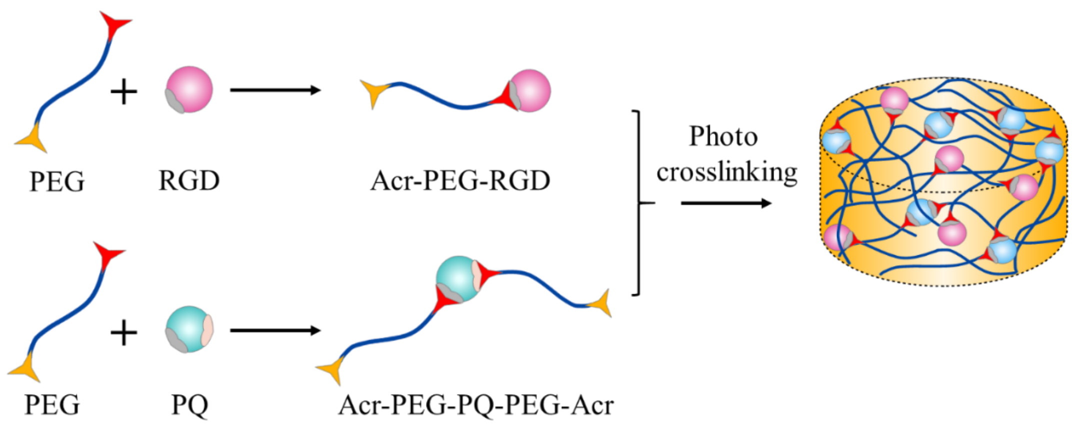

Figure 2.7. Schematic of PEG hydrogel system made of heterobifunctional PEG, MMP-sensitive peptide (PQ), and RGD peptide. Figure adapted from[74]**.**

2.6 Host tissue interaction with implanted biomaterial

There is a range of difference immune responses to the implanted scaffolds in tissue engineering and regenerative medicine. The scaffolds that are constructed by using synthetic or biological materials or derived from allogenic and xenogeneic tissues provoke different immunogenicity of the native tissue that are not the main focus of this review [111]. Synthetic biomaterials are among the most immunogenic biomaterials that can activate the innate immune system by triggering pathogen-associated molecular proteins [111].

There are many different proteins in blood plasma which depending on the nature of the biomaterial can be adsorbed to the surface of the implanted construct as the first interaction of the host tissue with the biomaterial, when it is implanted in the vascular tissues. In fact, the protein adsorption translates the structure and the composition of the implanted biomaterials to the corresponding cells [112]. This protein adsorption is followed by and affects the adhesion, proliferation, and differentiation of certain cell types that can influence the immunogenicity of the native tissue [106]. The cellular behavior followed by the protein adsorption can also influence the enzymatic degradation of the biomaterial [45]. For example, adsorption of fibronectin and vitronectin promotes the adhesion and spreading of specific cells such as fibroblasts and macrophages which secrete ECM remodeling enzymes [113].

2.7 Conclusion and perspectives

Biohybrid polymers, possessing the advantages of naturally-derived macromolecules and synthetic biopolymers, have gained much attention in the fields of tissue engineering and regenerative medicine during the past two decades. This group of biomaterials are promising for the reconstruction of many different types of damaged or lost tissues. However, the present literature on enzyme degradable biohybrid polymers lacks investigations of *in vivo* degradation profiles, the necessary moduli to match those of the various soft connective tissues, and the changes in the mechanical properties of these materials following implantation. With this knowledge, a library of cell-responsive, biodegradable, and though biohybrid polymers for applications in different soft connective tissue engineering and regenerative medicine applications would be possible.

Chapter 3

Scope

3.1 Proposed approach

The focus of this study was on developing an enzyme-degradable network for soft connective tissue engineering applications. To date, none of the tissue engineering approaches in soft connective tissue regeneration have been able to provide the mechanical, degradation, and biological aspects of the scaffold simultaneously. In this project, the first two aspects of such a material have been examined. It was a principal objective of this project to create a network degradable solely by enzyme action, such as it would be expected from cell growth and migration [98], [114], [115].

This work was guided by two hypotheses. It was hypothesized that networks prepared from end-functionalized poly(trimethylene carbonate) (PTMC) and peptide conjugates would have appropriate mechanical properties for use in soft connective tissue engineering. It was also hypothesized that the resulting network would be solely degraded by enzymes.

The approach involved development of a PTMC-based network that could be enzymatically degraded. The rationale of this approach was to maintain the mechanical properties of the network until the cells produce sufficient ECM to take up the applied loads. This aim is not reachable if any other cleavage mechanism dominates the final degradation rate [116]. To provide enzyme degradability a collagenase-cleavable (MMP-sensitive) peptide was conjugated to PTMC. PTMC was chosen because it has attractive mechanical properties for biomedical applications, as it has a rubbery and flexible structure at body temperature [117]. Furthermore, the carbonate linkage in PTMC undergoes a very slow degradation via hydrolysis [19], [118]. In this way, the degradation rate of the network was controlled by the cellular enzyme production rate. The PTMC degradation products were designed to be less than 1300 Da, as it has been shown previously that this low molecular weight PTMC is water soluble and can be eliminated from the body [110]. The final structure was a PTMC-peptide-PTMC triblock copolymer that was curable via free radical polymerization.

Two different approaches were explored to form PTMC-peptide networks. In the first approach, dual-functionalized PTMC was initially prepared having a vinyl sulfone (VS) at one end and a methacrylate (MA) at the other end. The VS enabled coupling of the PTMC to an MMP-sensitive peptide by reaction with the thiol group on a cysteine residue added to the peptides via Michael type addition of thiol to the activated olefin [119], while the MA enabled cross-linking of the resulting copolymers by free radical polymerization [120]. The thiol group on the cysteine amino acids preferentially reacted to the vinyl group of the VS end due to the steric hindrance of the methyl group on the MA end. Free radical polymerization was chosen in this design not only because of the fast and controllable crosslinking but also due to its ability to be carried out under ambient or physiological conditions [121]. In the second approach, a diblock of poly(ethylene glycol) (PEG)-PTMC was first formed and then end functionalized as in the first approach (i.e. one terminus with a VS group and the other with MA group). The addition of hydrophilic PEG to the hydrophobic PTMC backbone yielded an amphiphilic copolymer with an improved water solubility with aqueous crosslinking potential.

3.2 Objectives

The main objective of this work was to develop a biohybrid network with mechanical properties suitable for soft connective tissue engineering strategies that is degradable by matrix metalloproteinases (MMPs). Towards this objective, three specific aims were examined:

Specific Aim 1: Synthesis and *in vitro* characterization of a PTMC-based hybrid network.

A heterobifunctional MA-PTMC-VS was synthesized, that could be readily conjugated to a MMP-sensitive peptide, and form a crosslinkable triblock biohybrid prepolymer. A number of different molecular weights were prepared to study the effect of the PTMC block molecular weight on compressive moduli and *in vitro* degradation of the biohybrid networks. The structure, purity, water solubility, and thermal properties of the final prepolymer were characterized along with the stiffness, water content, and *in vitro* degradation of the biohybrid network.

Specific Aim 2: Synthesis and *in vitro* characterization of a PEG-PTMC hybrid network.

A heterobifunctional MA-PEG-PTMC-VS was synthesized, that could be readily conjugated to a MMP-sensitive peptide, and form a crosslinkable biohybrid prepolymer. The prepolymer and the networks prepared were characterized *in vitro*. The effect of the PEG addition on the compressive modulus and *in vitro* degradation of the biohybrid network was studied.

Specific Aim 3: *In vivo* degradation, mechanical property change assessment and tissue response to the networks prepared with chosen molecular weight PTMCs and PEG-PTMCs.

The tissue response following the implantation of the biohybrid networks and their degradation rate in a rat model were investigated following subcutaneous implantation in Wistar rats.

Chapter 4

Enzyme-degradable poly(trimethylene carbonate)-peptide biohybrid networks

An enzymatically degradable poly(trimethylene carbonate) (PTMC)-based hybrid network was developed with potential applications in soft connective tissue engineering. An α-vinyl sulfone (VS), ω-methacrylate (MA) heterobifunctional PTMC was prepared and conjugated to a di-cysteine containing matrix metalloproteinase (MMP)-sensitive peptide to form a curable triblock prepolymer. This prepolymer was photo-cured to form a biodegradable network. Three different number average molecular weights (500, 1100 and 1800 Da) of the heterobifunctional PTMC were used to adjust the mechanical properties and degradation rate of the networks prepared. The enzymatic degradation of the resulting networks was studied *in vitro* over 15 weeks. Networks prepared with PTMC-peptide conjugates with lower PTMC molecular weight showed higher water uptake, lower compressive moduli and faster degradation rates. 500 Da Poly(ethylene glycol) (PEG) was added to PTMC 1100 Da to improve its water solubility and study the effect of PEG addition on degradation of the hybrid network. This addition increased the water solubility of the biohybrid compound and the water content of the networks from 19 ± 1% to 69 ± 5%. A mass loss of 74 ± 2% was observed over 4 weeks of degradation in a collagenase-containing medium, whereas the mass loss of the networks prepared with PTMC 1100 Da was 18 ± 4% over the same period of time. The addition of PEG to the PTMC backbone also decreased the compressive modulus of the networks from 6.4 ± 0.7 to 1.1 ± 0.6 MPa.

4.1 Introduction

Tissue engineering is a multidisciplinary research field that aims to develop biological substitutes to improve, restore or maintain a tissue function. A common tissue engineering approach is to combine host-derived cells with a polymer scaffold that supports cellular function. An objective of many tissue engineering strategies, then, is to create suitable polymer scaffolds [7]. The most challenging features to be designed into these polymers are a stiffness equivalent to that of the tissue and a well-controlled degradation behavior [124].

The mechanical properties of the cell microenvironment control a number of cellular functions including proliferation, migration and morphogenesis [39]–[41]. This microenvironment includes the extracellular matrix (ECM), which determines the structure and mechanical properties of the tissue. The ECM mechanical properties regulate the behavior of different cells within the tissue [125], [126] and changes in these properties can initiate diseases [127]–[131]. For example, it has been shown that under otherwise identical conditions, the microenvironment elasticity can direct mesenchymal stem cell differentiation toward neurons, myoblasts and osteoblasts [131]. Cellular mechano-transducers generate signals based on the required force to deform the matrix. For example, when myoblasts feel higher resistance compared to normal sarcolemma while deforming their surrounding ECM, they differentiate into connective tissue rather than muscle [15]. Therefore, the mechanical properties of the engineered scaffold must be compatible with those of the innate microenvironment to mimic the natural mechanical stimulation of the cells [42]. These mechanical properties vary widely, depending on the function of the tissue. For example, the compressive moduli of soft connective tissues vary from 3 kPa for fat tissue to 1 MPa for load-bearing cartilage [25], [134], [135].

The ECM is also a dynamic structure that is constantly remodeled by specific cell-secreted enzymes like metalloproteinases [15], [136]. An ideal material for tissue engineering would have a degradation profile that would facilitate the regeneration of newly produced tissue. Such a design allows the load to be transferred from the implanted material to the regenerated tissue gradually, to provide continuous tissue function during healing. [72]

Enzyme degradable biomaterials are therefore advantageous for a range of soft connective tissue engineering applications [53], [54], [59], [60], [72], [73], [106], [137], [138]. Physiologically-derived polymers have been used widely in this regard, due to their suitable cellular interactions and enzyme mediated degradation [139]. However, the complications associated with this group of materials such as their poor mechanical properties, unpredictable degradation and lack of availability, limits their application [139]. Synthetic polymers, alternatively, have predictable and reproducible properties, but generally degrade principally through hydrolysis [140]. Hydrolytic degradation increases the risk of unpredictable loss of mechanical features and network collapse, which is not favorable for tissue engineering applications. One potential biomaterial design approach then is to combine the advantages of both materials through the incorporation of enzyme-cleavable peptide sequences to a synthetic polymer structure to form a biohybrid copolymer [67]. Limitations in current tissue engineering strategies for soft connective tissues with biomechanical function such as blood vessels, muscles and cartilage can thus be addressed by utilizing three-dimensional biohybrid networks. The synthetic phase of such a scaffold would provide mechanical support to the tissue during the healing process, while the peptide phase would provide enzyme-degradability.

The objective of this study was to create an enzyme degradable network suitable for soft tissue engineering applications. A triblock copolymer structure was chosen, wherein the central block was an MMP-sensitive peptide, flanked by synthetic hydrophobic blocks that would contribute the necessary mechanical properties. The peptide sequence chosen to demonstrate the potential of the design strategy was GCRDGPQG↓IWGQDRCG, which has shown sensitivity to a wide range of collagenases [116]. Poly(trimethylene carbonate) (PTMC) was chosen as the hydrophobic synthetic block because of its resistance to hydrolysis [110], its low glass transition temperature that makes it rubbery at physiologic temperature [118], its history of safe use in the body as a component of degradable Maxon sutures [141] and its ease of synthesis via controllable ring-opening polymerization [142]. Furthermore, low molecular weight PTMC is bio-absorbable and can be cleared from the body [110], [143].

A vinyl sulfone (VS) bearing molecule was used as an initiator in the PTMC polymerization process to functionalize one terminus of the polymer. Following polymerization the polymer was then functionalized at its other terminus with a methacrylate (MA) group. The VS enables the coupling of the thiol group on a cysteine residue on the MMP-sensitive peptide via Michael type addition [119]. The carbon double bond of VS is more electron-deficient compared to that in MA and is therefore more reactive in a Michael-type addition reaction [109], and so this coupling strategy should result in free terminal methacrylate groups [144]. The resulting thioether sulfone bond is hydrolytically stable, [109] which is a necessary feature in the design of our enzymatically degradable elastomer. Finally, the terminal methacrylate groups of the formed peptide-(PTMC-MA$)_2$ triblock copolymer provide crosslinking functionality and the resulting copolymer can be cured to form a network by free radical induced crosslinking of the MA groups [145], [146]. The advantage of this design is the simplified one-step cross-linking process by having both the synthetic polymer and the MMP-sensitive peptide components in a single prepolymer.

In a second polymer design, poly(ethylene glycol) (PEG) block was added to the PTMC block to improve the overall water solubility of the prepolymer, and to modify the mechanical properties of the previously described peptide-(PTMC-MA$)_2$ biohybrid networks. For this aim, methacrylate PEG was used as the initiator for the ring opening polymerization of TMC and the resulting diblock copolymer was subsequently functionalized at the PTMC terminus with a vinyl sulfone group. The MA-PEG-PTMC-VS thus formed was then conjugated to the dithiol peptide to form a peptide-(PTMC-PEG-MA)$_2$ prepolymer. A schematic of the peptide-(PTMC-MA)$_2$ and peptide-(PTMC-PEG-MA)$_2$ prepolymer formation strategy is illustrated in Figure 4.1.

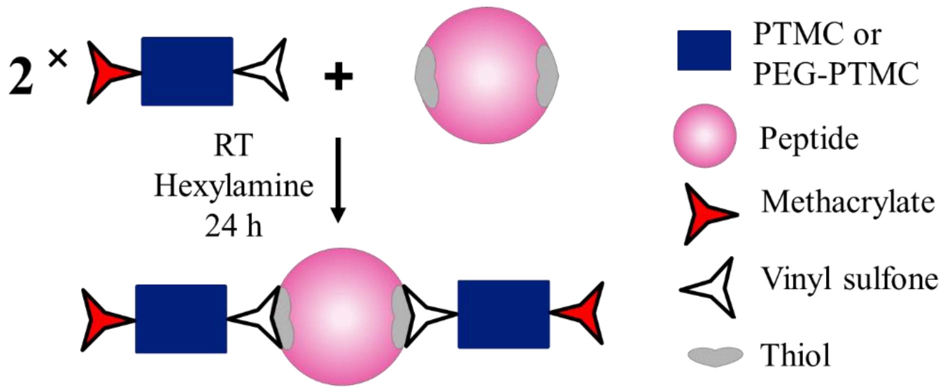

Figure 4.1. Schematic of the Michael-type addition reaction to yield the prepolymer.

Herein we describe the synthesis, and chemical and mechanical characterization of enzyme degradable networks formed from these prepolymers both following preparation and during *in vitro* degradation in an MMP-1 containing medium.

4.2 Materials and methods

4.2.1 Materials

1,3-Trimethylene carbonate (TMC) was obtained from LEAPChem, China. Stannous 2-ethylhexanoate was obtained from Alfa Aesar, USA. HPLC-grade toluene, hexylamine, dimethyl sulfoxide-d6 (DMSO), tetrahydrofuran (THF), dimethylformamide (DMF), divinyl sulfone (DVS) (97% purity), methacryloyl chloride, 2,2-dimethoxy-2-phenylacetophenone (DMPA), Irgacure 2959 photo initiator, 4-(2-hydroxyethyl)-1-piperazineethanesulfonic acid (HEPES), sodium azide, poly(ethylene glycol) (PEG) dithiol (182 Da), methacrylate PEG (500 Da), and 4-dimethylaminopyridine (DMAP) were purchased from Sigma-Aldrich, Canada. Dichloromethane, methanol, ethanol, 2-mercaptoethanol (99% purity), trimethylamine (TEA), and hydrochloric acid were obtained from Fisher Scientific, Canada. Collagenase type II from *Clostridium hyistolyticum* was purchased from MP Biomedicals LLC, USA. The collagenase-sensitive peptide (GCRDGPQGIWGQDRCG) was custom synthesized by CanPeptide Inc., Canada. Dialysis membranes with a molecular weight cut off of 100-500 Da were purchased from Biotech CE Tubing, USA. Deionized water was obtained from a Millipore Milli-Q Plus ultrapure water system. Dichloromethane was dried over molecular sieves for 72 h prior to use. All other reagents were used as received.

4.2.2 Initiator and PTMC synthesis

2-((2-vinylsulfonyl ethyl)thio)ethanol was synthesized by reaction of 2-mercaptoethanol with 4 equivalents of divinyl sulfone in the presence of TEA in methanol at 35 °C for 24 h (Figure 4.2a). The product was purified by silica gel column chromatography using ethyl acetate:petroleum ether, 70:30 as an eluent. The purified product was used as an initiator for 1,3-trimethylene carbonate (TMC) polymerization.

Low molecular weight PTMC containing 5-15 repeating units was synthesized by a stannous 2-ethylhexanoate-catalyzed ring opening melt polymerization of TMC in the presence of 2-((2-vinylsulfonyl ethyl)thio)ethanol as initiator (Figure 4.2b). A catalyst to initiator molar ratio of 3×10^{-3} was used and the catalyst was dissolved in toluene at 20% (w/w) concentration for accurate measurements [41]. All reactants were mixed in a 20 mL flame dried ampule, purged with argon, flame sealed under vacuum and then reacted overnight at 110 ºC. The resulting α-vinyl sulfone PTMC (VS-PTMC) was used in subsequent steps without purification.

Following formation of the VS-PTMC, methacryloyl chloride was reacted with the terminal hydroxyl groups of the PTMCin the presence of triethylamine and a catalyst, 4-dimethyl amino pyridine, in anhydrous toluene at room temperature (Figure 4.2c) to form α–vinyl sulfone, ω–methacrylate PTMC (VS-PTMC-MA). A molar amount of TEA equivalent to the moles of methacryloyl chloride was used to scavenge the hydrochloric acid formed during the reaction. All reactants were added to a flame-dried round bottom flask under an inert nitrogen atmosphere and within a dry box, and stirred for 48 h. The product was dissolved in ethyl acetate and filtered through filter paper to remove triethylamine HCl salt particles, followed by precipitation of the polymer in hexane to remove unreacted initiator and monomer.

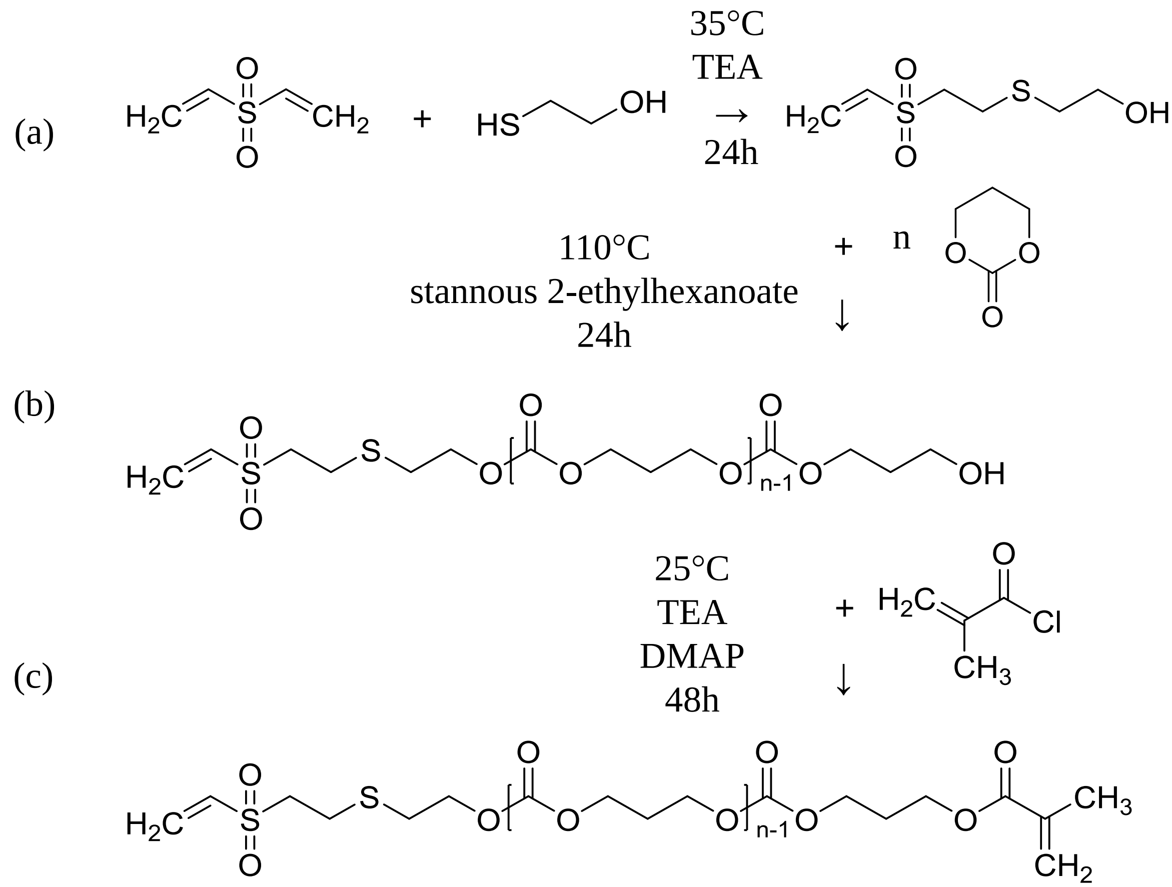

Figure 4.2. (a) Initiator synthesis; 4 molar equivalents of divinyl sulfone reacted with mercaptoethanol, (b) TMC polymerization; using 2-((2-(vinyl sulfonyl)ethyl)thio)ethanol as the initiator and stannous 2-ethylhexanoate as the catalyst, and (c) VS-PTMC-OH methacrylation; addition of methacryloyl chloride to the terminal hydroxyl group.

4.2.3 Synthesis of heterobifunctional PEG-PTMC

Methacrylate terminated poly(ethylene glycol)-*b*-poly(trimethylene carbonate) (MA-PEG-PTMC-OH) was first synthesised via a stannous(II) ethylhexanoate-catalyzed ring opening melt polymerization of 1,3-trimethylene carbonate (TMC) in the presence of PEG-methacrylate (500 Da) as the initiator (Figure 4.3a). The molar ratio of catalyst to initiator was 3×10^{-3} based on our previous results [110]. Following the polymerization, one equivalent of the MA-PEG-PTMC-OH in solution was added dropwise to a stirred round bottom flask containing four equivalents of divinyl sulfone in dichloromethane under argon over 3 h. The divinyl sulfone was then reacted to the terminal hydroxyl groups of the PTMC block in the presence of sodium hydride (NaH) as the catalyst over 72 h (Figure 4.3b) [107]. The final product was purified by adding 1.1 equivalents of acetic acid to the mixture and filtering the resulting salts through filter paper. The DCM was then removed in a rotary evaporator and excess divinyl sulfone was separated by precipitation of the copolymer in diethyl ether three times.

(a)

(b)

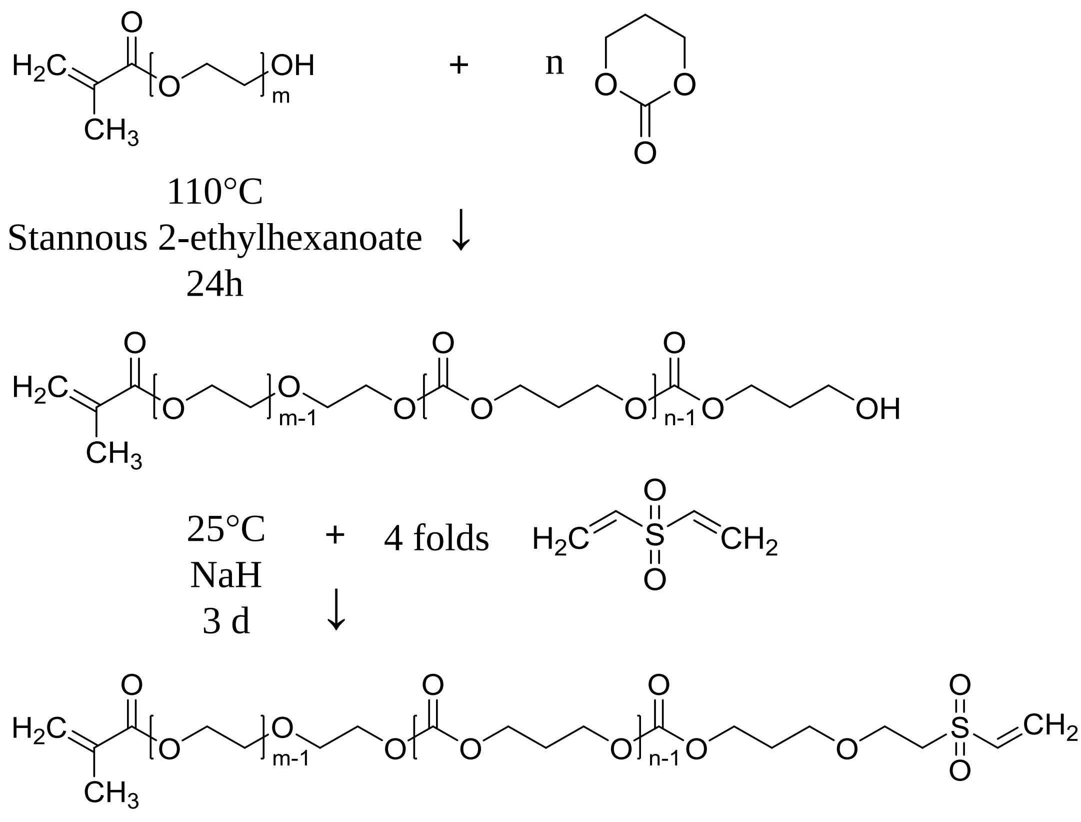

Figure 4.3. (a) TMC polymerization in presence of methacrylate-PEG as the initiator, and (b) vinyl sulfone functionalization of the hydroxyl end group of the MA-PEG-PTMC molecule.

4.2.4 Fractionation

Size exclusion chromatography was used to purify and fractionate the resulting heterobifunctional polymer into varying molecular weight size ranges. Porous hydroxylated acrylic gel beads (TOYOPEARL) were packed in a 4 cm × 50 cm glass column. The interstitial space between the gel particles was filled with solvent (ethyl acetate: methanol, 1:1). The VS-PTMC-MA and MA-PEG-PTMC-VS samples were separately dissolved in the same solvent and introduced into the gel column and eluted under gravity. Different molecular weight fractions were collected in 20 mL vials and evaluated by proton nuclear magnetic resonance spectroscopy (^{1}H NMR) and universal calibration gel permeation chromatography (GPC) using a styrene calibration curve for their number average molecular weight and molar mass dispersity ($Đ_M$), respectively. The GPC system was a Waters 2695 with THF as the mobile phase and 2 Phenogel 5 μm columns in series using a 5 mg/mL polymer solution in THF. In this way, PTMC molecular weight fractions of 500, 1100 and 1800 Da were obtained. ^{1}H NMR spectra were obtained in DMSO-d_6 using a Bruker Avance-400 NMR spectrometer. Chemical shifts were measured relative to the methyl proton resonance of an internal tetramethylsilane standard. The average number of TMC repeating units per macromolecule was calculated from the ^{1}H NMR spectra by comparing the integration of the methylene backbone peaks (δ = 1.93-1.96 ppm) of the TMC repeating units to the vinyl peaks (δ = 6.24-6.3 ppm and 6.95-7.04 ppm) of the vinyl sulfone terminal moiety. The number average molecular weight (M_n) was then calculated considering the molecular weight of the TMC repeating units, along with the initiator and methacrylate groups. A similar approach was used to obtain a PEG-PTMC molecular weight fraction of 1700 Da (PTMC block length of 1.2 kDa).

4.2.5 Peptide conjugation

The VS-PTMC-MA was reacted with a half equivalent of the di-cysteine, MMP-sensitive, GCRDGPQGIWGQDRCG peptide, to form a MA-PTMC-*b*-peptide-*b*-PTMC-MA triblock, (peptide-(PTMC-MA)$_2$). Similarly, the MA-PEG-PTMC-*b*-peptide-*b*-PTMC-PEG-MA copolymer, (peptide-(PTMC-PEG-MA)$_2$) was synthesized by peptide conjugation to MA-PEG-PTMC-VS. The thiol group on each cysteine end group was preferentially reacted with the vinyl sulfone terminal group via a Michael-type addition reaction in DMF in the presence of hexylamine for 24 h at room temperature. Purification of the final compound was carried out by dialysis in water for 48 h. The purified polymer was freeze-dried and stored at -20 ºC.

4.2.6 Prepolymer characterization

^{1}H NMR spectroscopy was performed to confirm the structure and relative purity of all products. The water solubility of the different polymer fractions was measured by adding 4 mL of distilled water into 100 mg of polymer sample. The mixture was stirred overnight at 37 ºC and then centrifuged at 3200 rpm for 10 min. The supernatant was separated and lyophilized and the weight of the dissolved material determined gravimetrically. The polymer glass transition temperatures were measured on a Mettler-Toledo differential scanning calorimeter (DSC) using a cooling-heating-cooling-heating cycle from 25 ºC to -60 ºC to 40 ºC to -60 ºC to 25 ºC at a rate of 30 ºC /min. Indium and gallium standards were used to calibrate the DSC. The glass transition temperature was determined from the inflection point of the second run endotherms using the internal DSC analysis software.

4.2.7 Network fabrication

Peptide-(PTMC-MA)$_2$ prepolymers of varying molecular weights and the peptide-(PTMC-PEG-MA)$_2$ prepolymer were dissolved to form a 25 % w/v solution in DMF:DMSO (1:1). To these solutions the photo-initiator, Irgacure 2959, was added to a final concentration of 0.1 % w/v. The resulting solution was mixed using a vortex mixer. A 1 mL plastic syringe was used as a mold; the syringe tip was cut and a stopper was used at the other end of the syringe in order to have flat surfaces at both sides of the elastomer discs (Figure 4.4). The syringe was filled with the prepolymer solution and exposed to long wave UV light (centered at 360 nm) at room temperature using an EXFO E3000 high-intensity lamp at a relative intensity of 20 mW/cm^2 for 5 min each side to yield a network. After crosslinking, the network was removed from the syringe by pushing the plunger, then dried under vacuum for 2 days. The resulting network was a cylindrical disc with dimensions of approximately 3.5 mm × 5.5 mm.

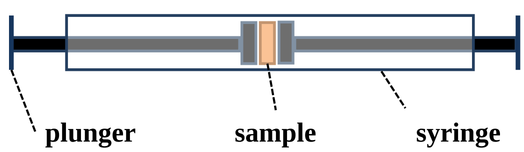

Figure 4.4. A schematic of the syringe mold used to prepare crosslinked samples.

4.2.8 Network characterization

The crosslinking efficiency was assessed by measuring the sol content after network formation. The sol content was determined by measuring the dry weight before and after immersing the network in DMSO at 37 ºC for 24 h. The DMSO was removed by immersing the networks in water with repeated water replacement for 24 h and then the networks were lyophilized. The aqueous swelling ratio of the network samples was determined by calculating the weight difference of the network disc before and after immersion in water at 37 ºC for 24 h. Following sol extraction, the glass transition temperature was measured via differential scanning calorimetry (DSC) using the cooling-heating-cooling-heating cycle described above.

To determine the instantaneous compressive modulus of the networks, indentation measurements were conducted. The measurements were performed on hydrated cylindrical samples (n = 5) pre-hydrated in water at 25 ºC. The measurements were conducted at a strain rate of 1%/s using a 1 mm diameter indenter and the resulting force was recorded. The compressive modulus was obtained from the following equation (Equation 1) assuming the rigidity of the indenter was infinite and the sample had a Poisson's ratio, ν, of 0.5. In the equation, E is the compressive modulus of the elastomer, F is the applied force, R is the radius of the indenter and d is the displacement of the indenter [147].

$$E = \frac{F}{2.67\,R\,d} \qquad \text{Equation 1}$$

4.2.9 *In vitro* degradation

The *in vitro* degradation was assessed by measuring the weight loss of the cross-linked networks in 3 mL of 10 mM HEPES buffered solution at pH 7.4 at 37 °C containing collagenase type 2 (0.1 mg/mL, 265 U/mg) and collagenase type 4 (0.1 mg/mL, 225 U/mg), along with calcium chloride (1 mM), sodium azide (0.2 mM) and bovine serum albumin (0.5 %w/v). The same media without collagenase was used to study the potential hydrolysis of control samples prepared from VS-PTMC-MA with a 1100 Da PTMC block conjugated with enzyme and hydrolysis stable 182 Da

PEG-dithiol instead of the MMP-sensitive peptide to form the triblock prepolymer. A similar approach was used to generate control samples prepared with MA-PEG-PTMC-VS conjugated to 182 Da PEG dithiol. The 2 mL tubes containing the cylindrical discs (n = 3) were placed in a thermomixer at 37 °C with horizontal shaking at 300 rpm. The weight loss, sol content, water content, glass transition temperature and the hydrated compressive modulus were measured and analyzed at given time points.

4.2.10 Statistical analysis

All data is expressed as the mean ± the standard deviation about the mean. One-way analysis of variance (ANOVA) with a Bonferroni post hoc test (Microsoft Excel) was performed where applicable. A paired t-test was conducted between samples for long-term studies. A p value of less than 0.05 was used to determine significant differences between population means.

4.3 Results

4.3.1 Peptide-(PTMC-MA)$_2$ prepolymer preparation and characterization

The reaction efficiency as well as chemical structure and purity of the compounds after each reaction were assessed via ^{1}H NMR spectroscopy. Figure 4.5a shows the ^{1}H NMR spectrum of the synthesized 2-((2-(vinylsulfonyl)ethyl)thio)ethanol initiator. The proton peaks at 6.25 and 7 ppm confirmed the presence of the carbon double bond of the vinyl sulfone group on the initiator. In addition, no impurity peaks appeared in the spectrum. The vinyl peaks of the sulfone group were preserved following ring-opening polymerization of TMC, and the resulting polymers possessed the characteristic peaks of poly(trimethylene carbonate) (Figure 4.5b) [110]. The proton peak at 4.55 ppm corresponds to the proton of the hydroxyl group, the triplet at 4.2 ppm corresponds to the protons of the methylene adjacent to the carbonates while the triplet at 2 ppm corresponds to the central methylene protons. Following methacrylation the peaks corresponding to the hydroxyl group disappeared while peaks corresponding to the vinyl protons and the methyl protons on the methacrylate group appeared at 5.6, 6, and 1.95 ppm, respectively (Figure 4.5c). Comparison of the integration of the peaks corresponding to the vinyl protons of the methacrylate group to those of the vinyl sulfone confirmed that degrees of methacrylation of greater than 98% were obtained. Finally, formation of the terminally methacrylated triblock copolymer through the Michael-type addition reaction was confirmed by the nearly complete disappearance of the vinyl protons of the VS group while all characteristic methacrylate peaks at 5.6, 6.1, and 1.95 ppm remained (Figure 4.5d). The conjugate addition reaction efficiency was greater than 95% as determined by integration of the VS peaks at 6.25 ppm before and after conjugation.

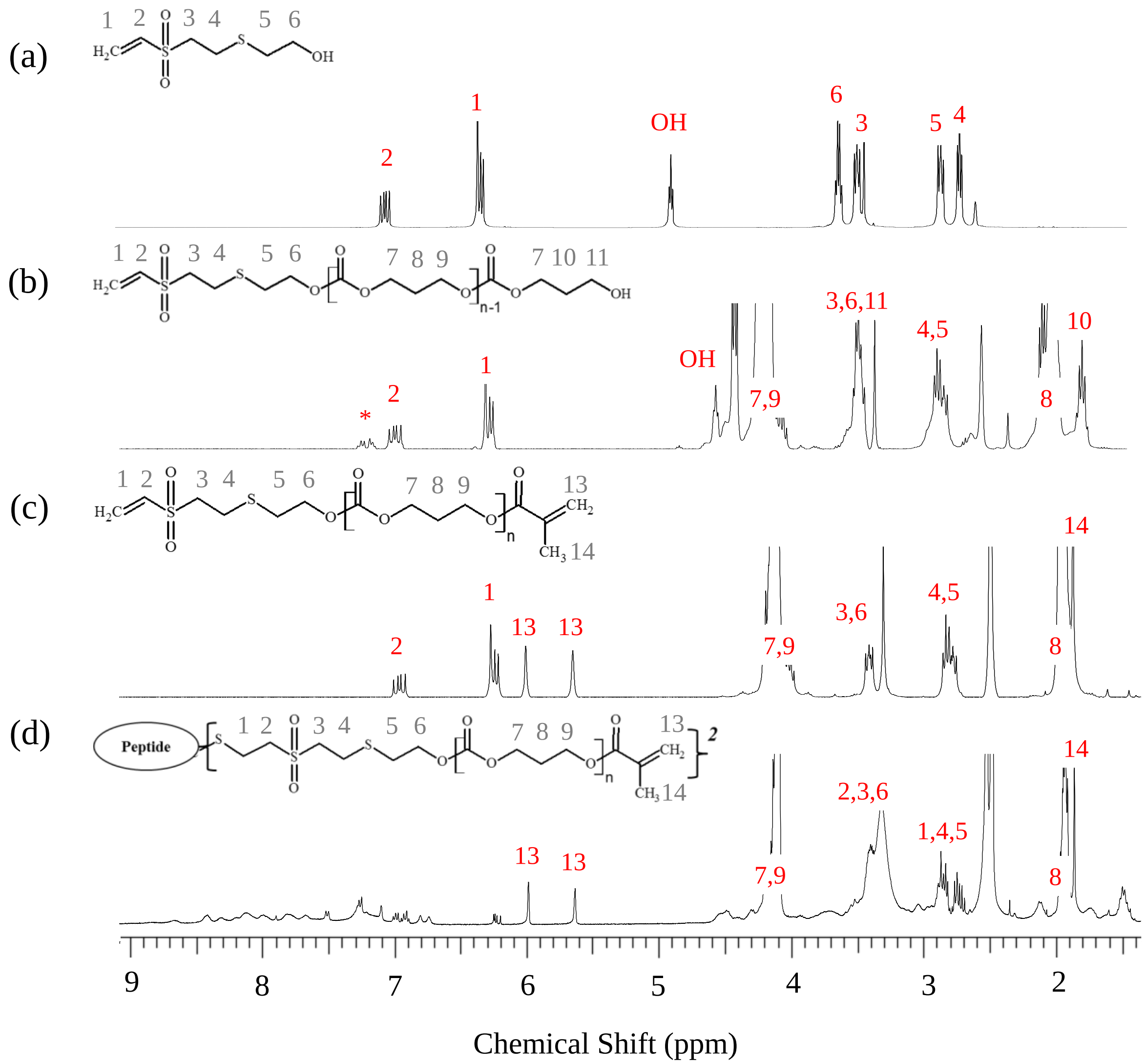

Figure 4.5. **^{1}H NMR spectra of (a) 2-((2-(vinylsulfonyl)ethyl)thio)ethanol initiator, (b) VS-PTMC-OH, (c) VS-PTMC-MA and (d) peptide-(PTMC-MA)$_2$, * Toluene residue at 7.18 ppm, DMSO at 2.54 ppm and water at 3.33 ppm.**

VS-PTMC-MAs with different molecular weights were analyzed by ^{1}H NMR, GPC and DSC. The results are shown in Table 4.1. Universal calibration GPC was used to measure the relative molar mass dispersity for the different fractions. There was relatively good agreement between the M_n calculated from ^{1}H NMR spectra via end-group analysis (M_{nNMR}) and that determined from GPC with universal calibration (M_{nGPC}). The relative molar mass dispersity increased slightly as the M_n increased, up to an M_{nNMR} of 1800 Da (Table 4.1). The T_g increased while the water solubility (WS) decreased as the average molecular weight increased, as expected.

Table 4.1. Number average molecular weight (M_n), glass transition temperature (T_g), water solubility (WS) and molar mass dispersity (ĐM) of fractionated VS-PTMC-MA samples.

M_{nNMR} (Da)	M_{nGPC} (Da)	T_g (°C)	WS (mg/mL)	$Đ_M$
500	600	-60	0.35 ± 0.07	1.1
850	950	-48	0.28 ± 0.05	1.2
1100	1300	-43	0.25 ± 0.05	1.3
1800	1950	-38	0.2 ± 0.03	1.5
2200	2400	-34	0.12 ± 0.04	1.2

4.3.2 Peptide-(PTMC-PEG-MA)$_2$ prepolymer preparation and characterization

Similarly, the reaction efficiency, chemical structure, and purity of the compounds after each reaction of peptide-(PTMC-PEG-MA)$_2$ synthesis were assessed using ^{1}H NMR spectroscopy. Figure 4.6 shows the ^{1}H NMR spectra the MA-PEG-OH initiator (Figure 4.6a), MA-PEG-PTMC-OH (Figure 4.6b), MA-PEG-PTMC-VS (Figure 4.6c) and peptide-(PETMC-PEG-MA)$_2$ (6d). The appearance of VS peaks at 6.25 ppm and 7 ppm after purification of the MA-PEG-PTMC-VS along with absence of the terminal hydroxyl proton peak at 4.5 ppm confirmed the divinyl sulfone addition to the hydroxyl end group (Figure 4.6c). In addition, no impurity peaks appeared in the spectrum after VS functionalization. The VS functionalization efficiency was greater than 90% as determined from a comparison of the integration of the VS peaks, at 6.25 and 7 ppm, to the integration of the methacrylate peaks and assuming that each MA-PEG-PTMC molecule had one methacrylate group. The dithiol MMP-sensitive peptide was successfully added to the VS functional group on the MA-PEG-PTMC-VS block copolymer. The absence of VS peaks at 6.25 and 7 ppm confirmed the Michael-type addition of the cysteine thiols on the peptide to the VS end group of the copolymer while the MA characteristic proton peaks at 5.6, 6.1 and 1.95 ppm remained, indicating that the methacrylate groups did not react (Figure 4.6d). The efficiency of the Michael-type addition reaction was more than 98%, as determined by measuring the integration of the peaks of the VS vinyl protons before and after the conjugation process. The water solubility of the resulting MA-PEG-PTMC block copolymer was 1.8 ± 0.5 mg/mL.

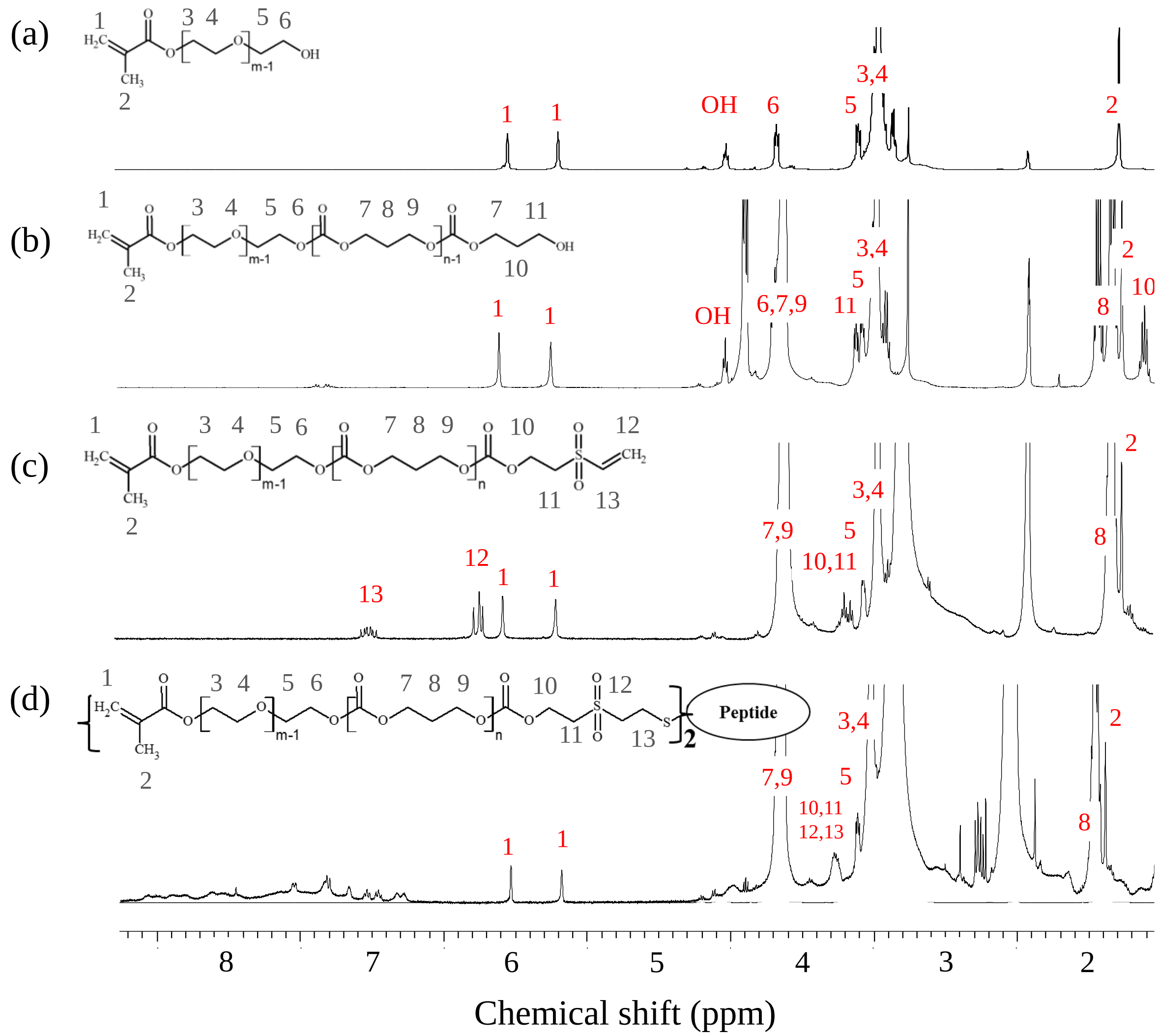

Figure 4.6. [1]H NMR spectra of (a) PEG-MA initiator, (b) MA-PEG-PTMC-OH, (c) MA-PEG-PTMC-VS, and (d) peptide-(PTMC-PEG-MA)$_2$. DMSO at 2.54 ppm and water at 3.33 ppm.

4.3.3 Network characterization

Sol content, water content and compressive modulus were measured for the networks prepared with peptide-(PTMC-MA)$_2$ having PTMC block molecular weights of 500, 1100 and 1800 Da and networks prepared with peptide-(PTMC-PEG-MA)$_2$ having a PTMC block molecular weight of 1200 Da (Figure 4.7). This range of distinct molecular weights was chosen to study the effect of the molecular weight of the PTMC block and the addition of PEG block to the backbone on degradation and mechanical characteristics of the networks. The sol content was below 10% for all the networks (Figure 4.7a). The water content decreased with increasing PTMC block molecular weight, from 26 ± 5% to 18 ± 4% for the peptide-(PTMC-MA)$_2$ networks made from 500 and 1800 Da PTMC blocks, respectively (Figure 4.7b). The addition of PEG block significantly increased the water content from 20 ± 2% in peptide-(PTMC-MA)$_2$ networks made from 1100 Da PTMc blocks to 72 ± 6% in peptide-(PTMC-PEG-MA)$_2$ networks containing roughly equivalent PTMC blocks of 1200 Da. The compressive moduli increased with increasing molecular weight of the PTMC block, ranging from 5 ± 1.5 to 11 ± 1.4 MPa for networks prepared with peptide-(PTMC-MA)$_2$ (Figure 4.7c). This value was significantly lower in the peptide-(PTMC-PEG-MA)$_2$ networks, at 1.2 ± 2 MPa, compared to that of networks prepared with peptide-(PTMC-MA)$_2$ containing a similar PTMC block molecular weight at 6.4 ± 0.7 MPa.

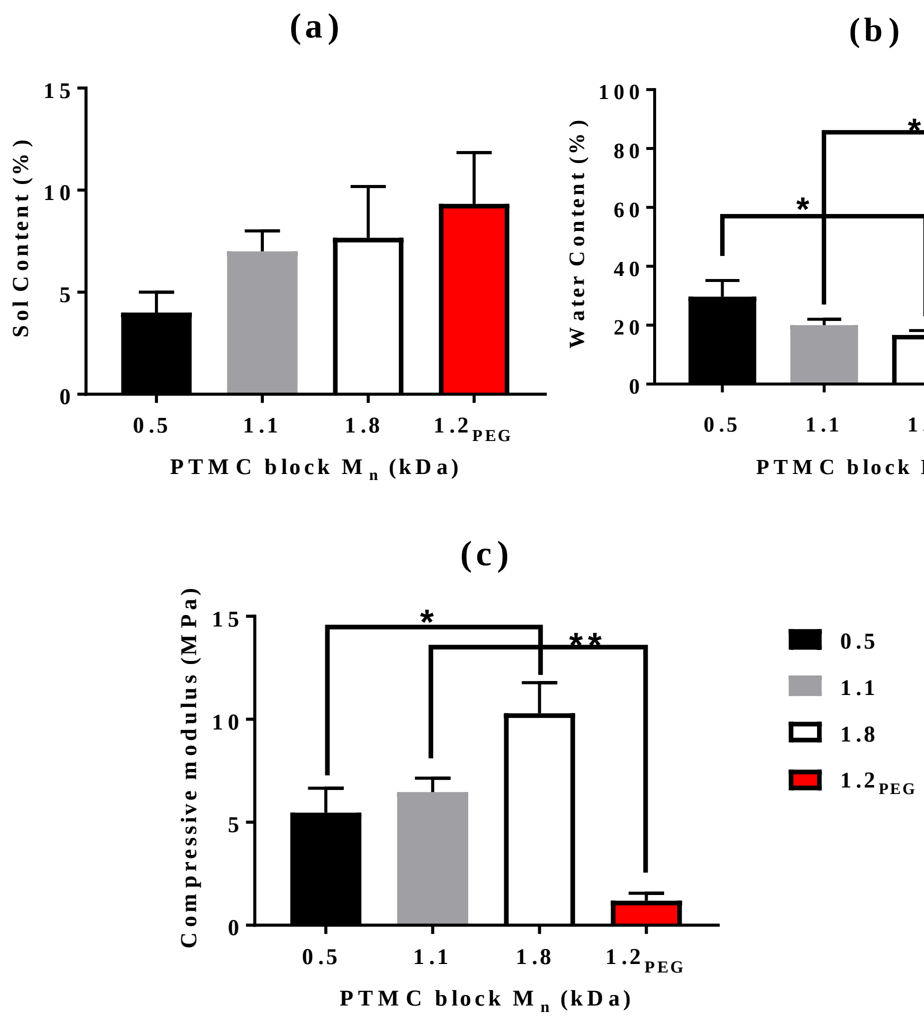

Figure 4.7. (a) Initial sol content, (b) water content and (c) compressive modulus of the networks prepared with peptide-(PTMC-MA)$_2$ having different PTMC block molecular weights and peptide-(PTM C-PEG-MA)$_2$ having PTMC block 1.2 kDa shown by 1.2PEG (n=5). Significant difference is shown by * for peptide-(PTMC-MA)$_2$ networks and ** for peptide-(PTMC-PEG-MA)$_2$ and peptide-(PTMC-MA)$_2$ networks prepared with similar PTMC block 1.1 kDa for $p < 0.05$.

4.3.4 *In vitro* Degradation

The mass loss, water content and compressive moduli of networks prepared from peptide-(PTMC-MA)$_2$ degraded in the presence of collagenase were measured over a period of 15 weeks (Figure 4.8). A control consisting of a network prepared with a triblock synthesized by reacting 1.1 kDa VS-PTMC-MA with 182 Da PEG-dithiol (PEG-(PTMC)$_2$) was incubated in collagenase-free medium to assess the hydrolytic stability of the thioether linkage. The mass loss versus time is shown in Figure 4.8a. The enzyme degradation was faster for elastomers possessing shorter PTMC block lengths, reaching 65 ± 6% mass loss in 15 weeks for the networks prepared with 0.5 kDa PTMC, compared to a mass loss of only 22 ± 1% for networks prepared with 1.8 kDa PTMC after the same time frame. The change in water content was highest for networks prepared with 0.5 kDa PTMC compared to all the other samples (Figure 4.8b). The water content was statistically constant over the first four weeks of degradation and it increased slightly with time as the degradation proceeded for all networks that contained a peptide block. The compressive modulus was constant over the first four weeks of degradation and then it decreased in all samples incubated in collagenase-containing medium over 15 weeks (Figure 4.8c). By contrast, the changes in modulus and water content were negligible in the control samples, confirming the hydrolytic stability of the thioether bond as well as the PTMC blocks.

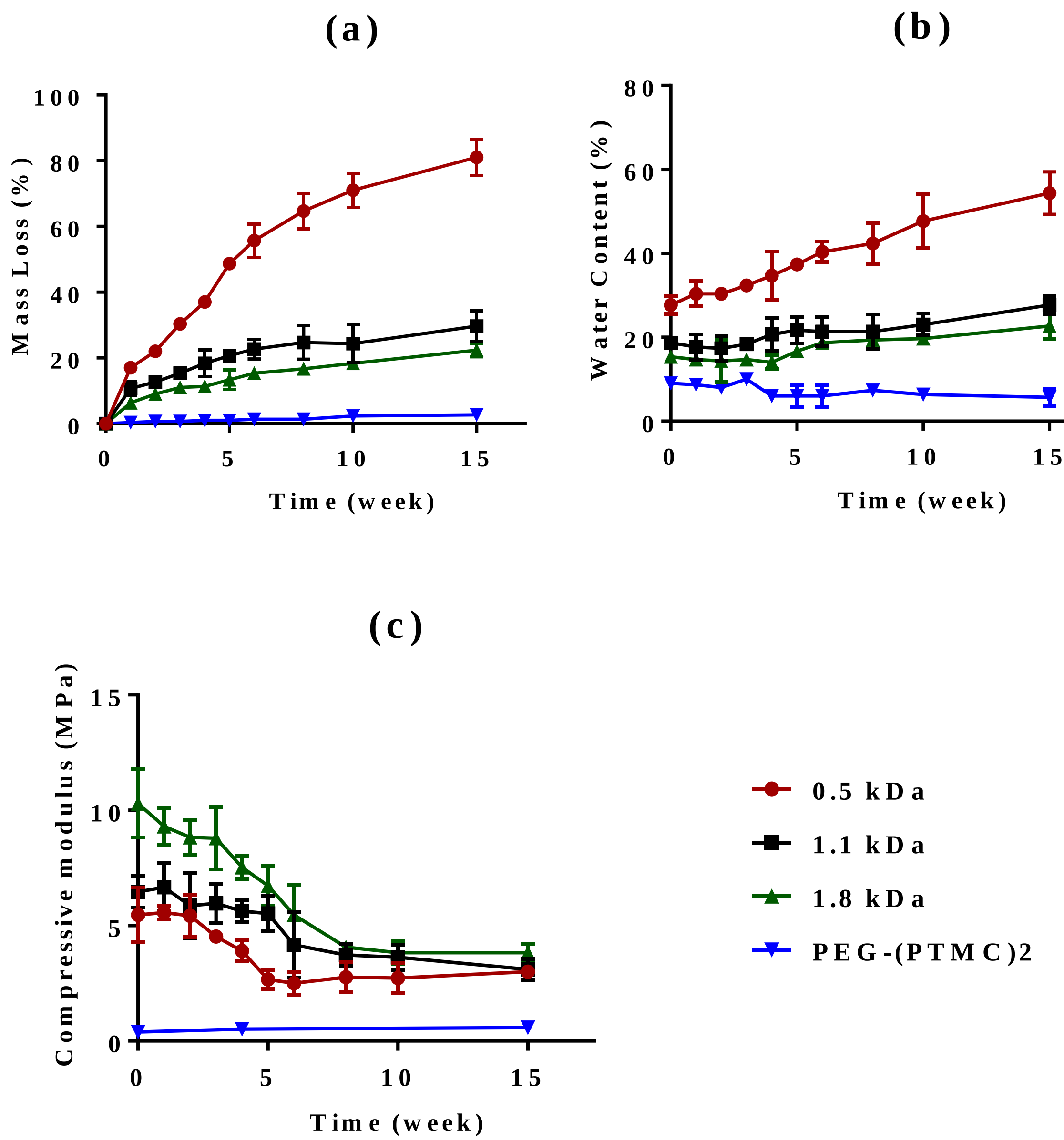

Figure 4.8. (a) Mass loss, (b) water content, and (c) compressive modulus of the networks prepared with peptide-(PTMC-MA)$_2$ having different PTMC block molecular weights (0.5, 1.1 and 1.8 kDa) in collagenase-containing media and PEG-(PTMC-MA)$_2$ sample in collagenase-free media (n=3).

Figure 4.9 shows the mass loss, change in water content, and compressive moduli of the hybrid networks prepared with peptide-(PTMC-PEG-MA)$_2$ (PEG block length of 500 Da, PTMC block length of 1.2 kDa) prepolymer during 28 days of incubation in a collagenase-containing medium. Once again, the PEG-(PTMC-PEG-MA)$_2$ control networks were incubated in a collagenase-free media to study the hydrolytic stability of the PEG-PTMC backbone and the thio-ether linkage. For the networks in a collagenase-containing medium a mass loss of 74 ± 2 %, a water content change from 69 ± 5 % to 89 ± 1 %, and a compressive modulus change from 1.1 ± 0.6 MPa to 0.2 ± 0.1 MPa were observed. Whereas, for the control sample, the mass loss, the water content change, and the compressive modulus change were negligible.

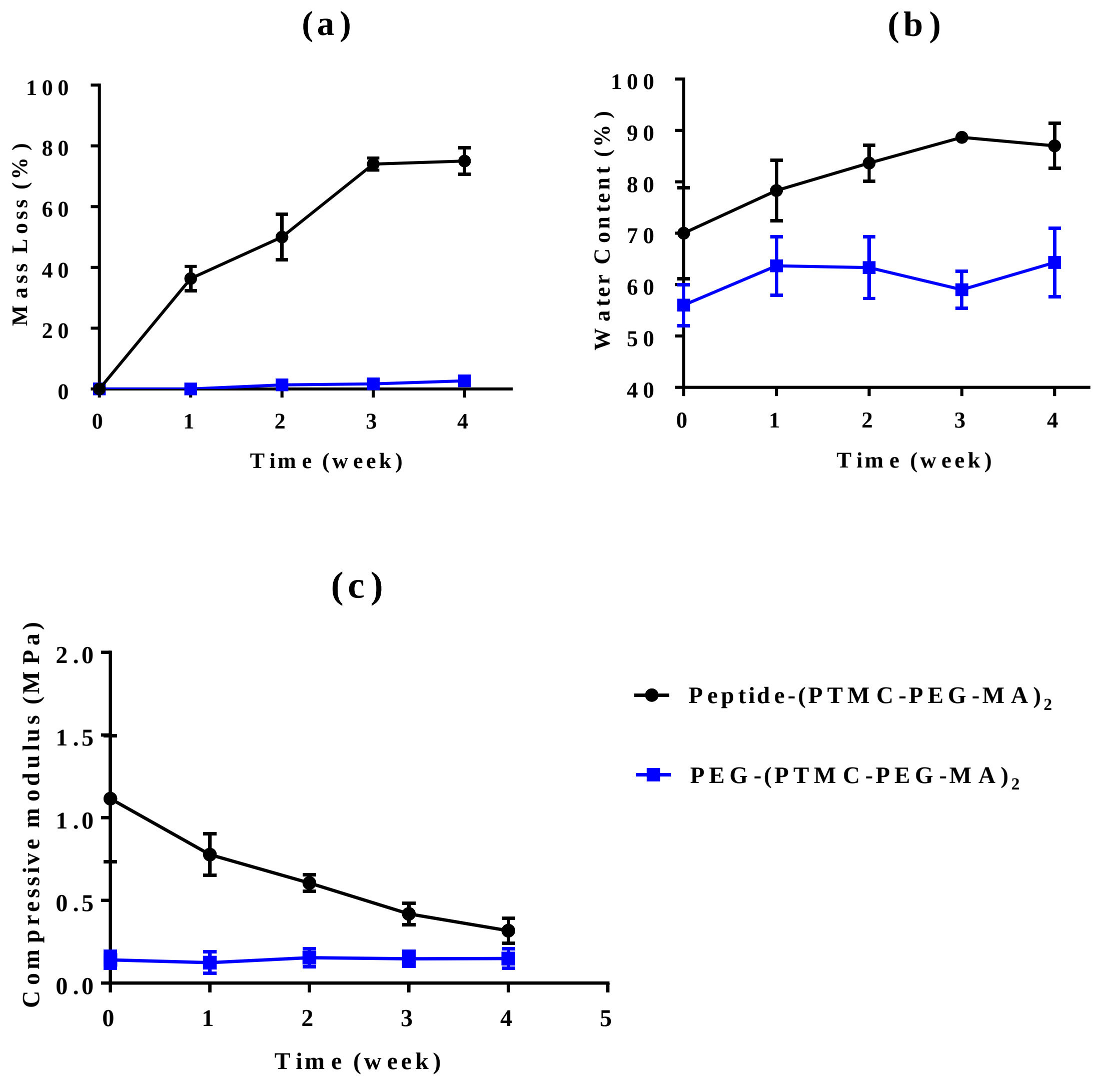

Figure 4.9. (a) Mass loss, and change in (b) water content and (c) compressive modulus of the networks prepared with peptide-(PTMC-PEG-MA)$_2$ in collagenase-containing media and the control networks prepared with PEG-(PTMC-PEG-MA)$_2$ in collagenase-free media.

A comparison of the degradation of the networks prepared with peptide-(PTMC-MA)$_2$, PTMC1.1 kDa, and peptide-(PTMC-PEG-MA)$_2$, PTMC 1.2 kDa, was done by comparing the mass loss, water content and compressive modulus changes over 28 days (Figures 4.10a to 4.10c). The mass loss of the networks prepared with peptide-(PTMC-PEG-MA)$_2$ was 74 ± 2% while this value for the networks prepared with peptide-(PTMC-MA)$_2$ with a similar PTMC block length was 18 ± 4%. The water content of the peptide-(PTMC-PEG-MA)$_2$ networks increased from 69 ± 5 % to 89 ± 1 %, while the water content of the peptide-(PTMC-MA)$_2$ networks was 19 ± 1% to 21 ± 2% with no significant change. Similarly, the compressive modulus of the peptide-(PTMC-PEG-MA)$_2$ networks decreased from 1.1 ± 0.6 MPa to 0.2 ± 0.1 MPa, while this value stayed constant from 6.4 ± 0.7 MPa to 5.6 ± 0.4 MPa with no significant change.

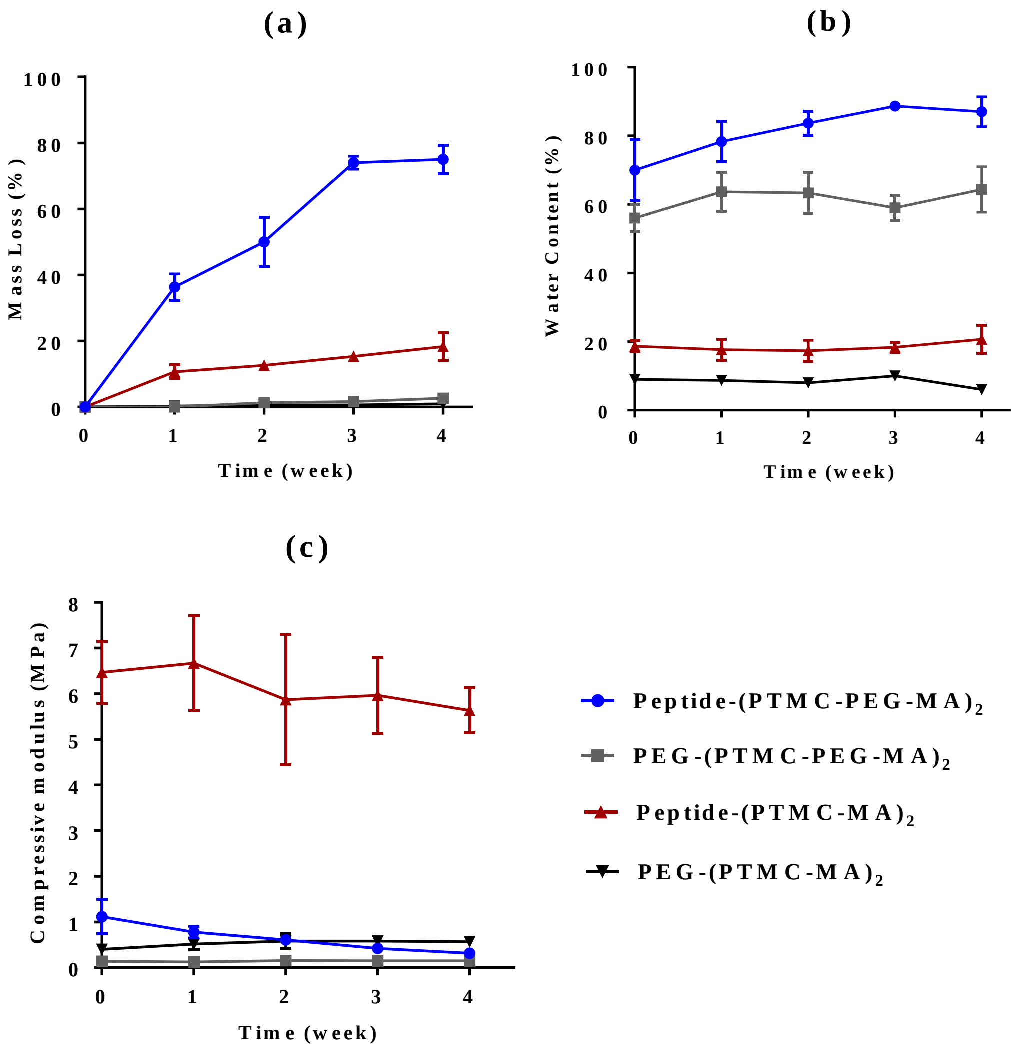

Figure 4.10. A comparison of the (a) mass loss, (b) water content, and (c) compressive modulus of the networks prepared with peptide-(PTMC-MA)$_2$ and peptide-(PTMC-PEG-MA)$_2$ along with the control samples of PEG-(PTMC-MA)$_2$ and PEG-(PTMC-PEG-MA)$_2$. The PTMC block lengths in these networks are approximately equal, thus showing the influence of the PEG on the degradation of the networks.

4.4 Discussion

A variety of elastomeric biomaterials have been developed over the past two decades to replace or assist in the function of soft tissues [148], [149]. However, a major challenge remaining to be addressed in such materials is the mechanical incompatibility with the target tissue [150]. Herein, we report on the design and characterization of a biohybrid network that can overcome limitations on degradability and stiffness of such biomaterials. The reported biohybrid network can provide an appropriate compressive modulus as well as a controllable degradation rate for soft connective tissue engineering applications. The main purpose of this study was to design a biohybrid material that can mimic the compressive modulus of the soft tissues while being solely enzyme degradable.

Biohybrid networks containing MMP-sensitive peptides and PTMC blocks (peptide-(PTMC-MA)$_2$) with three different PTMC block molecular weights (500, 1100, 1800 Da) were used to study the effect of PTMC molecular weight on scaffold characteristics and degradation rate. VS-PTMC-MA was successfully synthesized and fractionated to different molecular weights with low dispersity. The prepolymers were all amorphous with low T_g values (-60 to -30° C) that increased with increasing PTMC block length, in agreement with predictions of the Fox-Flory equation [142][151]. The low T_g is significant for potential tissue engineering applications as it provides for a rubbery nature of networks formed from these prepolymers.

The characterization of the different fractions confirmed previous results that low molecular weight PTMC possesses measurable water solubility and that its water solubility decreases with increasing molecular weight (Table 4.1), in accordance with the prediction of Flory-Huggins theory [110], [152], [153]. Addition of a 0.5 kDa PEG block to a 1.2 kDa PTMC block increased the water solubility of the biohybrid prepolymer and as a result the water content of the resulting network was significantly increased [154]. The water solubility of the 1.1 kDa VS-PTMC-MA was 0.25 ± 0.05 mg/mL while for the VS-PTMC-PEG-MA containing a similar PTMC block molecular weight of 1.2 kDa, this value was 1.8 ± 0.5 mg/mL. PEG addition changed the hydrophilicity of the biohybrid prepolymer and increased the water solubility [154]. Water solubility of the PTMC molecules is important for the intended application to ensure that the degradation products can readily dissolve into the degradation medium.

Triblock copolymers comprised of peptide-(PTMC-MA)$_2$ were synthesized by conjugating an MMP-sensitive peptide to VS-PTMC-MA via the α-VS terminus. Similarly, the triblock copolymer peptide-(PTMC-PEG-MA)$_2$ was synthesized by conjugation of MA-PEG-PTMC-VS with the peptide. The characterization of the resulting peptide-(PTMC-MA)$_2$ networks showed that the sol contents were between 5% and 10% (Figure 4.5a). Low sol contents confirmed the high degree conversion of the methacrylate during the crosslinking reaction. The water content of the peptide-(PTMC-MA)$_2$ networks showed that the samples prepared with PTMC 500 Da had a water content of 30% ± 5% which was significantly higher than the water contents of the networks prepared with PTMC 1100 Da and 1800 Da (Figure 4.5b). The water uptake of the network prepared with shorter PTMC blocks was higher due to the higher water solubility of the shorter PTMC chains as well as the higher weight ratio of the hydrophilic peptide to PTMC in these networks. The higher water uptake resulted in a lower compressive modulus in the networks of peptide-(PTMC-MA)$_2$ prepared using shorter PTMC blocks [155]. These data demonstrate that the mechanical and physical properties of the final biohybrid material can be tuned by the weight ratio of the PTMC block.

The higher *in vitro* mass loss of the networks prepared with shorter PTMC blocks was the result of the higher water solubility of the degradation products and the overall higher water uptake of the networks. The higher water uptake caused a greater accessibility of the collagenase to the peptide regions and their cleavable sites at the surface region of the networks. For all three groups of biohybrid networks the water content, as well as the compressive moduli, are statistically constant over 4 first weeks of degradation. This phenomenon confirmed the surface erosion of the networks that is a result of the low water content and limited accessibility of the cleaving enzymes. However, the water content started to increase after 4 weeks of degradation and subsequently the compressive moduli of the different networks decreased (Figures 4.6b and c). A schematic of the surface erosion process is shown in Figure 4.11. The reaction zone near the sample surface in this schematic is the volume accessible to the collagenase [156]. As degradation proceeds, the reaction zone moves toward the middle of the sample. After four weeks of degradation, the volume of the reaction zone was big enough in relation to the volume of non-degraded network that it could affect the network characteristics. Consequently, the water content increased and the modulus decreased after this time point. If mechanical support for a longer time period is needed for the target application a PTMC block with higher molecular weight could be chosen to make the peptide-(PTMC-MA)$_2$ networks. Using PTMC with higher molecular weights would minimize scaffold swelling due to the lower water solubility of the PTMC blocks as well as reduce the number of available peptide groups accessible for enzyme attack.

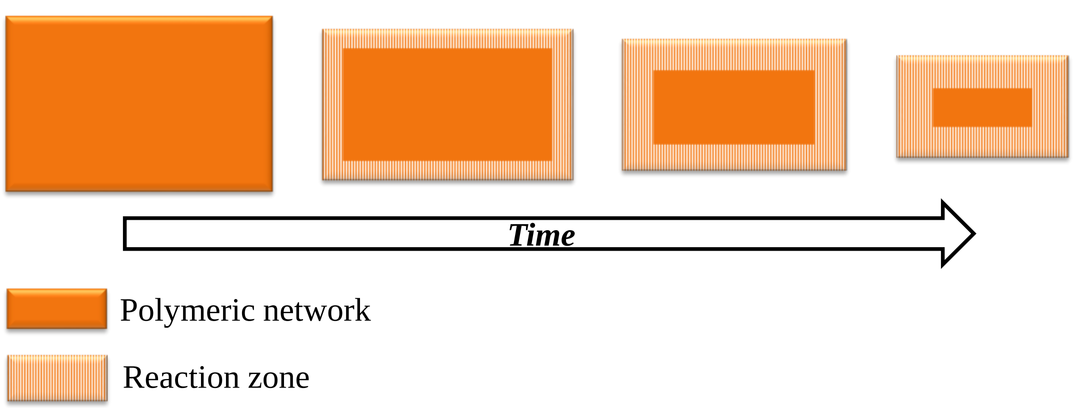

Figure 4.11. Schematic of surface erosion.

The control samples using the networks prepared with 1100 Da PTMC and PEG-dithiol (182 Da) showed negligible mass loss and compressive modulus change, and no change in water content in the absence of collagenase. The fact that degradation of the networks prepared with the peptide-(PTMC-MA)$_2$ was only observed in the presence of collagenase suggests that hydrolysis of PTMC or the thio-ether sulfone linkage did not affect the degradation rate. This conclusion suggests that the peptide-(PTMC-MA)$_2$ networks would maintain their mechanical properties in the absence of an MMP enzyme. Nevertheless, over longer degradation time frames (e.g. 40 weeks) the possibility of hydrolysis of the PTMC backbone must be considered [110]. In addition, other degradation mechanisms can be functional under physiological conditions that may catalyze the hydrolytic degradation of the PTMC backbone including the effect of different enzymes or reactive oxygen species [110].

The addition of the PEG block to the PTMC block resulted in a higher water uptake, lower compressive modulus, and a higher mass loss of the networks as compared to the networks prepared with a peptide-(PTMC-MA)$_2$ prepolymer of a similar PTMC block length. PEG addition to the PTMC backbone not only increased the water uptake of the networks resulting in quicker access of the water soluble enzymes to the peptide cleavable sites at the surface of the networks but also increased the water solubility of the degradation products. Both phenomena resulted in a faster mass loss of the network in the presence of collagenase.

The compressive moduli of all the networks were between 1.1 MPa to 10 MPa, which are comparable to the moduli of a range of load bearing cartilaginous tissues such as human knee meniscus (4.2-11.6 MPa), esophagus (1.2 MPa) and bronchioles (0.25-1.96 MPa) [157]–[159]. These results demonstrate that by choosing an appropriate molecular weight of the PTMC block or through the addition of a PEG block, the compressive modulus of the resulting network can be effectively tuned to that of a target soft connective tissue for tissue engineering applications.

The biohybrid polymeric network proposed and investigated in this study has the potential to be modified in different ways to adjust the compressive modulus and the degradation rate in order to fulfil a range of tissue engineering applications. The PTMC molecular weight affected both mechanical toughness and the degradation rate of the final component. The proposed peptide sequence can also be exchanged with another sequence that is susceptible to other groups of enzymes.

4.5 Conclusion

A hybrid network was developed in this study that combines the advantages of an enzyme-degradable peptide and rubbery PTMC. PTMC with three different molecular weights (500, 1100 and 1800 Da) were successfully synthesized and conjugated to an MMP-sensitive peptide to form the biohybrid prepolymer peptide-(PTMC-MA)$_2$. Similarly, PEG-PTMC 1700 Da was successfully synthesized and added to MMP-sensitive peptide to form peptide-(PTMC-PEG-MA)$_2$ prepolymer. The resulting prepolymers were photo-cured to form crosslinked networks and then characterized in order to study the effect of PTMC molecular weight on final degradation rate and mechanical deterioration of the network. It was shown that the dominant mechanism of degradation was the enzyme-cleavage of MMP-sensitive peptide segments. No hydrolysis of the PTMC backbone and thio-ether linkage was observed. It was also shown that the degradation rate and the mechanical deterioration rate are faster for the elastomers prepared by PTMC with lower molecular weight. The addition of PEG to the PTMC backbone resulted in an increased water content and concomitant reduction in modulus and increase in degradation rate. This new material is promising for soft connective tissue engineering applications due to the similar mechanical aspects to the native ECM and a tunable degradation profile.

Chapter 5

In vivo degradation and tissue response to the enzyme-degradable biohybrid poly(trimethylene carbonate) (PTMC)-based networks

5.1 Abstract

In the previous chapter we reported on the development of matrix metalloproteinase (MMP)-degradable poly(trimethylene carbonate) (PTMC)-based hybrid networks. In this study the *in vivo* degradation and tissue response following implantation of the networks were assessed in a male Wistar rat model. Two formulations, possessing either PTMC or poly(ethylene glycol) (PEG)-PTMC conjugated to a MMP-sensitive peptide, were subcutaneously implanted in rats. Total mass loss of 72 ± 3% and 65 ± 6% were measured over 6 weeks of implantation for the networks prepared with peptide-$(PTMC\text{-}MA)_2$ and peptide-$(PTMC\text{-}PEG\text{-}MA)_2$ respectively; the mass loss of the peptide-free networks was negligible over this period of time. The compressive modulus and glass transition temperature measurements indicated that the implants underwent surface erosion, in agreement with our previous *in vitro* findings. Immunohistochemistry analysis of the tissue surrounding the implants confirmed a moderate tissue response comparable to that observed towards a Vicryl™ suture, suggesting that these new materials can be considered biocompatible.

5.2 Introduction

The successful development of biomaterials for tissue engineering and regenerative medicine will require a combination of different characteristics and functionalities in order to mimic the complexity of the native structures. The implanted biomaterial must have enough mechanical integrity to function from implantation time to completion of the regeneration process. In addition, it needs to be degradable via a cell-dependent mechanism to mimic the ECM remodeling process, and thereby enable migration and proliferation of target cells in the implanted material. Enzyme-degradable biohybrid materials may be able to provide these necessary features [35], [36], [137], [160]. These materials combine the mechanical stiffness of the synthetic polymers, their ease of synthesis with relatively low cost, reproducibility and well-controlled mechanical properties, with the biocompatibility and the enzyme-degradability of components derived from the extracellular matrix of native tissues.

A number of enzyme-degradable biohybrid networks have been developed over the last decade, which can mimic the mechanical features of soft connective tissues [74], [88], [94], [107], [116], [161]–[163]. To date, none of the tissue engineering approaches in such applications have been able to provide the mechanical, degradation, and biological aspects of the network simultaneously. Most of the developed biohybrid polymeric materials are hydrogels with low stiffness, which are not appropriate for many load-bearing soft connective tissue engineering applications. In addition, the synthesis strategies of these biohybrid materials are mostly based on mixing the separate functionalized polymer and peptide components. Therefore, a clinical strategy using a simplified one-step crosslinking process having both components in a single prepolymer with tunable mechanical properties for soft connective tissue repair is needed.

We have recently reported on the development and *in vitro* characterization of enzyme-degradable poly(trimethylene carbonate) (PTMC)-based networks. α-Vinyl sulfone (VS), ω-methacrylate (MA) heterobifunctional PTMC and PEG-*b*-PTMC were prepared and conjugated to a di-cysteine containing matrix metalloproteinase (MMP)-sensitive peptide to form curable triblock prepolymers. These prepolymers were photo-cured to form enzyme-degradable networks. Surface erosion via cleavage of MMP-sensitive peptides was the dominant degradation mechanism of these networks *in vitro*. Faster degradation was observed for networks prepared with shorter PTMC block lengths while the addition of PEG increased the water content, reduced the modulus, and increased the degradation rate of the biohybrid network.

As a natural progression in the development of the polymeric biomaterials, it is necessary to investigate the nature of the tissue response following their implantation and their *in vivo* degradation rate. It is also important to determine factors influencing the degradation rate of the biomaterials *in vivo*. Moreover, a comparison between *in vitro* and *in vivo* degradation would be beneficial in further development of these materials.

The overall goal of the current study was to investigate the tissue response and *in vivo* degradation of the previously developed polymers. Herein, the inflammatory response upon subcutaneous implantation of the biohybrid networks in a rat model was studied compared to that of the commercially available Vicryl™ suture.

5.3 Materials and methods

5.3.1 Materials

1,3-Trimethylene carbonate (TMC) was obtained from LEAPChem, Zhejiang, China. Stannous 2-ethylhexanoate was obtained from Alfa Aesar, Tewksbury, USA. HPLC-grade toluene, hexylamine, dimethyl sulfoxide-d6, divinyl sulfone, methacryloyl chloride, 2,2-dimethoxy-2-phenylacetophenone (DMPA), Irgacure 2959 photo initiator, 4-(2-hydroxyethyl)-1-piperazineethanesulfonic acid (HEPES), sodium azide, Tween 20, poly(ethylene glycol) (PEG) dithiol (182 Da), PEG methacrylate (500 Da), and 4-dimethylaminopyridine (DMAP) were purchased from Sigma-Aldrich, Mississauga, Ontario, Canada. Dichloromethane, ethyl acetate, dimethylformamide, sodium chloride, methanol, ethanol, xylene, 2-mercaptoethanol, trimethylamine (TEA), diethyl ether, Permount resin, phosphate buffered saline (PBS), Tris-buffered saline (TBS) and hydrochloric acid were obtained from Fisher Scientific, Mississauga, Ontario, Canada. Collagenase type II from *Clostridium hyistolyticum* was purchased from MP Biomedicals LLC, Santa Ana, California, USA. The collagenase-sensitive peptide (GCRDGPQGIWGQDRCG) was custom synthesized by CanPeptide Inc., Pointe-Claire, Quebec, Canada. Mouse anti-rat (ED1) primary antibody for CD68 staining, goat anti-mouse Alexia 488 and fluoroshield mounting medium with 4',6-diamidino-2-phenylindole (DAPI) were purchased from Abcam Inc., Toronto, Ontario. A Masson's trichrome kit was purchased from Polysciences Inc. Warrington, Pennsylvania. Coated antibacterial Vicryl^{TM} suture, polyglactin 910, was purchased from Ethicon, New Jersey, USA. Dialysis membranes with a molecular weight cut off of 100-500 Da were purchased from Biotech CE Tubing, Wilmington, Delaware, USA. Deionized water was obtained from a Millipore Milli-Q Plus ultrapure water system. Dichloromethane was dried over molecular sieves for 72 h prior to use. All other reagents were used as received.

5.3.2 Network preparation

Heterobifunctional PTMC and PEG-PTMC were synthesised, fractionated, and characterized as described previously in Chapter 4. Briefly, PTMC was synthesized by a stannous 2-ethylhexanoate-catalyzed ring opening melt polymerization of TMC in the presence of 2-((2-vinylsulfonyl ethyl)thio)ethanol as initiator and then methacrylated by reaction of methacryloyl chloride with the terminal hydroxyl group. Methacrylate terminated poly(ethylene glycol)-*b*-poly(trimethylene carbonate) (MA-PEG-PTMC-OH) was first synthesised via a stannous(II) ethylhexanoate-catalyzed ring opening melt polymerization of 1,3-trimethylene carbonate (TMC) in the presence of PEG-methacrylate (500 Da) as the initiator and then it was functionalized by reaction of divinyl sulfone with the terminal hydroxyl group. Size exclusion chromatography was used to purify and fractionate both formulations. The target molecular weight of the PTMC block for each prepolymer was 1100 Da. The chemical structure of the VS-PTMC-MA and VS-PTMC-PEG-MA are illustrated in Figure 5.1a and Figure 5.1b, respectively.

(a)

(b)

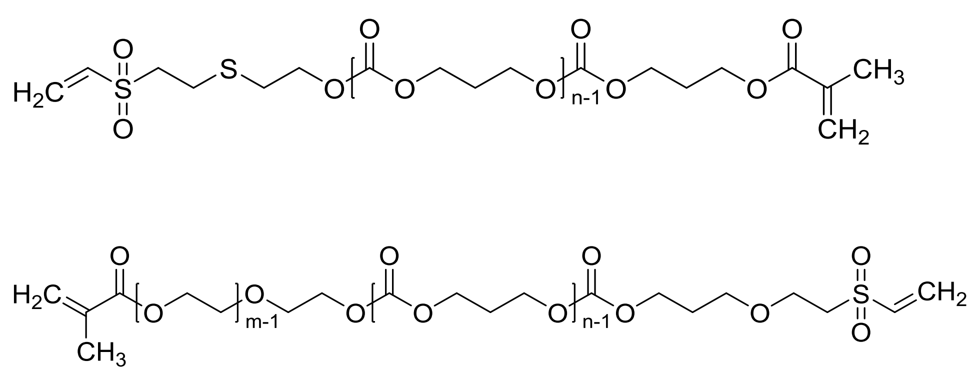

Figure 5.1. Chemical structure of the heterobifunctional (a) VS-PTMC-MA and (b) VS-PTMC-PEG-MA

The resulting heterobifunctional copolymers were separately conjugated to a half equivalent of the di-cysteine, MMP-sensitive, GCRDGPQGIWGQDRCG peptide to form the bio-hybrid prepolymers peptide-$(PTMC\text{-}MA)_2$ and peptide-$(PTMC\text{-}PEG\text{-}MA)_2$. ^{1}H NMR spectroscopy was performed to confirm the structure and relative purity of all products after each step of the synthesis process. These prepolymers were then photo-crosslinked using the photo-initiator, Irgacure 2959, to form biohybrid networks. As controls, networks were also prepared with PEG-dithiol instead of the MMP-sensitive peptide.

5.3.3 *In vivo* degradation

The *in vivo* degradation rate and host response to the networks were assessed in a subcutaneous implant model in male Wistar rats [164]–[166]. The animal study was performed in accordance with the guidelines of the Canadian Council on Animal Care code of ethics governing animal experimentation (protocol #Amsden 2007-043-R1). Anesthetization was performed with 2% isoflurane in oxygen a flow rate of 0.2 mL/min. Following anesthetization, the dorsal area of the rats was shaved, disinfected with Hibitane and three samples of UV sterilized networks prepared from the peptide-$(PTMC\text{-}MA)_2$ prepolymer, the peptide-$(PTMC\text{-}PEG\text{-}MA)_2$ prepolymer, enzyme resistant control samples prepared using PEG-dithiol (182 Da) conjugated to VS-PTMC-MA (PEG-$(PTMC\text{-}MA)_2$), and tissue response control samples of Vicryl™ suture, were implanted subcutaneously (n = 2 per sample, per time point for 6 time points). The implantation location of the samples is illustrated in Figure 5.2.

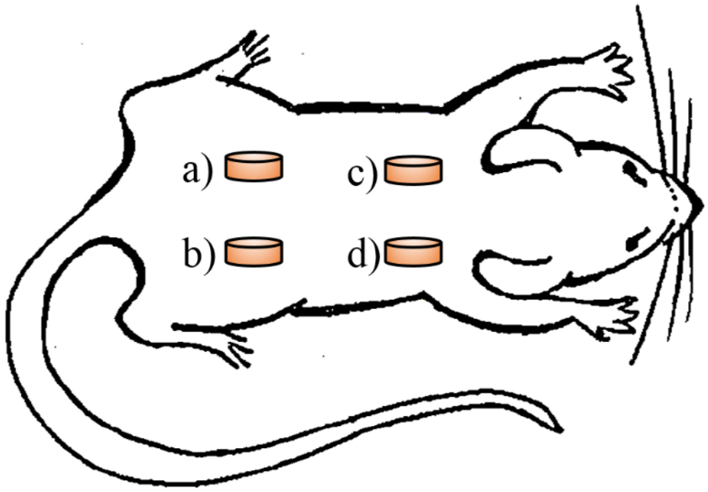

Figure 5.2. Location of samples implantation; a) peptide-(PTMC-MA)$_2$ network, b) peptide-(PTMC-PEG-MA)$_2$ network, c) Vicryl^{TM} suture, and d) PEG-(PTMC-MA)$_2$ network

At 1, 2, 3, 4, 5 and 6 weeks post-implantation, two rats at each time point were humanely euthanized by 2% isoflurane in oxygen followed by intraperitoneal injection of Somnotol (65 mg/kg) and the implant areas were analyzed macroscopically and microscopically. The skin was shaved, all the implants were excised and the surrounding tissue was removed and fixed in 4% paraformaldehyde in PBS overnight, then transferred to 70% ethanol and stored at 4 °C until being processed for histological analysis. Following separation of the polymer networks from the tissue, the mass loss, sol content, and compressive modulus were assessed. The mass loss was measured by comparing the dry mass of the networks before and after implantation. The compressive modulus of each rehydrated polymer network was measured by unconfined indentation as described above. The sol content of each network was measured by soaking them in dimethyl sulfoxide (DMSO) overnight at room temperature and comparing the dry weight before and after sol removal. The glass transition temperature (T_g) of the networks were measured using a cooling-heating-cooling-heating cycle as was previously described in Chapter 4 and the

T_g values were compared to those from the *in vitro* study. The harvested tissues were dehydrated in graded ethanol and xylene, embedded in paraffin, and sectioned into 10 μm thick sections.

5.3.4 Tissue response

5.3.4.1 Masson's Trichrome

Masson's trichrome staining was used to assess the host tissue reaction to the implanted polymeric networks. The sections were deparaffinised by xylene and graded ethanol then cleared in PBS, followed by a Masson's trichrome staining procedure, according to the manufacturer`s instruction, then dehydrated and cover-slipped with Permount mounting media. The stained sections were observed and photographed using a Zeiss optical microscope with Zeiss Axio Vision software (version 4.7.1.0). The thickness of the fibrous layer around the implant was measured using Image J. For these measurements, the fibrous capsule was considered the collagen region that was stained in blue by Masson's trichrome [167]. Newly deposited collagen was differentiated from pre-existing collagen by its striated appearance.

5.3.4.2 CD68 staining

The total macrophage response to the implant was assessed by using a CD-68 antibody stain. Following deparaffinization and rehydration the sections were antigen retrieved in citrate buffer, pH 6, at 60 °C overnight. Tris-buffered saline (TBS) containing 0.025% Tween-20 was used to permeabilize the tissue sections. The sections were blocked by incubation in 5000 μg/mL BSA in TBS for 30 min at room temperature. The tissues were then incubated with the primary antibody mouse anti-rat CD68 diluted in 1% BSA at a concentration of 2.5 μg/mL at 4°C overnight. The secondary antibody goat anti-mouse Alexafluor 488 was diluted to 2 μg/mL in TBS and then used to incubate the sections for one hour at room temperature. The stained tissues were then rinsed by

TBS mounted in DAPI mounting medium. The negative control was prepared on each microscope slide by applying TBS without the primary antibody. The sections were photographed using a Zeiss AxioImager M1 fluorescent microscope with ZEN Blue software. The macrophage density in the fibrous layer was measured by counting the number of green-stained cells co-stained with DAPI per mm^2.

5.3.5 Statistical analysis

All data is expressed as the mean ± the standard deviation about the mean. One way analysis of variance (ANOVA) with a Bonferroni post hoc test (Microsoft Excel) was performed where applicable. A paired t-test was conducted between samples for long-term studies. A p value of less than 0.05 was used to determine significant differences between population means.

5.4 Results

5.4.1 Polymer characterization

A target average PTMC block length of 8 repeating TMC units was chosen based on the *in vitro* results to obtain a prolonged degradation time *in vivo*. This PTMC block length was achieved for the VS-PTMC-MA, while an average block length of 9 TMC units was obtained for the VS-PTMC-PEG-MA. The two PTMC block lengths were considered approximately equivalent.

5.4.2 *In vivo* degradation

5.4.2.1 Macroscopic examination of tissue response

Following implantation of the samples, all the rats gained weight and were active and healthy prior to implant removal. Figure 5.3 shows the macroscopic appearance of the implants and the tissue around them after 6 weeks of implantation. The physical appearance of the PEG-(PTMC-MA)$_2$ control sample after 6 weeks of implantation (Figure 5.3 and Figure A.12a) was similar to the initially prepared samples, but with a slight color tint to darker yellow. The inflammation of the tissue surrounding the peptide-(PTMC-PEG-MA)$_2$ and peptide-(PTMC-MA)$_2$ networks was visually similar to that around the Vicryl^{TM} suture (Figure 5.3 and figure A.12b-d). Moreover, the peptide-(PTMC-MA)$_2$ networks decreased in size but remained a single solid piece. In contrast, the peptide-(PTMC-PEG-MA)$_2$ networks had broken into smaller pieces over 6 weeks of degradation.

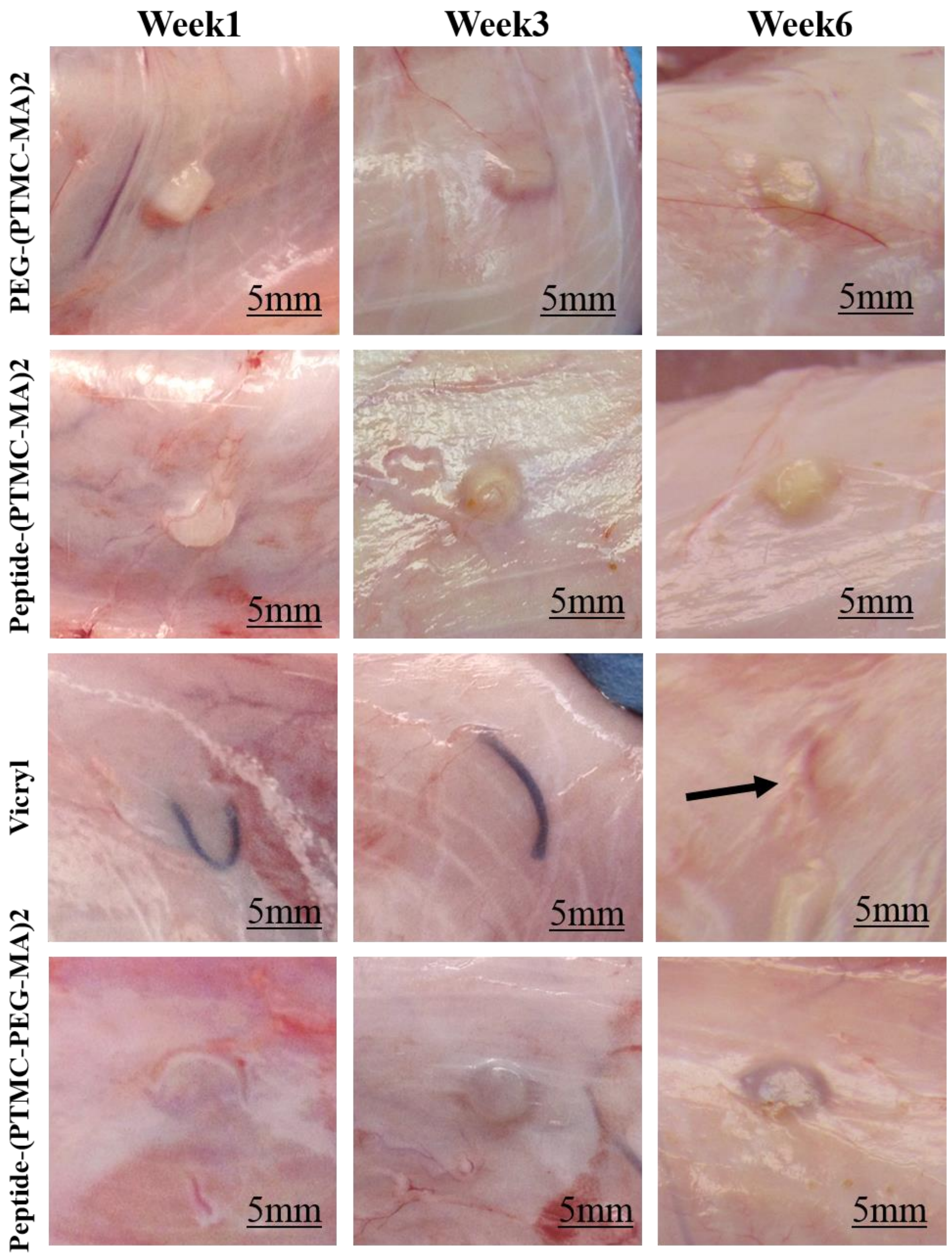

Figure 5.3. Physical appearance of the implants and tissue from PEG-(PTMC-MA)$_2$, peptide-(PTMC-PEG-MA)$_2$, peptide-(PTMC-MA)$_2$ and Vicryl^{TM} suture, after 1, 3, and 6 weeks of implantation. The implant area is shown by the arrow at week 6 for the Vicryl^{TM} suture.

5.4.2.2 Network property changes with time

Figure 5.4 shows the mass loss, sol content and the compressive modulus of three groups of samples over 6 weeks of implantation. The peptide-(PTMC-MA)$_2$ samples initially steadily lost mass until week 4. After this time, the mass loss plateaued at 68 ± 2%. The peptide-(PTMC-PEG-MA)$_2$ samples lost mass at an equivalent rate as the peptide-(PTMC-MA)$_2$ samples until week 3 then, mass loss remained at 40 ± 6% for two weeks, then increased to 55 ± 10 % by week 6. In contrast, the PEG-(PTMC-MA)$_2$ control implants showed negligible mass loss throughout the entire time frame (Figure 5.4a). The sol content increased over the implantation time for all groups of samples. However, the change in the sol content was highest for the peptide-(PTMC-PEG-MA)$_2$ samples, 28 ± 7%, moderate for the peptide-(PTMC-MA)$_2$ samples, 12 ± 3%, and low for the PEG-(PTMC-MA)$_2$ control samples, 6 ± 2% (Figure 5.4b). The compressive modulus of the peptide-(PTMC-MA)$_2$ implants also decreased steadily over time from an initial value of 7.1 ± 0.1 MPa to 1 ± 0.1 MPa. Similarly, the compressive modulus of the peptide-(PTMC-PEG-MA)$_2$ implants decreased steadily over time from an individual value of 1.5 ± 0.4 MPa to 0.35 ± 0.05 MPa. In contrast, the modulus of the PEG-(PTMC-MA)$_2$ samples remained constant (Figure 5.4c). No significant difference in compressive moduli was observed for thre peptide-(PTMC-MA)$_2$ and peptide-(PTMC-PEG-MA)$_2$ implants over two weeks post implantation. It was not possible to measure the compressive modulus of the peptide-containing networks at week 6 due to size limitations.

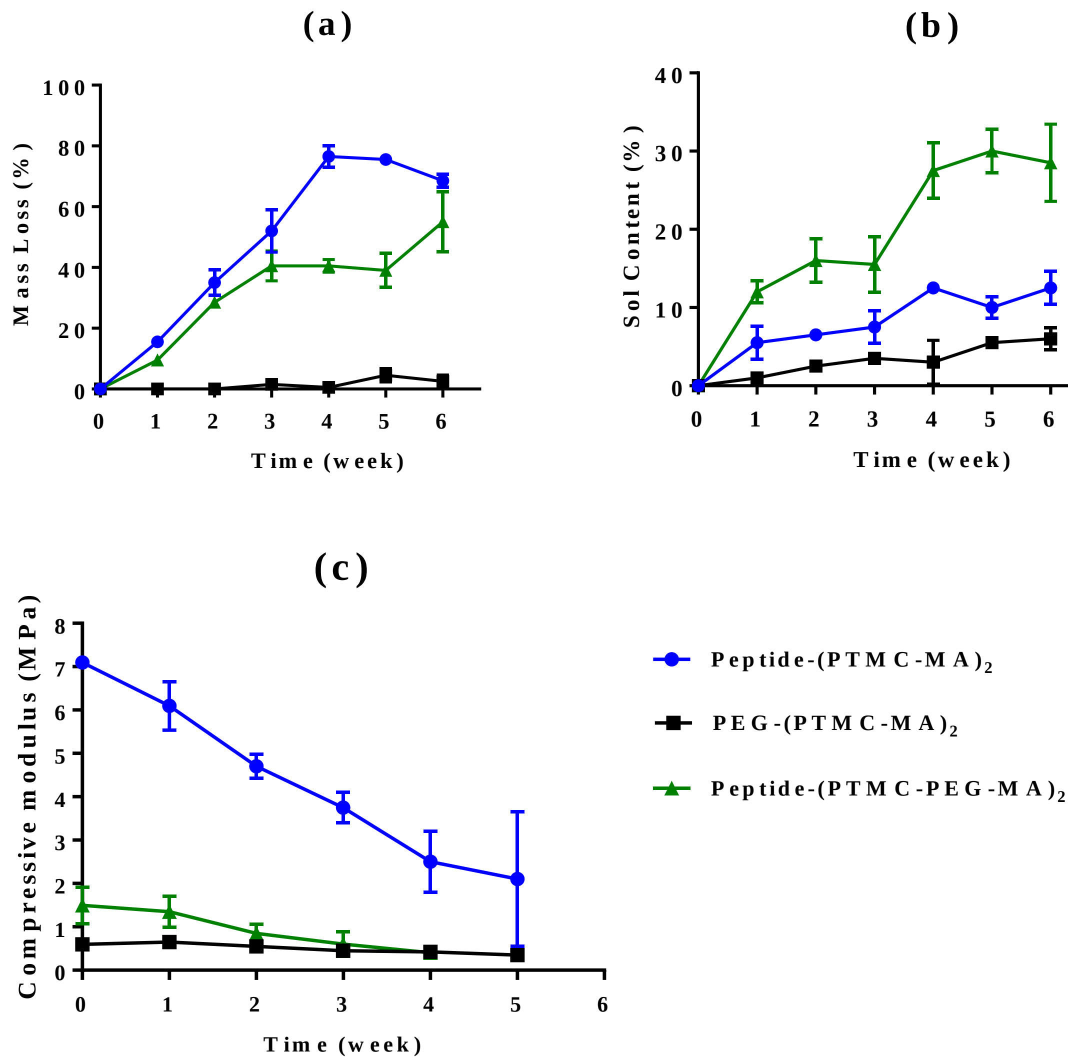

Figure 5.4. (a) Mass loss, (b) sol content, and (c) compressive moduli of the peptide-(PTMC-MA)$_2$, peptide-(PTMC-PEG-MA)$_2$, and PEG-(PTMC-MA)$_2$ implants over 6 weeks (n=2).

Figure 5.5 shows the thermographs of the peptide-(PTMC-MA)$_2$ and peptide-(PTMC-PEG-MA)$_2$ networks over the degradation time *in vitro* and *in vivo* after 4 weeks. There was one T_g (1) at – 4 °C in the thermographs of the peptide-(PTMC-MA)$_2$ samples that were degrading *in vitro* while a second T_g (2) at 20 °C appeared in the thermographs of the samples that were degrading *in vivo* (Figure 5.5a). Similarly, there was only one T_g (1) at –18 °C in the thermographs of the peptide-(PTMC-PEG-MA)$_2$ samples *in vitro* while a second T_g (2) appeared at 20 °C *in vivo* samples (Figure 5.5b). The change in the T_g of the peptide-(PTMC-MA)$_2$ and PEG-(PTMC-MA)$_2$ networks prepared with PTMC 1100 Da *in vivo* are given in Table 5.1. The T_g of the control samples stayed constant with small fluctuation over the degradation time while for the peptide-(PTMC-MA)$_2$ and peptide-(PTMC-PEG-MA)$_2$ networks T_g values slightly decreased.

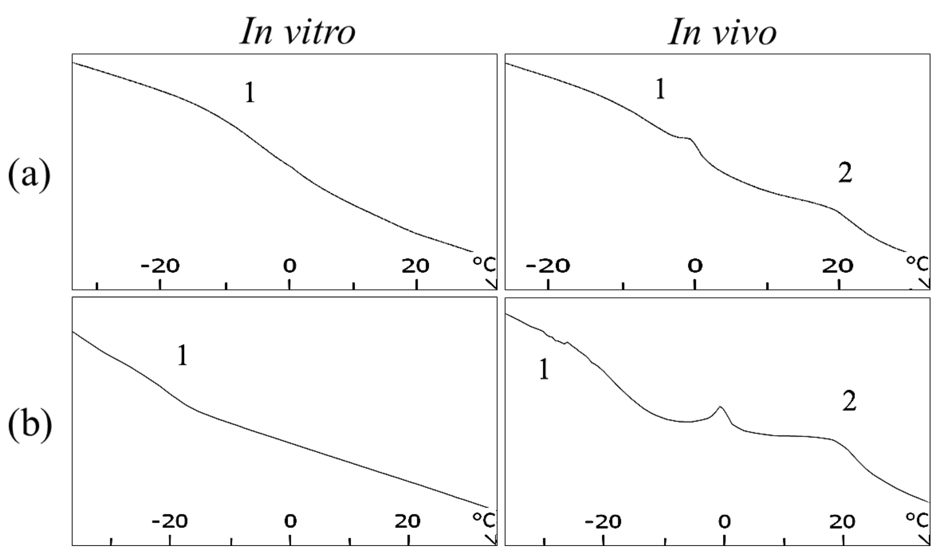

Figure 5.5. Thermographs of the networks prepared from (a) peptide-(PTMC-MA)$_2$ and (b) peptide-(PTMC-PEG-MA)$_2$ after 4 weeks of degradation *in vivo* and *in vitro*.

Table 5.1. T_g values (°C) of hydrated peptide-(PTMC-MA)$_2$, peptide-(PTMC-PEG-MA)$_2$ and PEG-(PTMC-MA)$_2$ networks over 4 weeks

Samples	Weeks				
	0	1	2	3	4
peptide-(PTMC-MA)$_2$	0	-2	-3	-4	-4
PEG-(PTMC-MA)$_2$	-11	-11	-12	-12	-12
peptide-(PTMC-PEG-MA)$_2$	-16	-16	-17	-18	-18

5.4.2.3 Histology

Figure 5.6 shows representative photomicrographs of tissue sections at weeks 1, 3 and 6 stained with Masson's trichrome. These photomicrographs were used to measure the thickness of the inflammatory zone, the cell density in the inflammatory zone, and the thickness of the fibrous capsule at the interface of implanted materials using Image J. These data are presented in Figures 5.7a-c.

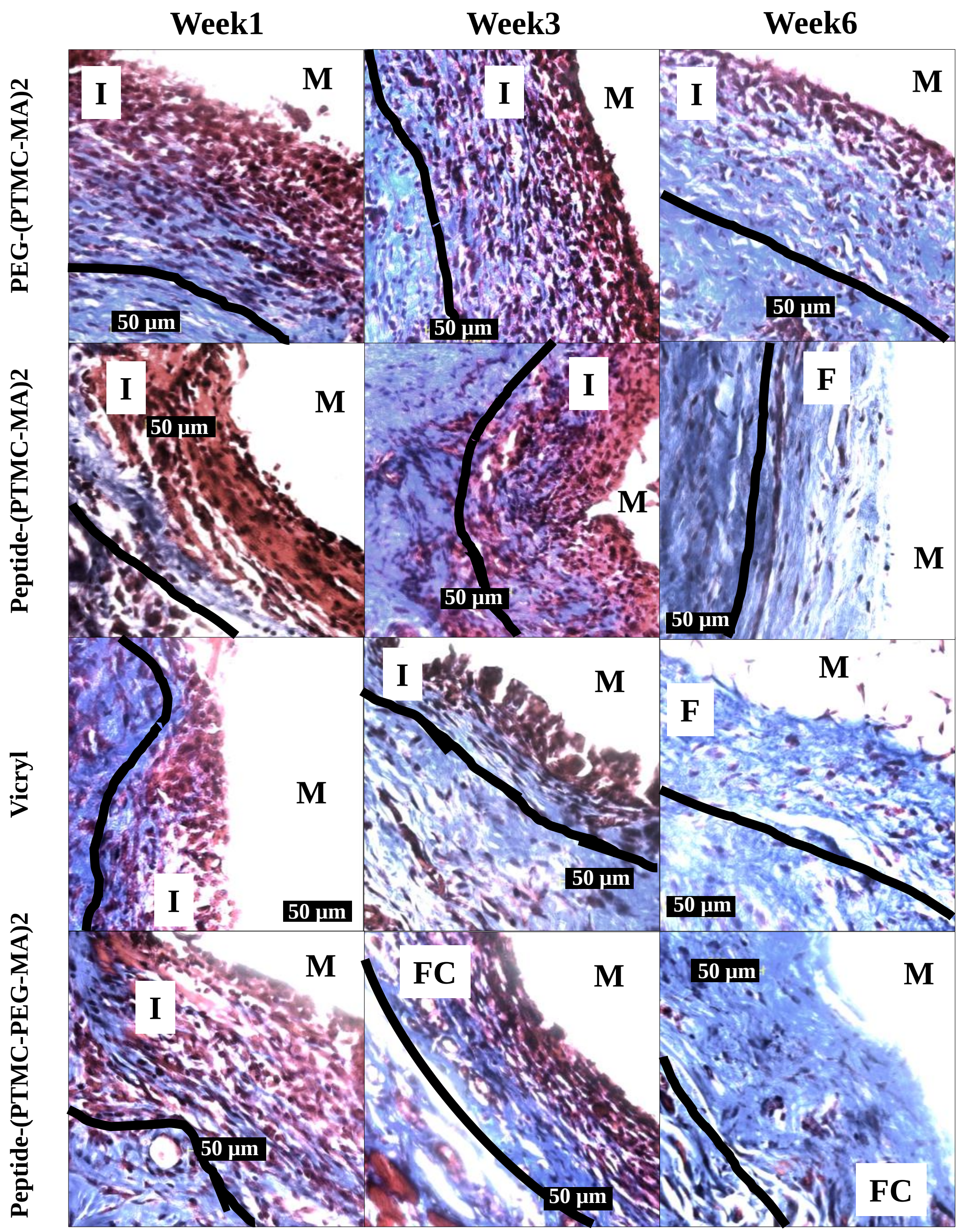

Figure 5.6. Masson's trichrome stained sections of the tissue surrounding implants at week 1, 3 and 6. The implant area (M) is on the right side of each image. The extent of the inflammatory zone (I) and the fibrous capsule area (F) are indicated by the black line. The scale bar is 50 µm.

There was no significant difference in the thickness of the inflammatory zone around the implanted area between the groups of material implants at weeks, 1, 4, and 5 post implantation (Figure 5.7a). However, this value was statistically lower for the Vicryl™ suture implants compared to the peptide-(PTMC-MA)$_2$, peptide-(PTMC-PEG-MA)$_2$, and PEG-(PTMC-MA)$_2$ samples at weeks 2 and 3 post implantation. The Vicryl™ suture implants were totally degraded at week 6, and no inflammatory zone was observed at the implantation area. The cell density in the inflammatory zone decreased with time at a similar rate for all four groups of implants with no significant differences between the different materials (Figure 5.7b). A fibrous capsule was present around the PEG-(PTMC-MA)$_2$ and peptide-(PTMC-PEG-MA)$_2$ implants at week 1, while it gradually appeared around the peptide-(PTMC-MA)$_2$ and Vicryl™ implants with time (Figure 5.7c). The thickness of the fibrous capsule around the implants increased over time up until 4 weeks for all the materials and was significantly greater around the peptide-(PTMC-MA)$_2$ implants compared to the peptide-(PTMC-PEG-MA)$_2$, Vicryl™, and PEG-(PTMC-MA)$_2$ implants at times beyond 2 weeks (Figure 5.7c). After 4 weeks, the capsule thickness plateaued for the peptide-(PTMC-MA)$_2$ implants, decreased for the Vicryl™ implants, but continued to steadily increase for the peptide-(PTMC-PEG-MA)$_2$ and PEG-(PTMC-MA)$_2$ control implants.

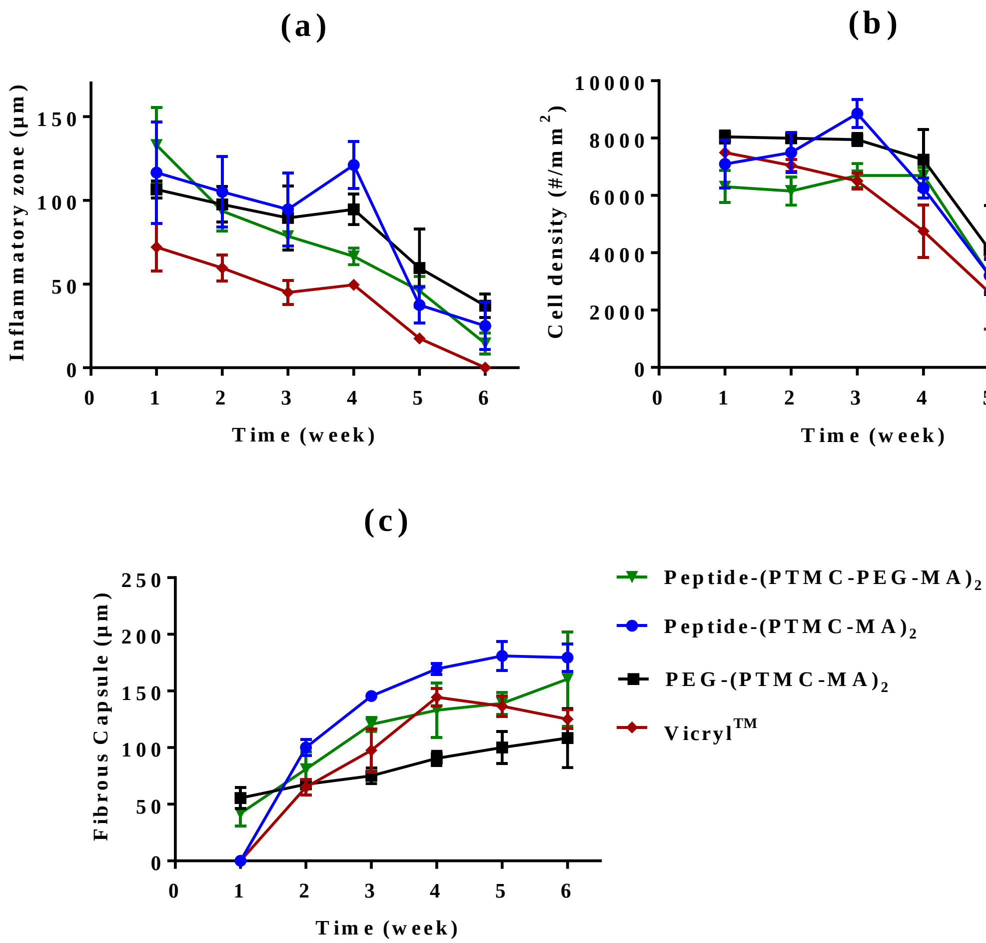

Figure 5.7. (a) The inflammatory zone thickness, (b) cell density, (c) the thickness of the fibrous capsule around the implanted area (n=2).

Figure 5.8 shows representative photomicrographs of tissue sections at week 1, 3 and 6 that were stained for the pan-macrophage marker CD68. These photomicrographs were used to measure the macrophage density and the ratio of macrophage number to total number of cells in the inflammatory zone. These data are presented in Figures 5.9a and b.

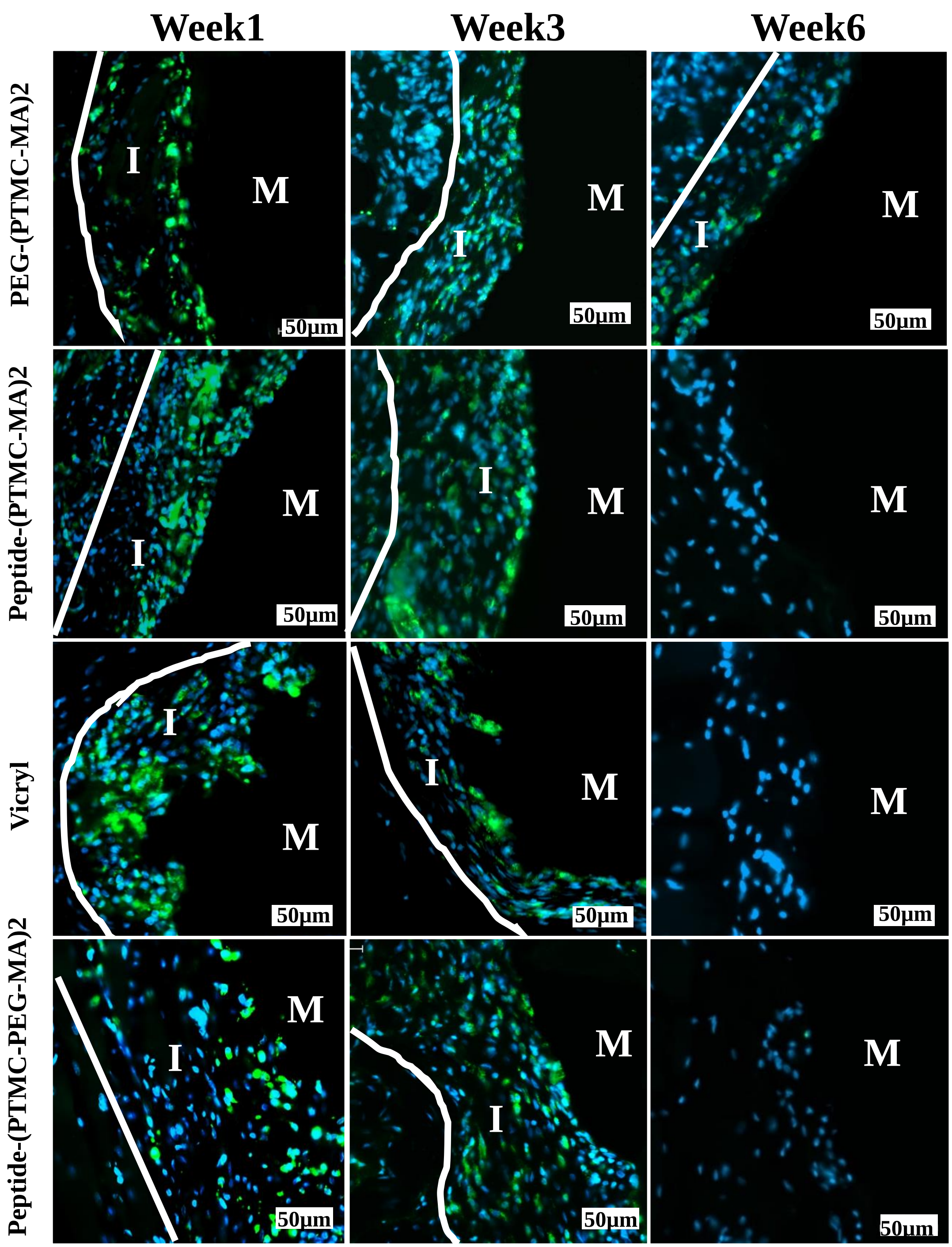

Figure 5.8. Fluorescent CD68 staining of the tissues surrounding implants at week 1, 3 and 6. The implanted area is indicated by (M) on the right side of each image. The white line indicates the extent of the inflammatory zone at the boundary of the implant. The scale bar is 50 µm. Macrophages are stained green while all cell nuclei are blue (n=2).

Similarly to the total cell density, the macrophage density also decreased over time for all implanted materials with no significant differences found between macrophage densities around any of the materials (Figure 5.9a). The ratio of the macrophage density to total cell density also decreased around all the implanted materials, with no significant differences in the first 4 weeks (Figure 5.9b). However, this ratio was significantly lower for the Vicryl™ control implants compared to the other groups of implants at weeks 5 and 6.

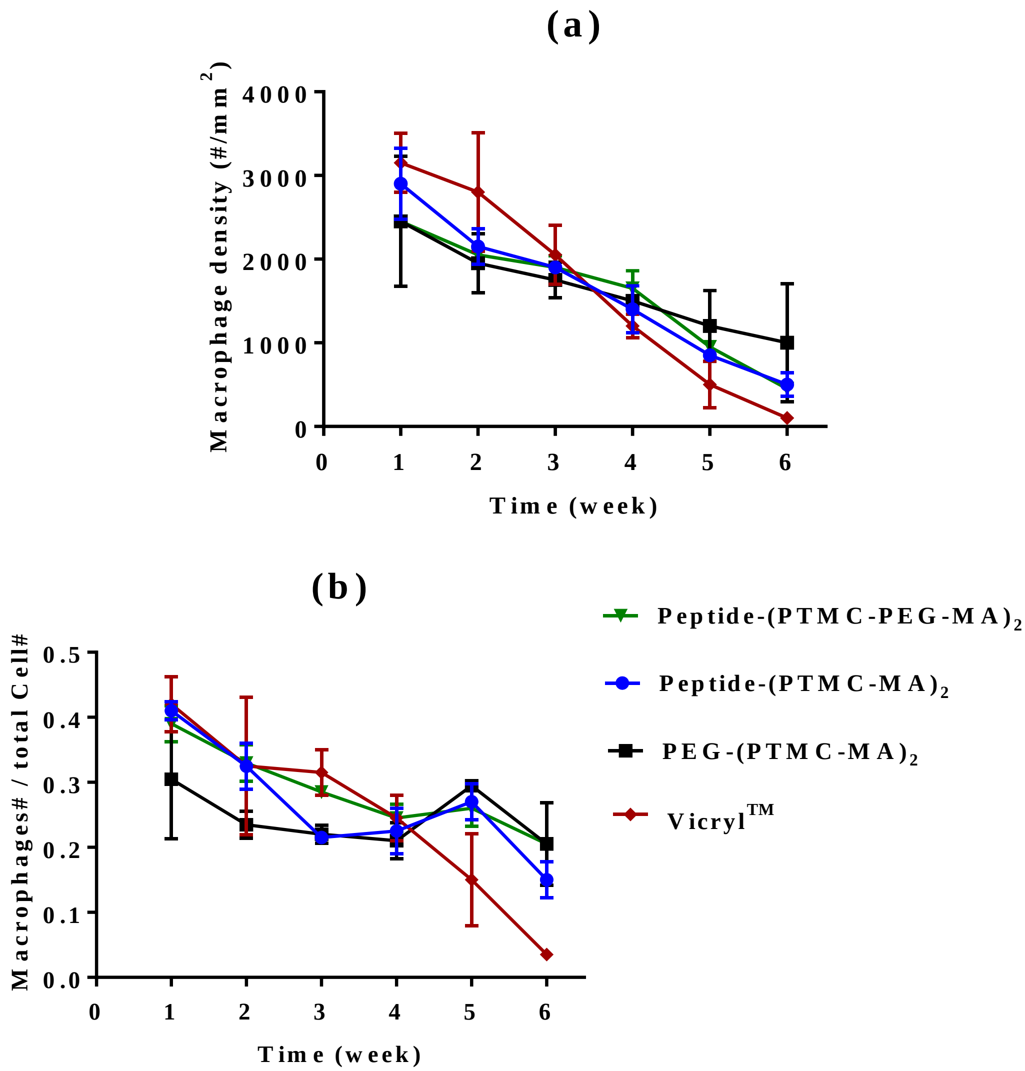

Figure 5.9. (a) The macrophage density, and (b) the ratio of macrophage to total cell number, in the inflammatory zone (n=2).

5.5 Discussion

The subcutaneous implantation study was performed to investigate the tissue response to the implanted materials as well as their *in vivo* degradation profiles. It is known that the hydrolytic degradation of these materials in the body is accelerated by secretion of cell-derived hydrolytic enzymes [107]. The reduction in volume of the peptide-(PTMC-MA)$_2$ implants with no signs of fragmentation suggests that surface erosion was the primary mode of degradation. The degradation via the surface erosion was also observed *in vitro* using collagenase-containing medium. In contrast, the peptide-(PTMC-PEG-MA)$_2$ sample had broken into smaller pieces, which could be due to the lower compressive modulus of this material making it less able to withstand the mechanical forces associated with tissue movements. The compressive modulus is affected by the molecular weight, the crosslink density, and the water content [88]. During the degradation process the crosslink density is being decreased by cleavage of the peptide sequence. A lower crosslink density resulted in greater mobility of the polymer molecules and therefore lowered the modulus. This phenomena happened after two weeks of implantation for peptide-(PTMC-MA)$_2$ and peptide-(PTMC-PEG-MA)$_2$ samples. The compressive moduli of these groups of implants decreased from week 3 post implantation, while this value stayed constant for the PEG-(PTMC-MA)$_2$ control samples over the entire implantation time.

The mass loss measurement of the implants showed that the mass actually increased for the peptide-(PTMC-MA)$_2$ samples after 4 weeks, and for the peptide-(PTMC-MA)$_2$ samples after 3 weeks. This mass increase can be attributed to ECM protein deposition and tissue ingrowth into the degrading implants [168]. The appearance of a second T_g at 20 °C in the DSC thermograph of both materials at week 4 is evidence of this protein deposition [169], [170]. The T_g of 20% hydrated collagen is around 20 °C that is in agreement with our finding [171].

Considering the mass loss and the sol content together, the total degradation of the peptide-(PTMC-MA)$_2$ and peptide-(PTMC-PEG-MA)$_2$ implants were 72 ± 3% and 65 ± 6%, respectively, over 6 weeks. In contrast, the PEG-(PTMC-MA)$_2$ control samples did not degrade and possessed negligible sol content. This observation along with the constant compressive modulus confirmed the hydrolytic stability of the copolymer backbone and the thio-ether sulfone linkage between vinyl sulfone at the polymer end and the thiol group at the dithiol PEG. It is proposed that the oxidation by reactive oxygen species (ROSs) has a dominant role in PTMC backbone degradation *in vivo* [172]. The lack of significant sol content also confirmed the resistance of the PTMC backbone to degradation by ROSs over this period of time. Therefore, the observed degradation in the peptide-containing networks was considered to be due primarily to enzymatic cleavage of the peptide regions.

The thickness of the inflammatory zones around all groups of implants were comparable to each other, except two time points in the middle of the experimental time frame. The thickness of this zone around the suture control material was lower than the other implants at weeks 2 and 3 post implantation. However, this difference was not biologically significant for these time points. The biological significance is related to the concept of clinically relevant difference (CRD), which is the smallest meaningful effect [173]. The thickness of the inflammatory zone decreased with time for all the implants. For degradable implants it is proposed that when they became softer over the degradation process their mechanical irritation to the surrounding tissue decreases [174], [175]. In addition, the formation of the fibrous capsule at the interface of tissue and implant isolated the biomaterial from the local tissue environment and it mediated the inflammatory response around the control samples [176]. The thickness of the fibrous capsule around the implantation area also increased over time. Fibrous encapsulation is the end stage of healing response to the implantation of biomaterials in vascularized tissues [176].

Similar to the cell density, the macrophage density in the inflammatory zone decreased over the degradation time for all four materials. Over the degradation process, it is proposed that the degradable materials became smaller in size and this reduction in size resulted in a lower amount of degradation products that along with the subsided inflammation affected the macrophage density [177], [178]. The macrophage response was statistically similar to all four groups of implants. In the earlier time points the ratio of macrophage density to the total cell density in the inflammatory zone was 42 ± 4% in the peptide-$(PTMC\text{-}MA)_2$ networks, 39 ± 3% in the peptide-$(PTMC\text{-}PEG\text{-}MA)_2$ networks, and 30 ± 9% in PEG-$(PTMC\text{-}MA)_2$ networks. This ratio was statistically constant for the PEG-$(PTMC\text{-}MA)_2$ control implant while it decreased over time for the other groups of implants. This result could be due to the ongoing inflammation caused by the macrophages' inability to degrade the PEG-$(PTMC\text{-}MA)_2$ control samples.

Despite all the recent studies on degradable biohybrid networks there are only a few solely enzymatically degradable materials. Some recent approaches include the proteinase-sensitive PEG-based hydrogel [74], the enzyme-degradable zwitterionic dextran hydrogels [179] and MMP-sensitive hyaluronic acid (HA) [180]. The main drawback of the naturally-sourced materials such as HA and dextran is the high swelling ratio and unpredictable degradability. Generally, the PEG-based hydrogels are not mechanically strong enough to withstand the forces in load-bearing soft connective tissues due to their high water content. However, by incorporating the hydrophobic blocks to the PEG structure the mechanical features of the final copolymer can be improved via controlling its water content. Recently, an enzyme-degradable biohybrid hydrogel has been reported entailing the addition of TMC blocks onto a 4-arm PEG that showed improved mechanical properties [88]. The advantage of the current strategy is the simplified one-step crosslinking without using two separate functionalized components such as were used in the previous approach.

Considering the *in vivo* observations, the hybrid polymeric network proposed and investigated in this study has a moderate tissue response which is comparable to that of the Vicryl™ suture. Therefore, the proposed PTMC-based formulation has the potential to be considered for clinical applications. It also can be modified in different ways to adjust the compressive modulus by tuning the ratio of hydrophilic block to hydrophobic block, or the degradation rate and the susceptibility to various enzymes by using different peptide sequences in order to fulfil a range of tissue engineering applications.

5.6 Conclusion

Herein, a new biohybrid PTMC-based network has been developed that has the potential to overcome limitations of current strategies in soft connective tissue engineering. The new formulation may be able to support the damaged tissue mechanically, with identical mechanical features, and a controlled degradation behavior until the healing process is completed. The previous *in vitro* degradation study of the developed materials had confirmed their enzyme-degradation via surface erosion. This *in vivo* study supported the previous *in vitro* finding under the physiological conditions in a rat model. The negative control sample without the enzyme-sensitive fractions showed negligible mass loss over 6 weeks of implantation. Importantly, the MMP-sensitive peptide containing samples showed comparable moderate inflammatory response to that observed towards commercially available Vicryl™ suture.

Chapter 6

Aqueous crosslinking of the poly(trimethylene carbonate)-poly(ethylene glycol) biohybrid networks

6.1 Abstract

The aqueous crosslinking of the previously described biohybrid copolymer made of poly(ethylene glycol) (PEG) and poly(trimethylene carbonate) (PTMC) conjugated to a matrix metalloproteinase (MMP)-sensitive peptide (peptide(PTMC-PEG-MA)$_2$) was investigated. The prepolymer with different molar ratios of PEG to PTMC blocks were characterized. The thermo-gelation of the aqueous suspension occurred at 37 °C for the prepolymer with a number average molecular weight of 1700 Da and a PEG to PTMC weight ratio of 30%. The covalent crosslinking of the 30% w/v aqueous suspension of the prepolymer was successfully done via a free radical polymerization using Ammonium persulfate (APS) and N,N,N',N'-tetrametylethylenediamine (TEMED). The crosslink efficiency, water content, instantaneous compressive modulus, and the glass transition temperature of the final networks were measured at room temperature.

6.2 Introduction

In situ formable polymeric networks for tissue engineering and regenerative medicine applications have been intensively examined over the past decade. Use of these materials not only minimizes the risk of infection and scar formation, but also facilitates cell encapsulation [19]. Another advantage is their ability to fill and reproduce even large irregular geometrically complex defects [2],[3]. Networks can be formed *in situ* via a number of covalent crosslinking strategies such as free radical polymerization, carbonyl-base condensation, addition reactions, or in response to environmental stimuli such as temperature or pH of the surrounding media [181], [182]. Stimuli-responsive polymers have been widely investigated due to their ability to form gels upon injection with no other requirements of chemical agents. Thermoresponsive amphiphilic block copolymers have received the most interest in biomedical applications as their sol to gel transition happens by a temperature increase from ambient to physiological [4]. The physical formation of the networks via a thermal gelation process can also be combined with a covalent polymerization method in order to achieve better mechanical properties [183].

Herein, the thermal gelation and the aqueous crosslinking of the previously developed peptide-$(PTMC\text{-}PEG\text{-}MA)_2$ prepolymer was investigated in order to assess its potential for *in situ* formation in the presence of cells.

6.3 Materials and methods

6.3.1 Materials

The materials used for block copolymer synthesis and purification were provided in previous chapters. N,N,N',N'-tetrametylethylenediamine (TEMED) was obtained from Fisher Scientific, Mississauga, Ontario Canada. Ammonium persulfate (APS) was purchased from BioShop Canada Inc. Burlington, Ontario.

6.3.2 Synthesis of Heterobifunctional PEG-PTMC, MMP-sensitive peptide conjugation, and characterization

Methacrylate-poly(ethylene glycol)-*b*-poly(trimethylene carbonate)-vinyl sulfone (MA-PEG-PTMC-VS) was synthesized as previously described in Chapter 4. The final block copolymer was fractionated using size exclusion chromatography and evaluated by proton nuclear magnetic resonance (^{1}H NMR) to calculate the number average molecular weight, confirm the structure and determine the vinyl sulfone addition efficiency as described in the previous chapters.

Heterobifunctional MA-PEG-PTMC-VS's with different molecular weights were then reacted with a half equivalent of a dithiol containing MMP-sensitive peptide (GCRDGPQGIWGQDRCG, 1704 Da) to form MA-PEG-*b*-PTMC-*b*-peptide-*b*-PTMC-*b*-PEG-MA block copolymers (peptide-(PTMC-PEG-MA)$_2$). The final conjugates were purified by dialysis in water for 24 h using a 500 Da cut-off membrane. The final product was lyophilized and stored at -20 °C.

6.3.3 Peptide-(PTMC-PEG-MA)$_2$ prepolymer characterization

The structure confirmation, purity, and reaction efficiency of the final prepolymer were analyzed by ^{1}H NMR spectroscopy. The water solubility of the final prepolymer were measured by mixing

100 mg of the sample in 1mL of distilled water. The suspension was stirred at 37 °C overnight and then centrifuged at 3200 rpm for 10 minutes. The supernatant was collected and lyophilized for further studies. To assess the ability of the copolymer to undergo thermal gelation, an aqueous suspension of 5% (w/v) was prepared with each fraction and then put at 37 °C. The thermal gelation behavior was investigated by vial tilting method [184]. The polymer glass transition temperatures were measured on a Mettler-Toledo differential scanning calorimeter (DSC) using a cooling-heating-cooling-heating cycle from 25 °C to -60 °C to 40 °C to -60 °C to 25 °C at a rate of 30 °C /min. Indium and gallium standards were used to calibrate the DSC. The glass transition temperature was determined from the inflection point of the second run endotherms using the internal DSC analysis software.

6.3.4 Network formation in aqueous condition

Purified prepolymer of peptide-(PTMC-PEG-MA)$_2$ containing 1.7 kDa PEG-PTMC was mixed with distilled water to form a 30% w/v aqueous suspension (n=3). Ammonium persulfate (APS) and N,N,N',N'-tetrametylethylenediamine (TEMED) were used at a 75 mM final concentration as a thermal free-radical initiator for chemical crosslinking. APS and TEMED solutions were added to the prepolymer suspension immediately before crosslinking, which was then gently agitated and quickly pipetted into a 1mL syringe mold. The networks were then formed over 15 min at 37 °C. Following network formation, the sol content, the water content, and the compressive moduli of the networks were measured as described below.

6.3.5 Network characterization

The crosslinking efficiency was assessed by measuring the sol content after network formation. The sol content was determined by measuring the dry weight before and after immersing the network in DMSO at 37 ºC for 24 h. The DMSO was removed by immersing the networks in water, with repeated water replacement, for 24 h and then the networks were lyophilized. The aqueous swelling ratio of the samples was determined by calculating the weight difference of the elastomer disc before and after immersion in water at 37 ºC for 24 h. Following sol extraction, the glass transition temperature was measured via DSC using the cooling-heating-cooling-heating cycle described above.

To determine the instantaneous compressive modulus of the networks measurements were performed on hydrated cylindrical samples (n = 5) pre-hydrated in water at 25 ºC. The measurements were conducted to 20 % strain at a strain rate of 1 %/s using a 1 mm indenter and the resulting force was recorded. The compressive modulus was obtained from Equation 1 assuming the rigidity of the indenter was infinite and the sample had a Poisson's ratio ν of 0.5 [147].

6.3.6 Statistical analysis

Final quantitative data was expressed as the mean ± the standard deviation about the mean. One-way analysis of variance (ANOVA) with a Bonferroni post hoc test was performed where applicable. A paired t test was conducted between different samples for long-term studies with the assigned significance at p values less than 0.05.

6.4 Results

6.4.1 Prepolymer characterization

The reaction efficiency, chemical structure, and purity of the compounds after each reaction were assessed using ^{1}H NMR spectroscopy as previously described. The final peptide-(PTMC-PEG-MA)$_2$ was fractionated into different molecular weight fractions and the average molecular weight, T_g, water solubility, PEG/PTMC ratio and thermal gelation behaviour of each prepolymer molecular weight fraction assessed (Table 6.1). The number average molecular weight (M_n) of the different fractions were calculated from the ^{1}H NMR spectra by comparing the integrals of the methacrylate peaks and the methylene protons of the TMC units as described in Chapter 4. The water solubility of the prepolymers with different M_ns ranged from 0.5 to 5.1 %w/v. As would be expected, a higher water solubility was obtained for copolymers with a higher ratio of PEG to PTMC. Generally, the existence of the hydrophilic PEG in the copolymer backbone improves the water solubility and attracts more water molecules to the polymer structure [185].

Table 6.1. Number average molecular weights (M_n), glass transition temperature (T_g), and water solubility of different fractions of PEG-PTMC. PEG/PTMC ratio is the molecular weight ratio of the PEG block to the PEG-PTMC block.

PEG-PTMC M_n (Da)	**1300**	**1700**	**2000**	**2400**	**3000**
PEG/PTMC ratio	34%	30%	32%	28%	14%
MA-PEG-PTMC-VS T_g (°C)	-44	-42	-41	-39	-35
peptide-(PTMC-PEG-MA)$_2$ solubility (% w/v)	5.1 ± 0.8	3.5 ± 0.5	3.3 ± 0.3	1.2 ± 0.4	0.5 ± 0.1
5% w/v suspension at 37°C	-	Thermal gelation		Precipitation	

The vial tilting method was used to illustrate the thermal gelation behavior of the peptide-(PTMC-PEG-MA)$_2$ with different molecular weights. The aqueous suspension of peptide-(PTMC-PEG-MA)$_2$ prepolymer containing PEG-PTMC 1700-2000 Da and the PEG/PTMC ratio of 30-32% at 5% w/v concentration showed the thermal gelation behavior at 37 °C. For PEG-PTMC 1300 Da copolymer 5% w/v suspension stayed stable at 37 °C, while, for the PEG-PTMC 2400 Da and 3000 Da the 5% w/v aqueous suspension collapsed and precipitation occurred upon a temperature change from 25 °C to 37 °C. Figure 6.1 illustrates the thermal gelation of the aqueous suspension of prepolymer fraction with PEG-PTMC of 1.7 kDa and 30% PEG/PTMC weight ratio upon a temperature increase to 37 °C.

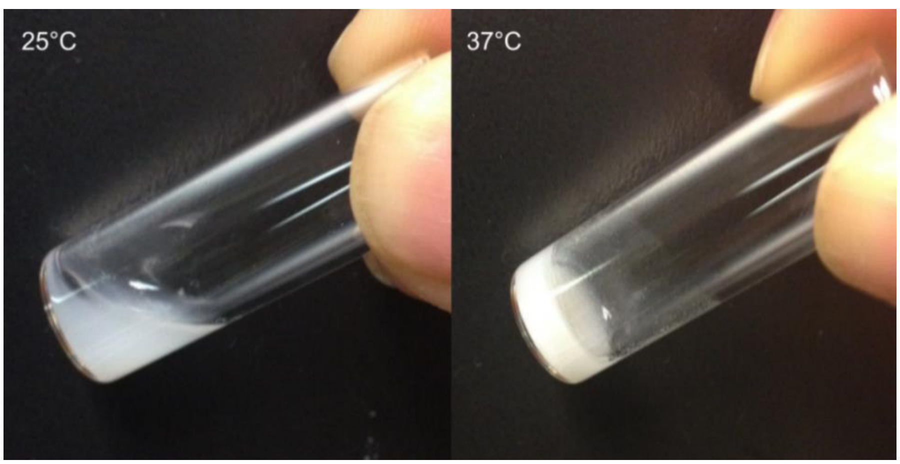

Figure 6.1. Thermal gelation of peptide-(PTMC-PEG-MA)$_2$ aqueous suspension, PEG-PTMC 1.7 kDa and PEG/PTMC weight fraction of 30%.

6.4.2 The characterization of the crosslinked networks in aqueous suspension

The sol content, water content, and the compressive moduli of the networks prepared with peptide-(PTMC-PEG-MA)$_2$ in aqueous suspension were measured as described above (Table 6.2). The sol content upon network formation was 18% ± 2%, the water content of the networks was 65% ± 4%, and the compressive modulus was 243 ± 80 kPa.

Table 6.2. Characterization of the networks prepared with peptide-(PTMC-PEG-MA)$_2$ formed in aqueous suspension.

PEG-PTMC M_n	Sol content	Water content	Compress. Mod
1.7 kDa	18% ± 2%	65% ± 4%	243 ± 80 (kPa)

6.5 Discussion

A biohybrid prepolymer of peptide-(PTMC-PEG-MA)$_2$, were successfully synthesized and fractionated to study the effect of the molecular weight and the PEG/PTMC ratio on water solubility and thermal gelation behavior. Biohybrid networks were fabricated from the chosen prepolymer M_n with thermal gelation behavior at 37 °C in an aqueous suspension and their sol content, water content, and compressive moduli were measured.

The characterization of the peptide-(PTMC-PEG-MA)$_2$ prepolymer with different weight ratios of PTMC confirmed that by increasing the molecular ratio of the hydrophobic PTMC block the water solubility of the compound decreased at room temperature (Table 6.1) [186]. It was also shown that by increasing the molecular weight of the prepolymer, the T_g increased (Table 6.1). T_g is associated with the molecular motions and the chain rotational movements and lower T_g means a higher molecular mobility [187], [188]. Larger PEG-PTMC molecules have higher T_g due to the lower mobility that affects the overall flexibility of the polymer chains [189].

The 5% w/v aqueous suspension of peptide-(PTMC-PEG-MA)$_2$ prepolymer containing PEG-PTMC 1700-2000 Da and the PEG/PTMC ratio of 30-32% showed a thermal gelation behavior at 37 °C (Figure 6.1). 5% w/v suspension was chosen due to its stablility with no precipitation at room temperature. For lower molecular weight PEG-PTMC and a higher PEG/PTMC ratio, the copolymer suspension stayed stable at 37 °C. This was due to the stronger hydrogen bonding between water molecules and the polymer chains compared to the hydrophobic interactions of the PTMC blocks [190]. Whereas, for PEG-PTMC of higher molecular weights and lower weight ratios of PEG to PTMC the aqueous suspension collapsed and precipitation occurred upon a temperature change from 25 °C to 37 °C. For these cases, as when the temperature was raised the hydrogen bonding was weakened by random thermal motions of the polymer molecules and the hydrophobic interactions dominated to form reversible crosslinking domains [191]. At a weight ratio of PEG to PTMC of 30-32%, the balance between hydrogen bonding and hydrophobic interactions held the physical structure of the gel.

The sol content of the networks was 18% ± 2%, which was higher than the sol content measured for the photo-cured networks in Chapter 4. The higher sol content indicates a lower crosslinking efficiency using the chemical crosslinking in aqueous suspension. This can be due to the low solubility in water compared to DMF of the peptide-(PTMC-PEG-MA)$_2$ prepolymer and limited access of the chemical reagents to the methacrylate groups. The thermally-initiated polymerization method was previously used to form a PTMC-*b*-PEG-*b*-PTMC diacrylate and methacrylated glycol chitosan hydrogels by using a low initiator concentration (5mM) [192]. However, in this study a 75 mM initiator concentration was needed in order to form the biohybrid network. The need for higher concentration of the initiator could also be due to the limited water solubility of the peptide-(PTMC-PEG-MA)$_2$ prepolymers and limited availability of the methacrylate groups for crosslinking. This high radical concentration could potentially be cytotoxic for cells in future applications. The compressive modulus was also lower than the one measured for photo-cured networks in Chapter 4. The compressive modulus is affected by the molecular weight, the crosslink density, and the water content [88]. The lower crosslink efficiency not only increased the sol content but also decreased the crosslink density of the biohybrid networks, which affected the compressive modulus.

Despite the high number of recent studies of thermoresponsive degradable polymeric biomaterials [101], [193]–[201], few simultaneously possesses a high compressive modulus, enzyme degradation ability, and thermal gelation properties. A biodegradable thermosensitive triblock copolymer of poly(δ-valerolactone-co-D,L-lactide)-*b*-PEG-*b*-poly(δ-valerolactone-co-D,L-lactide) (PVLA-PEG-PVLA) has recently been reported [194]. The mechanical properties of the PVLA-PEG-PVLA copolymers are promising for future biomedical applications. However, this formulation undergoes hydrolysis under physiological conditions that causes uncontrolled mechanical failure that is not favorable for tissue engineering applications. A PNIPAAm–gelatin-based thermoresponsive injectable hydrogel for cardiac tissue engineering has been recently reported [195]. Although this biohybrid hydrogel offers a high bioactivity for cell survival and adhesion, the degradation and the mechanical deterioration were not investigated.

The biohybrid network that is reported herein can overcome the limitations associated with low mechanical properties and the unfavorable degradation mechanisms. The networks prepared with peptide-$(PTMC\text{-}PEG\text{-}MA)_2$ have well-defined mechanical properties and an enzyme-degradation behavior. The initial assessment also confirmed the potential of thermal gelation of the biohybrid networks.

6.6 Conclusion

Enzymatically degradable PTMC-based hybrid scaffold was successfully developed with potential application in soft connective tissue engineering. Heterobifunctional PEG-PTMC block copolymer was conjugated to a MMP-sensitive peptide. Different prepolymers of peptide-$(PTMC\text{-}PEG\text{-}MA)_2$ with different hydrophilic to hydrophobic ratios were synthesized and analyzed for thermal gelation properties. The thermal gelation behavior was assessed in order to evaluate the potential of the quick formation of the biohybrid networks *in situ*. Furthermore, a chemical crosslinking method was used to form a covalently bound network with improved compressive modulus. The best candidate with thermal gelation behavior at biological conditions was chosen for the next characterizations (PEG-PTMC1.7 kDa with PEG/PTMC ratio of 30%). The initial assessment of the peptide-$(PTMC\text{-}PEG\text{-}MA)_2$ prepolymer aqueous crosslinking showed promising results for future *in situ* formation of the biohybrid networks. More investigation is needed to optimize the crosslinking conditions and cell-seeding potential of these biohybrid networks.

Chapter 7

Conclusion and Recommendations

7.1 Conclusion

Herein, a new biohybrid material was developed that has the potential to overcome limitations of current materials used in soft connective tissue engineering strategies. The formation of an enzyme-degradable biohybrid network was achieved by photo-crosslinking a methacrylate functionalized prepolymer following the conjugation of MMP-sensitive peptide to heterobifunctional PTMC/PEG-PTMC. The compressive moduli and the degradation rate of the final networks *in vitro* were dependent on the initial molecular weight of the PTMC block. The addition of PEG block to PTMC block increased the water content of the resulting networks and subsequently decreased their compressive modulus.

The *in vitro* degradation of the networks in collagenase-containing media happened via surface erosion through enzyme-degradation of the MMP-sensitive peptide. Controls consisting of networks prepared from a peptide-free prepolymer confirmed the resistance of the PTMC/PEG-PTMC backbone and the thio-ether linkage to hydrolysis. *In vitro* degradation rates increased by decreasing the M_n of the PTMC block or addition of the PEG block to the prepolymer backbone.

The subcutaneous implantation of peptide containing biohybrid networks prepared with selected PTMC molecular weight along with a peptide-free control and the commercially available Vicryl^{TM} suture in rat model showed the same degradation mechanism *in vivo*. The inflammatory response to the implanted biohybrid network was the same as to the Vicryl^{TM} suture, suggesting that the new materials could be considered biocompatible.

The aqueous crosslinking of the biohybrid prepolymer was assessed and the network was successfully fabricated and characterized. The aqueous network formation confirmed the cell-seeding potential of biohybrid prepolymers as well as their *in situ* formation.

The new formulation may be able to support the damaged tissue mechanically, with identical mechanical features, until the healing process is completed. The network degradation rate can be tuned according to the estimated healing time by optimizing the PTMC/PEG-PTMC molecular weight, and enzymatic-degradable peptide type and concentration.

7.2 Recommendations for future work

The focus of this study was on design and development of enzyme degradable biohybrid materials for soft connective tissue engineering. It is recommended that a protocol be developed to aid in manufacture of the biohybrid prepolymer and the network for soft connective tissue engineering. The current developed biohybrid material has limited water solubility that affects the potential of cell-seeding and *in situ* formation of the final network. It is recommended to improve the water solubility of the PEG-PTMC copolymer by increasing the molar ratio of PEG block to PTMC block. However, it will be challenging for load bearing soft connective tissue to maintain the stiffness of the crosslinked network. It is also recommended to investigate the thermal gelation behavior of the biohybrid prepolymer to have a quick network formation upon injection before the covalent crosslinking occurs. A systematic study is needed to optimize the water solubility, thermal gelation behavior, and the stiffness of the biohybrid networks by tuning the PEG molar ratio and the peptide sequence being used for different applications.

The next step of the project will be to investigate cartilage secretion *in vitro* by chondrocyte encapsulation in the biohybrid networks. Chondrocytes, adipose derived stem cells, and mesenchymal stem cells are the potential cell sources for load-bearing soft connective tissue engineering considering their effectiveness on cartilage synthesizing. The culture conditions should be optimized for the chosen cell type. Dynamic culture systems are recommended to be used for a better nutrient delivery to the cells in the center of the networks. Biological segments such as hyaluronic acid and/or chondroitin sulfate are suggested to be mixed with the biohybrid prepolymer to improve the cellular activities throughout the network.

For load-bearing soft connective tissue engineering it is also recommended to use larger animals such as sheep to investigate the cartilage injection. The larger animal model will help provide information on the cartilage regeneration under the biological loading over the degradation time. Cells and growth factors are also recommended to be encapsulated in the injecting prepolymer. Growth factors facilitate and promote cells to regenerate new tissue.

7.3 Contributions to Knowledge

- The development of a heterobifunctional PTMC structure that can be readily conjugated to a dithiol MMP-sensitive peptide.
- The development of a simplified one-step crosslinking strategy to form biohybrid networks.
- The fabrication of the biohybrid networks with high stiffness appropriate for a range of load-bearing soft connective tissue engineering that is solely degradable by the action of enzymes.

References

[1] G. Chen, T. Ushida, and T. Tateishi, "Scaffold design for tissue engineering," *Macromol. Biosci.*, vol. 2, no. 2, pp. 67–77, 2002.

[2] H. Shin, S. Jo, and A. G. Mikos, "Biomimetic materials for tissue engineering," *Biomaterials*, vol. 24, no. 24, pp. 4353–4364, 2003.

[3] A. Heidary Rouchi and M. Mahdavi-Mazdeh, "Regenerative medicine in organ and tissue transplantation: Shortly and practically achievable?," *Int. J. organ Transplant. Med.*, vol. 6, no. 3, pp. 93–8, 2015.

[4] L. S. Nair and C. T. Laurencin, "Biodegradable polymers as biomaterials," *Prog. Polym. Sci.*, vol. 32, no. 8–9, pp. 762–798, 2007.

[5] J. M. Morais, F. Papadimitrakopoulos, and D. J. Burgess, "Biomaterials/tissue interactions: possible solutions to overcome foreign body response.," *AAPS J.*, vol. 12, no. 2, pp. 188–196, 2010.

[6] J. M. Anderson, A. Rodriguez, and D. T. Chang, "Foreign body reaction to biomaterials," *Semin. Immunol.*, vol. 20, no. 2, pp. 86–100, Apr. 2008.

[7] R. Langer and J. Vacanti, "Tissue engineering," *Science (80-.).*, vol. 260, no. 5110, pp. 920–926, 1993.

[8] F. Berthiaume, T. J. Maguire, and M. L. Yarmush, "Tissue engineering and regenerative medicine: history, progress, and challenges," *Annu Rev Chem Biomol Eng*, vol. 2, pp. 403–430, 2011.

[9] J. W. Nichol and A. Khademhosseini, "Modular tissue engineering: Engineering biological tissues from the bottom up," *Soft Matters*, vol. 5, no. 7, pp. 1312–1319, 2010.

[10] G. Steinhoff, *Regenerative medicine*. 2011.

[11] Y. Ikada, "Challenges in tissue engineering," *J. R. Soc. Interface*, vol. 3, no. 10, pp. 589–601, 2006.

[12] S. Bhatia, *Engineering Biomaterials for Regenerative Medicine*. New York, NY: Springer New York, 2012.

[13] C. Chung and J. Burdick, "Engineering cartilage tissue," *Adv Drug Deliv Rev.*, vol. 60, no. 2, pp. 243–62, 2008.

[14] A. Atala, "Tissue engineering and regenerative medicine: Concepts for clinical applications," *Rejuvenation Res.*, vol. 7, no. 1, 2004.

[15] P. Lu, K. Takai, V. M. Weaver, and Z. Werb, "Extracellular matrix degradation and remodeling in development and disease.," *Cold Spring Harb Perspect Biol*, vol. 3, no. 12, pp. 1–24, 2011.

[16] D. Narasipura, Srinivas, M. R. King, B. N. Mason, J. P. Califano, C. a. Reinhart-King, W. L. Stoppel, S. C. Roberts, S. Kundu, E. P. Chan, G. N. Tew, S. R. Bhatia, A. L. Gonzalez-Simon, O. Eniola-Adefeso, P. P. Wattamwar, T. D. Dziubla, W. K. Cho, M. J. M. Nunes Pereira, N. Lang, K. Lee, *et al.*, *Engineering Biomaterials for Regenerative Medicine*. New York, NY: Springer New York, 2012.

[17] D. S. Kohane and R. Langer, "Polymeric biomaterials in tissue engineering," *Pediatr. Res.*, vol. 63, no. 5, pp. 487–491, 2008.

[18] A. R. Amini, J. S. Wallace, and S. P. Nukavarapu, “Short-term and long-term effects of orthopedic biodegradable implants.,” *J. Long. Term. Eff. Med. Implants*, vol. 21, no. 2, pp. 93–122, 2011.

[19] Q. P. Hou, P. a. De Bank, and K. M. Shakesheff, “Injectable scaffolds for tissue regeneration,” *J. Mater. Chem.*, vol. 14, no. 13, pp. 1915–1923, 2004.

[20] B. Balakrishnan, N. Joshi, A. Jayakrishnan, and R. Banerjee, “Self-crosslinked oxidized alginate/gelatin hydrogel as injectable, adhesive biomimetic scaffolds for cartilage regeneration,” *Acta Biomater.*, vol. 10, no. 8, pp. 3650–3663, 2014.

[21] J. S. Kwon, S. M. Yoon, D. Y. Kwon, D. Y. Kim, G. Z. Tai, L. M. Jin, B. Song, B. Lee, J. H. Kim, D. K. Han, B. H. Min, and M. S. Kim, “Injectable in situ-forming hydrogel for cartilage tissue engineering,” *J. Mater. Chem. B*, vol. 1, no. 26, pp. 3314–3321, 2013.

[22] F. Gattazzo, A. Urciuolo, and P. Bonaldo, “Extracellular matrix : A dynamic microenvironment for stem cell niche,” *Biochim. Biophys. Acta - Gen. Subj.*, vol. 1840, no. 8, pp. 2506–2519, 2014.

[23] W. D. Callister, “Materials science and engineering: An introduction,” *Mater. Sci. Eng.*, vol. 94, p. 975, Oct. 1987.

[24] D. A. Fletcher and R. D. Mullins, “Cell mechanics and the cytoskeleton,” *Nature*, vol. 463, no. 7280, pp. 485–492, 2010.

[25] S. Pal, *Design of Artificial Human Joints & Organs*. Boston, MA: Springer US, 2014.

[26] N. Newell, J. P. Little, A. Christou, M. A. Adams, C. J. Adam, and S. D. Masouros, “Biomechanics of the human intervertebral disc: A review of testing techniques and results,” *J. Mech. Behav. Biomed. Mater.*, vol. 69, no. August 2016, pp. 420–434, 2017.

[27] I. Levental, P. C. Georges, and P. A. Janmey, “Soft biological materials and their impact on cell function,” *Soft Matter*, vol. 3, no. 3, pp. 299–306, 2007.

[28] N. Alkhouli, J. Mansfield, E. Green, J. Bell, B. Knight, N. Liversedge, J. C. Tham, R. Welbourn, A. C. Shore, K. Kos, and C. P. Winlove, “The mechanical properties of human adipose tissues and their relationships to the structure and composition of the extracellular matrix,” *AJP Endocrinol. Metab.*, vol. 305, no. 12, pp. E1427–E1435, Dec. 2013.

[29] P. B. Malafaya, G. A. Silva, and R. L. Reis, “Natural – origin polymers as carriers and scaffolds for biomolecules and cell delivery in tissue engineering applications,” *Adv. Drug Deliv. Rev.*, vol. 59, pp. 207–233, 2007.

[30] T. V. Ojumu, J. Yu, and B. O. Solomon, “Production of Polyhydroxyalkanoates, a bacterial biodegradable polymer,” *African J. Biotechnol.*, vol. 3, no. 1, pp. 18–24, 2004.

[31] A. P. Bonartsev, V. L. Myshkina, D. A. Nikolaeva, E. K. Furina, and T. A. Makhina, “Biosynthesis , biodegradation , and application of poly (3- hydroxybutyrate) and its copolymers - natural polyesters produced by diazotrophic bacteria,” *FORMATEX*, pp. 295–307, 2007.

[32] G. Chen and Q. Wu, “The application of polyhydroxyalkanoates as tissue engineering materials,” *Biomaterials*, vol. 26, pp. 6565–6578, 2005.

[33] B. Guo and P. X. Ma, “Synthetic biodegradable functional polymers for tissue engineering: a brief review,” *Sci. China Chem.*, vol. 57, no. 4, pp. 490–500, Apr. 2014.

[34] C. S. Mahon and D. A. Fulton, “Mimicking nature with synthetic macromolecules capable of recognition,” *Nat. Chem.*, vol. 6, no. 8, pp. 665–672, 2014.

[35] C. M. Magin, D. L. Alge, and K. S. Anseth, "Bio-inspired 3D microenvironments: a new dimension in tissue engineering," *Biomed. Mater.*, vol. 11, no. 2, p. 22001, Mar. 2016.

[36] X. Jia and K. L. Kiick, "Hybrid multicomponent hydrogels for tissue engineering," *Macromol. Biosci.*, vol. 9, no. 2, pp. 140–156, Feb. 2009.

[37] B. K. G. Theng, "Interactions of clay minerals with organic polymers. Some practical applications," *Clays Clay Miner.*, vol. 18, no. 6, pp. 357–362, 1970.

[38] S. Lecommandoux and É. Garanger, "Precision polymers with biological activity: Design towards self-assembly and bioactivity," *Comptes Rendus Chim.*, vol. 19, no. 1–2, pp. 143–147, Jan. 2016.

[39] A. J. Grodzinsky, M. E. Levenston, M. Jin, and E. H. Frank, "Cartilage tissue remodeling in response to mechanical forces," *Annu. Rev. Biomed. Eng.*, vol. 2, pp. 691–713, 2000.

[40] P. Y. Hwang, J. Chen, L. Jing, B. D. Hoffman, and L. A. Setton, "The role of extracellular matrix elasticity and composition in regulating the nucleus pulposus cell phenotype in the intervertebral disc: A narrative review," *J. Biomech. Eng.*, vol. 136, no. 2, p. 21010, 2014.

[41] J. Eyckmans, T. Boudou, X. Yu, and C. S. Chen, "A Hitchhiker's guide to mechanobiology," *Developmental Cell*, vol. 21, no. 1. Elsevier Inc., pp. 35–47, 2011.

[42] H. Yu, J. K. Mouw, and V. M. Weaver, "Forcing form and function: Biomechanical regulation of tumor evolution," *Trends in Cell Biology*, vol. 21, no. 1. Elsevier Ltd, pp. 47–56, 2011.

[43] S. J. Millward-Sadler and D. M. Salter, "Integrin-dependent signal cascades in chondrocyte mechanotransduction," *Ann. Biomed. Eng.*, vol. 32, no. 3, pp. 435–446, 2004.

[44] D. Rajgor and C. M. Shanahan, "Nesprins: from the nuclear envelope and beyond," *Expert Rev. Mol. Med.*, vol. 15, no. July, p. e5, Jan. 2013.

[45] S. Van Rossom, C. R. Smith, L. Zevenbergen, D. G. Thelen, B. Vanwanseele, D. Van Assche, and I. Jonkers, "Knee Cartilage Thickness, T1ρ and T2 Relaxation Time Are Related to Articular Cartilage Loading in Healthy Adults," *PLoS One*, vol. 12, no. 1, p. e0170002, Jan. 2017.

[46] S. Gobaa, S. Hoehnel, M. Roccio, A. Negro, S. Kobel, and M. P. Lutolf, "Artificial niche microarrays for probing single stem cell fate in high throughput," *Nat. Methods*, vol. 8, no. 11, pp. 949–955, Nov. 2011.

[47] Y. Navaro, N. Bleich-Kimelman, L. Hazanov, I. Mironi-Harpaz, Y. Shachaf, S. Garty, Y. Smith, G. Pelled, D. Gazit, D. Seliktar, and Z. Gazit, "Matrix stiffness determines the fate of nucleus pulposus–derived stem cells," *Biomaterials*, vol. 49, pp. 68–76, May 2015.

[48] J. Patterson and J. A. Hubbell, "Enhanced proteolytic degradation of molecularly engineered PEG hydrogels in response to MMP-1 and MMP-2," *Biomaterials*, vol. 31, no. 30, pp. 7836–7845, 2010.

[49] S. A. Syggelos, A. J. Aletras, I. Smirlaki, and S. S. Skandalis, "Extracellular matrix degradation and tissue remodeling in periprosthetic loosening and osteolysis : Focus on matrix metalloproteinases , their endogenous tissue inhibitors , and the proteasome," *Biomed Res. Int.*, vol. 2013, p. 18, 2013.

[50] H. S. Azevedo and R. R. L. Reis, "Understanding the enzymatic degradation of biodegradable polymers and strategies to control their degradation rate," *Biodegrad. Syst. tissue …*, pp. 177–202, 2005.

[51] M. C. Actuator, J. Thongrueng, T. Tsuchiya, K. Nagata, B. S. Valves, K. Muramoto, M.

Shiraishi, K. Chino, and Y. Wada, “Preparation and degradation mechanisms of biodegradable polymer : a review,” *Mater. Sci. Eng. C*, vol. 137, 2016.

[52] A. Banerjee, K. Chatterjee, and G. Madras, “Enzymatic degradation of polymers: a brief review,” *Mater. Sci. Technol.*, vol. 30, no. 5, pp. 567–573, May 2014.

[53] J. M. Sand, L. Larsen, C. Hogaboam, F. Martinez, M. Han, M. Røssel Larsen, A. Nawrocki, Q. Zheng, M. Asser Karsdal, and D. J. Leeming, “MMP mediated degradation of type IV collagen alpha 1 and alpha 3 chains reflects basement membrane remodeling in experimental and clinical fibrosis – validation of two novel biomarker assays,” *PLoS One*, vol. 8, no. 12, p. e84934, Dec. 2013.

[54] P. A. Parmar, S. C. Skaalure, L. W. Chow, J. P. St-Pierre, V. Stoichevska, Y. Y. Peng, J. A. Werkmeister, J. A. M. Ramshaw, and M. M. Stevens, “Temporally degradable collagen-mimetic hydrogels tuned to chondrogenesis of human mesenchymal stem cells,” *Biomaterials*, vol. 99, pp. 56–71, 2016.

[55] K. A. Woodhouse, P. Klement, V. Chen, M. B. Gorbet, F. W. Keeley, R. Stahl, J. D. Fromstein, and C. M. Bellingham, “Investigation of recombinant human elastin polypeptides as non-thrombogenic coatings,” *Biomaterials*, vol. 25, no. 19, pp. 4543–4553, Aug. 2004.

[56] R. A. McMillan and V. P. Conticello, “Synthesis and Characterization of Elastin-Mimetic Protein Gels Derived from a Well-Defined Polypeptide Precursor,” *Macromolecules*, vol. 33, no. 13, pp. 4809–4821, Jun. 2000.

[57] A. Chilkoti, T. Christensen, and J. Mackay, “Stimulus responsive elastin biopolymers: applications in medicine and biotechnology,” *Curr. Opin. Chem. Biol.*, vol. 10, no. 6, pp. 652–657, Dec. 2006.

[58] T. Osathanon, M. L. Linnes, R. M. Rajachar, B. D. Ratner, M. J. Somerman, and C. M. Giachelli, “Microporous nanofibrous fibrin-based scaffolds for bone tissue engineering,” *Biomaterials*, vol. 29, no. 30, pp. 4091–4099, Oct. 2008.

[59] R. J. Wade, E. J. Bassin, C. B. Rodell, and J. A. Burdick, “Protease-degradable electrospun fibrous hydrogels,” *Nat. Commun.*, vol. 6, p. 6639, Mar. 2015.

[60] A. K. Jha, K. M. Tharp, S. Browne, J. Ye, A. Stahl, Y. Yeghiazarians, and K. E. Healy, “Matrix metalloproteinase-13 mediated degradation of hyaluronic acid-based matrices orchestrates stem cell engraftment through vascular integration,” *Biomaterials*, vol. 89, pp. 136–147, 2016.

[61] P. a Parmar, L. W. Chow, J.-P. St-Pierre, C.-M. Horejs, Y. Y. Peng, J. a Werkmeister, J. a M. Ramshaw, and M. M. Stevens, “Collagen-mimetic peptide-modifiable hydrogels for articular cartilage regeneration.,” *Biomaterials*, vol. 54, pp. 213–25, 2015.

[62] D.-A. Wang, S. Varghese, B. Sharma, I. Strehin, S. Fermanian, J. Gorham, D. H. Fairbrother, B. Cascio, and J. H. Elisseeff, “Multifunctional chondroitin sulphate for cartilage tissue-biomaterial integration.,” *Nat. Mater.*, vol. 6, no. 5, pp. 385–392, 2007.

[63] H. Naderi-Meshkin, K. Andreas, M. M. Matin, M. Sittinger, H. R. Bidkhori, N. Ahmadiankia, A. R. Bahrami, and J. Ringe, “Chitosan-based injectable hydrogel as a promising in situ forming scaffold for cartilage tissue engineering,” *Cell Biol. Int.*, vol. 38, no. 1, pp. 72–84, 2014.

[64] B. D. Ulery, L. S. Nair, and C. T. Laurencin, “Biomedical applications of biodegradable polymers,” *J. Polym. Sci. Part B Polym. Phys.*, vol. 49, no. 12, pp. 832–864, 2011.

[65] D. F. Williams and S. P. Zhong, “Biodeterioration / Biodegradation of Polymeric Medical

Devices In Situ," *lnternational Biodeterior. Biodegrad.*, vol. 95, no. 130, pp. 95–130, 1994.

[66] P. X. Ma, "Biomimetic materials for tissue engineering," *Adv. Drug Deliv. Rev.*, vol. 60, no. 2, pp. 184–198, 2008.

[67] M. Demoor, D. Ollitrault, T. Gomez-Leduc, M. Bouyoucef, M. Hervieu, H. Fabre, J. Lafont, J.-M. Denoix, F. Audigié, F. Mallein-Gerin, F. Legendre, and P. Galera, "Cartilage tissue engineering: Molecular control of chondrocyte differentiation for proper cartilage matrix reconstruction," *Biochim. Biophys. Acta - Gen. Subj.*, vol. 1840, no. 8, pp. 2414–2440, 2014.

[68] A. Sionkowska, "Current research on the blends of natural and synthetic polymers as new biomaterials: Review," *Prog. Polym. Sci.*, vol. 36, no. 9, pp. 1254–1276, Sep. 2011.

[69] K. M. Shakesheff, S. M. Cannizzaro, and R. Langer, "Creating biomimetic micro-environments with synthetic polymer-peptide hybrid molecules," *J. Biomater. Sci. Polym. Ed.*, vol. 9, no. 5, pp. 507–518, Jan. 1998.

[70] B. Scholz, C. Kinzelmann, K. Benz, J. Mollenhauer, H. Wurst, and B. Schlosshauer, "Suppression of adverse angiogenesis in an albumin-based hydrogel for articular cartilage and intervertebral disc regeneration," *Eur. Cells Mater.*, vol. 20, pp. 24–37, 2010.

[71] R. Jin, L. S. M. Teixeira, A. Krouwels, P. J. Dijkstra, C. A. Van Blitterswijk, M. Karperien, and J. Feijen, "Synthesis and characterization of hyaluronic acid-poly(ethylene glycol) hydrogels via Michael addition: An injectable biomaterial for cartilage repair," *Acta Biomater.*, vol. 6, no. 6, pp. 1968–1977, 2010.

[72] L. D. Amer and S. J. Bryant, "The in vitro and in vivo response to MMP-sensitive poly(ethylene glycol) hydrogels," *Ann. Biomed. Eng.*, vol. 44, no. 6, pp. 1959–1969, Jun. 2016.

[73] J. Yu, F. Chen, X. Wang, N. Dong, C. Lu, G. Yang, and Z. Chen, "Synthesis and characterization of MMP degradable and maleimide cross-linked PEG hydrogels for tissue engineering scaffolds," *Polym. Degrad. Stab.*, vol. 133, pp. 312–320, Nov. 2016.

[74] E. B. Peters, N. Christoforou, K. W. Leong, G. A. Truskey, and J. L. West, "Poly(Ethylene Glycol) Hydrogel Scaffolds Containing Cell-Adhesive and Protease-Sensitive Peptides Support Microvessel Formation by Endothelial Progenitor Cells," *Cell. Mol. Bioeng.*, vol. 9, no. 1, pp. 38–54, Mar. 2016.

[75] K. R. Stevens, J. S. Miller, B. L. Blakely, C. S. Chen, and S. N. Bhatia, "Degradable hydrogels derived from PEG-diacrylamide for hepatic tissue engineering," *J. Biomed. Mater. Res. Part A*, vol. 103, no. 10, pp. 3331–3338, Oct. 2015.

[76] H. Shin, P. Quinten Ruhé, A. G. Mikos, and J. A. Jansen, "In vivo bone and soft tissue response to injectable, biodegradable oligo(poly(ethylene glycol) fumarate) hydrogels," *Biomaterials*, vol. 24, no. 19, pp. 3201–3211, 2003.

[77] J. S. Temenoff, H. Shin, D. E. Conway, P. S. Engel, and A. G. Mikos, "In vitro cytotoxicity of redox radical initiators for cross-linking of oligo(poly(ethylene glycol) fumarate) macromers," *Biomacromolecules*, vol. 4, no. 6, pp. 1605–1613, 2003.

[78] T. A. Holland, Y. Tabata, and A. G. Mikos, "Dual growth factor delivery from degradable oligo(poly(ethylene glycol) fumarate) hydrogel scaffolds for cartilage tissue engineering," in *Journal of Controlled Release*, 2005, vol. 101, no. 1–3 SPEC. ISS., pp. 111–125.

[79] Y. Park, M. P. Lutolf, J. A. Hubbell, E. B. Hunziker, and M. Wong, "Bovine primary chondrocyte culture in synthetic matrix metalloproteinase-sensitive poly(ethylene glycol)-

based hydrogels as a scaffold for cartilage repair.," *Tissue Eng.*, vol. 10, no. 3–4, pp. 515–522, 2004.

[80] M. E. Hoque, T. T. H. Meng, Y. L. Chuan, M. Chowdhury, and R. G. S. V. Prasad, "Fabrication and characterization of hybrid PCL/PEG 3D scaffolds for potential tissue engineering applications," *Mater. Lett.*, vol. 131, pp. 255–258, Sep. 2014.

[81] L. Li, L. Lu, and C. Zhou, "Fabrication of injectable PLLA / alginate hydrogel for tissue engineering," *IEEE Int. Conf. Semicond. Electron. Proceedings, ICSE*, 2011.

[82] B. Jeong, Y. H. Bae, and S. W. Kim, "Drug release from biodegradable injectable thermosensitive hydrogel of PEG – PLGA – PEG triblock copolymers," *J. Control. Release*, vol. 63, pp. 155–163, 2000.

[83] M. Qiao, D. Chen, X. Ma, and Y. Liu, "Injectable biodegradable temperature-responsive PLGA-PEG-PLGA copolymers: Synthesis and effect of copolymer composition on the drug release from the copolymer-based hydrogels," *Int. J. Pharm.*, vol. 294, no. 1–2, pp. 103–112, 2005.

[84] A. López, C. Persson, J. Hilborn, and H. Engqvist, "Synthesis and characterization of injectable composites of poly[D,L-lactide-co-(ε-caprolactone)] reinforced with β-TCP and CaCO3 for intervertebral disk augmentation," *J. Biomed. Mater. Res. Part B Appl. Biomater.*, vol. 95B, no. 1, pp. 75–83, Oct. 2010.

[85] D. Hannouche, H. Terai, J. R. Fuchs, S. Terada, S. Zand, B. a Nasseri, H. Petite, L. Sedel, and J. P. Vacanti, "Engineering of implantable cartilaginous structures from bone marrow-derived mesenchymal stem cells.," *Tissue Eng.*, vol. 13, no. 1, pp. 87–99, 2007.

[86] F. T. Moutos, L. E. Freed, and F. Guilak, "A biomimetic three-dimensional woven composite scaffold for functional tissue engineering of cartilage," *Nat. Mater.*, vol. 6, no. 2, pp. 162–167, 2007.

[87] L. Zhang, S. Dou, Y. Li, Y. Yuan, Y. Ji, Y. Wang, and Y. Yang, "Degradation and compatibility behaviors of poly(glycolic acid) grafted chitosan," *Mater. Sci. Eng. C*, vol. 33, no. 5, pp. 2626–2631, 2013.

[88] G. Chen, S. Taghavi, D. Marecak, and B. G. Amsden, "Tough and Enzyme-Degradable Hydrogels," *Macromol. Mater. Eng.*, vol. 1700162, p. 1700162, Jul. 2017.

[89] S. Kim and K. E. Healy, "Synthesis and characterization of injectable poly(N-isopropylacrylamide-co-acrylic acid) hydrogels with proteolytically degradable cross-links," *Biomacromolecules*, vol. 4, no. 5, pp. 1214–1223, 2003.

[90] S. Ibusuki, Y. Fujii, D. Ph, Y. Iwamoto, and D. Ph, "Tissue-Engineered Cartilage Using an Injectable and in Situ Gelable Thermoresponsive Gelatin : Fabrication and in Vitro Performance," vol. 9, no. 2, 2003.

[91] J. P. Chen and T. H. Cheng, "Thermo-responsive chitosan-graft-poly(N-isopropylacrylamide) injectable hydrogel for cultivation of chondrocytes and meniscus cells," *Macromol. Biosci.*, vol. 6, no. 12, pp. 1026–1039, 2006.

[92] E. Larraz, C. Elvira, and J. San Román, "Design and properties of novel self-curing acrylic formulations for application in intervertebral disks restoration," *Biomacromolecules*, vol. 6, no. 4, pp. 2058–2066, 2005.

[93] A. Thiem, M. Bagheri, C. Große-Siestrup, and R. Zehbe, "Gelatin-poly(lactic-co-glycolic acid) scaffolds with oriented pore channel architecture — From in vitro to in vivo testing," *Mater. Sci. Eng. C*, vol. 62, pp. 585–595, May 2016.

[94] G. Chen, T. Sato, T. Ushida, N. Ochiai, and T. Tateishi, "Tissue Engineering of Cartilage Using a Hybrid Scaffold of Synthetic Polymer and Collagen," *Tissue Eng.*, vol. 10, no. 3–4, pp. 323–330, Mar. 2004.

[95] Y. Hong, A. Huber, K. Takanari, N. J. Amoroso, R. Hashizume, S. F. Badylak, and W. R. Wagner, "Biomaterials Mechanical properties and in vivo behavior of a biodegradable synthetic polymer micro fi ber e extracellular matrix hydrogel biohybrid scaffold," *Biomaterials*, vol. 32, no. 13, pp. 3387–3394, 2011.

[96] J. Kundu, J. Shim, J. Jang, S. Kim, and D. Cho, "An additive manufacturing-based PCL – alginate – chondrocyte bioprinted scaffold for cartilage tissue engineering," no. January 2013, pp. 1286–1297, 2015.

[97] N. T. Dai, M. R. Williamson, N. Khammo, E. F. Adams, and A. G. A. Coombes, "Composite cell support membranes based on collagen and polycaprolactone for tissue engineering of skin," *Biomaterials*, vol. 25, no. 18, pp. 4263–4271, 2004.

[98] J. W. S. Hayami, S. D. Waldman, and B. G. Amsden, "Injectable, High Modulus, And Fatigue Resistant Composite Scaffold for Load-Bearing Soft Tissue Regeneration," *Biomacromolecules*, vol. 14, no. 12, pp. 4236–4247, 2013.

[99] P. S. Lienemann, Y. R. Devaud, R. Reuten, B. R. Simona, M. Karlsson, W. Weber, M. Koch, M. P. Lutolf, V. Milleret, and M. Ehrbar, "Locally controlling mesenchymal stem cell morphogenesis by 3D PDGF-BB gradients towards the establishment of an in vitro perivascular niche," *Integr. Biol.*, vol. 7, no. 1, pp. 101–111, 2015.

[100] A. D. Cook, J. S. Hrkach, N. N. Gao, I. M. Johnson, U. B. Pajvani, S. M. Cannizzaro, and R. Langer, "Characterization and development of RGD-peptide-modified poly(lactic acid-co-lysine) as an interactive, resorbable biomaterial," *J. Biomed. Mater. Res.*, vol. 35, no. 4, pp. 513–523, 1997.

[101] C. Wiltsey, T. Christiani, J. Williams, J. Scaramazza, C. V. Van Sciver, K. Toomer, J. Sheehan, A. Branda, A. Nitzl, E. England, J. Kadlowec, C. Iftode, and J. Vernengo, "Thermogelling bioadhesive scaffolds for intervertebral disk tissue engineering: Preliminary in vitro comparison of aldehyde-based versus alginate microparticle-mediated adhesion," *Acta Biomater.*, vol. 16, no. 1, pp. 71–80, 2015.

[102] C. Wiltsey, P. Kubinski, T. Christiani, K. Toomer, J. Sheehan, A. Branda, J. Kadlowec, C. Iftode, and J. Vernengo, "Characterization of injectable hydrogels based on poly(N-isopropylacrylamide)-g-chondroitin sulfate with adhesive properties for nucleus pulposus tissue engineering," *J. Mater. Sci. Mater. Med.*, vol. 24, no. 4, pp. 837–847, Apr. 2013.

[103] M. A. Cooperstein and H. E. Canavan, "Assessment of cytotoxicity of (N -isopropyl acrylamide) and poly (N -isopropyl acrylamide) - coated surfaces," *Biointerphases*, pp. 1–12, 2013.

[104] J. Zhu and R. E. Marchant, "Design properties of hydrogel tissue-engineering scaffolds," *Expert Rev. Med. Devices*, vol. 8, no. 5, pp. 607–626, Sep. 2011.

[105] B. V. Sridhar, J. L. Brock, J. S. Silver, J. L. Leight, M. A. Randolph, and K. S. Anseth, "Development of a Cellularly Degradable PEG Hydrogel to Promote Articular Cartilage Extracellular Matrix Deposition," *Adv. Healthc. Mater.*, vol. 4, no. 5, pp. 702–713, Apr. 2015.

[106] L. D. Amer, A. Holtzinger, G. Keller, M. J. Mahoney, and S. J. Bryant, "Enzymatically degradable poly(ethylene glycol) hydrogels for the 3D culture and release of human embryonic stem cell derived pancreatic precursor cell aggregates," *Acta Biomater.*, vol. 22, pp. 103–110, Aug. 2015.

[107] M. P. Lutolf, J. L. Lauer-Fields, H. G. Schmoekel, A. T. Metters, F. E. Weber, G. B. Fields, and J. A. Hubbell, "Synthetic matrix metalloproteinase-sensitive hydrogels for the conduction of tissue regeneration: Engineering cell-invasion characteristics," *Proc. Natl. Acad. Sci.*, vol. 100, no. 9, pp. 5413–5418, Apr. 2003.

[108] Y. Park, D. Ph, M. P. Lutolf, D. Ph, J. A. Hubbell, D. Ph, E. B. Hunziker, M. Wong, D. Ph, and P. E. T. Al, "Bovine Primary Chondrocyte Culture in Synthetic Matrix Hydrogels as a Scaffold for Cartilage Repair," *Tissue Eng.*, vol. 10, no. 3, 2004.

[109] D. P. Nair, M. Podgórski, S. Chatani, T. Gong, W. Xi, C. R. Fenoli, and C. N. Bowman, "The thiol-michael addition click reaction: A powerful and widely used tool in materials chemistry," *Chem. Mater.*, vol. 26, no. 1, pp. 724–744, Jan. 2014.

[110] L. Timbart, M. Y. Tse, S. C. Pang, O. Babasola, and B. G. Amsden, "Low viscosity poly(trimethylene carbonate) for localized drug delivery: Rheological properties and in vivo degradation," *Macromol. Biosci.*, vol. 9, pp. 786–794, 2009.

[111] K. Wiles, J. M. Fishman, and B. M. Bch, "The Host Immune Response to Tissue-Engineered Organs :," *Tissue Eng. Part B Rev.*, vol. 22, no. 3, pp. 208–219, 2016.

[112] C. J. Wilson, R. E. Clegg, D. I. Leavesley, and M. J. Pearcy, "Mediation of Biomaterial–Cell Interactions by Adsorbed Proteins: A Review," *Tissue Eng.*, vol. 11, no. 1–2, pp. 1–18, 2005.

[113] S. Franz, S. Rammelt, D. Scharnweber, and J. C. Simon, "Immune responses to implants - A review of the implications for the design of immunomodulatory biomaterials," *Biomaterials*, vol. 32, no. 28, pp. 6692–6709, 2011.

[114] A. Page-McCaw, A. J. Ewald, and Z. Werb, "Matrix metalloproteinases and the regulation of tissue remodelling," *Nat. Rev. Mol. Cell Biol.*, vol. 8, no. 3, pp. 221–233, 2007.

[115] L. Troeberg and H. Nagase, "Proteases involved in cartilage matrix degradation in osteoarthritis.," *Biochim. Biophys. Acta*, vol. 1824, no. 1, pp. 133–45, 2012.

[116] J. Patterson and J. A. Hubbell, "Enhanced proteolytic degradation of molecularly engineered PEG hydrogels in response to MMP-1 and MMP-2," *Biomaterials*, vol. 31, no. 30, pp. 7836–7845, 2010.

[117] L. Q. Yang, B. He, S. Meng, J. Z. Zhang, M. Li, J. Guo, Y. M. Guan, J. X. Li, and Z. W. Gu, "Biodegradable cross-linked poly(trimethylene carbonate) networks for implant applications: Synthesis and properties," *Polym. (United Kingdom)*, vol. 54, no. 11, pp. 2668–2675, 2013.

[118] Q. Hou, D. W. Grijpma, and J. Feijen, "Creep-resistant elastomeric networks prepared by photocrosslinking fumaric acid monoethyl ester-functionalized poly(trimethylene carbonate) oligomers.," *Acta Biomater.*, vol. 5, no. 5, pp. 1543–51, 2009.

[119] B. D. Mather, K. Viswanathan, K. M. Miller, and T. E. Long, "Michael addition reactions in macromolecular design for emerging technologies," *Prog. Polym. Sci.*, vol. 31, no. 5, pp. 487–531, 2006.

[120] L. Garamszegi, C. Donzel, G. É. Carrot, T. Q. Nguyen, and J. Hilborn, "Synthesis of thiol end-functional polystyrene via atom transfer radical polymerization," *React. Funct. Polym.*, vol. 55, no. 2, pp. 179–183, 2003.

[121] Rong JinPieter J. Dijkstra, *Biomedical applications of hydrogels handbook*. Springer, 2010.

[122] S. Jo, J. Kim, and S. W. Kim, "Reverse thermal gelation of aliphatically modified

biodegradable triblock copolymers.," *Macromol. Biosci.*, vol. 6, no. 11, pp. 923–8, 2006.

[123] X. Zhang, R. Zhuo, and Y. Yang, "Using mixed solvent to synthesize temperature sensitive poly(N-isopropylacrylamide) gel with rapid dynamics properties," *Biomaterials*, vol. 23, no. 5, pp. 1313–1318, 2002.

[124] P. X. Ma, "Biomimetic materials for tissue engineering," *Advanced Drug Delivery Reviews*, vol. 60, no. 2. pp. 184–198, 2008.

[125] C. M. Metallo, J. C. Mohr, C. J. Detzel, J. J. De Pablo, B. J. Van Wie, and S. P. Palecek, "Engineering the stem cell microenvironment," *Biotechnol. Prog.*, vol. 23, no. 1, pp. 18–23, 2007.

[126] N. F. Boyd, L. J. Martin, M. J. Yaffe, and S. Minkin, "Mammographic density and breast cancer risk: current understanding and future prospects," *Breast Cancer Res.*, vol. 13, no. 6, p. 223, Dec. 2011.

[127] D. E. Discher, "Tissue cells feel and respond to the stiffness of their substrate," *Science (80-.).*, vol. 310, no. 5751, pp. 1139–1143, Nov. 2005.

[128] F. Kai, H. Laklai, and V. M. Weaver, "Force matters: Biomechanical regulation of cell invasion and migration in disease," *Trends Cell Biol.*, vol. 26, no. 7, pp. 486–497, Jul. 2016.

[129] K. M. Riching, B. L. Cox, M. R. Salick, C. Pehlke, A. S. Riching, S. M. Ponik, B. R. Bass, W. C. Crone, Y. Jiang, A. M. Weaver, K. W. Eliceiri, and P. J. Keely, "3D Collagen Alignment Limits Protrusions to Enhance Breast Cancer Cell Persistence," *Biophys. J.*, vol. 107, no. 11, pp. 2546–2558, Dec. 2014.

[130] O. Chaudhuri, S. T. Koshy, C. Branco da Cunha, J. Shin, C. S. Verbeke, K. H. Allison, and D. J. Mooney, "Extracellular matrix stiffness and composition jointly regulate the induction of malignant phenotypes in mammary epithelium," *Nat. Mater.*, vol. 13, no. 10, pp. 970–978, Jun. 2014.

[131] A. J. Engler, S. Sen, H. L. Sweeney, and D. E. Discher, "Matrix elasticity directs stem cell lineage specification," *Cell*, vol. 126, no. 4, pp. 677–689, Aug. 2006.

[132] L. a Flanagan, Y.-E. Ju, B. Marg, M. Osterfield, and P. a Janmey, "Neurite branching on deformable substrates," *Neuroreport*, vol. 13, no. 18, pp. 2411–2415, Dec. 2002.

[133] A. J. Engler, M. A. Griffin, S. Sen, C. G. Bönnemann, H. L. Sweeney, and D. E. Discher, "Myotubes differentiate optimally on substrates with tissue-like stiffness," *J. Cell Biol.*, vol. 166, no. 6, pp. 877–887, Sep. 2004.

[134] A. Samani, J. Zubovits, and D. Plewes, "Elastic moduli of normal and pathological human breast tissues: an inversion-technique-based investigation of 169 samples," *Phys. Med. Biol.*, vol. 52, no. 6, pp. 1565–1576, Mar. 2007.

[135] T. R. Cox and J. T. Erler, "Remodeling and homeostasis of the extracellular matrix: implications for fibrotic diseases and cancer," *Dis. Model. Mech.*, vol. 4, no. 2, pp. 165–178, Mar. 2011.

[136] C. Bonnans, J. Chou, and Z. Werb, "Remodelling the extracellular matrix in development and disease," *Nat. Rev. Mol. Cell Biol.*, vol. 15, no. 12, pp. 786–801, Nov. 2014.

[137] S. Chu, S. L. Sridhar, U. Akalp, S. C. Skaalure, F. J. Vernerey, and S. J. Bryant, "Understanding the spatiotemporal degradation behavior of aggrecanase-sensitive poly(ethylene glycol) hydrogels for use in cartilage tissue engineering," *Tissue Eng. Part A*, vol. 23, no. 15–16, pp. 795–810, Aug. 2017.

[138] S. G. Lévesque and M. S. Shoichet, “Synthesis of enzyme-degradable, peptide-cross-linked dextran hydrogels,” *Bioconjug. Chem.*, vol. 18, no. 3, pp. 874–885, 2007.

[139] A. B. Allen, L. B. Priddy, M.-T. A. Li, and R. E. Guldberg, “Functional augmentation of naturally-derived materials for tissue regeneration,” *Ann. Biomed. Eng.*, vol. 43, no. 3, pp. 555–567, Mar. 2015.

[140] Q. Chen, S. Liang, and G. A. Thouas, “Elastomeric biomaterials for tissue engineering,” *Prog. Polym. Sci.*, vol. 38, no. 3–4, pp. 584–671, 2013.

[141] J. Hochberg, K. M. Meyer, and M. D. Marion, “Suture choice a nd other methods of skin closure,” *Surg. Clin. NA*, vol. 89, no. 3, pp. 627–641, 2009.

[142] K. Zhu, R. Hendren, K. Jensen, and C. Pitt, “Synthesis, properties, and biodegradation of poly (1, 3-trimethylene carbonate),” *Macromolecules*, pp. 1736–1740, 1991.

[143] S. Q. Liu, Q. Tian, L. Wang, J. L. Hedrick, J. H. P. Hui, Y. Y. Yang, and P. L. R. Ee, “Injectable biodegradable poly(ethylene glycol)/RGD peptide hybrid hydrogels for in vitro chondrogenesis of human mesenchymal stem cells.,” *Macromol. Rapid Commun.*, vol. 31, no. 13, pp. 1148–54, 2010.

[144] G.-Z. Li, R. K. Randev, A. H. Soeriyadi, G. Rees, C. Boyer, Z. Tong, T. P. Davis, C. R. Becer, and D. M. Haddleton, “Investigation into thiol-(meth)acrylate Michael addition reactions using amine and phosphine catalysts,” *Polym. Chem.*, vol. 1, no. 8, p. 1196, 2010.

[145] A. Takao, M. Fusae, and N. Yu, “Preparation of cross-linked aliphatic polyester and application to thermo-responsive material,” *J. Control. Release*, vol. 32, no. 1, pp. 87–96, Nov. 1994.

[146] K. T. Nguyen and J. L. West, “Photopolymerizable hydrogels for tissue engineering applications,” *Biomaterials*, vol. 23, no. 22, pp. 4307–4314, 2002.

[147] C. T. McKee, J. a Last, P. Russell, and C. J. Murphy, “Indentation versus tensile measurements of Young’s modulus for soft biological tissues,” *Tissue Eng. Part B Rev.*, vol. 17, no. 3, pp. 155–164, Jun. 2011.

[148] B. Amsden, “Curable, biodegradable elastomers: emerging biomaterials for drug delivery and tissue engineering,” *Soft Matter*, vol. 3, no. 11, p. 1335, 2007.

[149] E. Bat, Z. Zhang, J. Feijen, D. W. Grijpma, and A. A. Poot, “Biodegradable elastomers for biomedical applications and regenerative medicine,” *Regen. Med.*, vol. 9, no. 3, pp. 385–398, May 2014.

[150] Y. Li, Y. Xiao, and C. Liu, “The horizon of materiobiology: A perspective on material-guided cell behaviors and tissue engineering,” *Chem. Rev.*, vol. 117, no. 5, pp. 4376–4421, Mar. 2017.

[151] A. Albertsson and M. Eklund, “Influence of molecular structure on the degradation mechanism of degradable polymers: in vitro degradation of poly(trimethylene carbonate), poly(trimethylene carbonate-co-caprolactone), and poly(adipic anhydride),” *J. Appl. Polym. Sci.*, vol. 57, no. 1, pp. 87–103, 1995.

[152] D. Patterson, “Free volume and polymer solubility. A qualitative view,” *Macromolecules*, vol. 2, no. 6, pp. 672–677, 1969.

[153] B. a. Wolf, “Solubility of polymers,” *Pure Appl. Chem.*, vol. 57, no. 2, pp. 323–336, 1985.

[154] V. G. Kadajji and G. V. Betageri, “Water soluble polymers for pharmaceutical applications,” *Polymers (Basel).*, vol. 3, no. 4, pp. 1972–2009, 2011.

[155] K. S. Anseth, C. N. Bowman, and L. Brannon-Peppas, “Mechanical properties of hydrogels and their experimental determination,” *Biomaterials*, vol. 17, no. 17, pp. 1647–1657, Jan. 1996.

[156] S. Lyu and D. Untereker, “Degradability of polymers for implantable biomedical devices,” *Int. J. Mol. Sci.*, vol. 10, no. 9, pp. 4033–4065, Sep. 2009.

[157] D. E. T. Shepherd and B. B. Seedhom, “Thickness of human articular cartilage in joints of the lower limb,” *Ann. Rheum. Dis.*, vol. 58, no. 1, pp. 27–34, 1999.

[158] V. I. Egorov, I. V Schastlivtsev, E. V Prut, A. O. Baranov, and R. A. Turusov, “Mechanical properties of the human gastrointestinal tract,” *J. Biomech.*, vol. 35, no. 10, pp. 1417–1425, 2002.

[159] J.-Y. Wang, P. Mesquida, P. Pallai, C. J. Corrigan, and T. H. Lee, “Dynamic properties of human bronchial airway tissues,” *Biol. Phys.*, pp. 1–8, Nov. 2011.

[160] E. Ruiz-Hitzky, M. Darder, P. Aranda, and K. Ariga, “Advances in biomimetic and nanostructured biohybrid materials,” *Adv. Mater.*, vol. 22, no. 3, pp. 323–336, 2010.

[161] A. Mellati, M. V. Kiamahalleh, S. H. Madani, S. Dai, J. Bi, B. Jin, and H. Zhang, “Poly(N -isopropylacrylamide) hydrogel/chitosan scaffold hybrid for three-dimensional stem cell culture and cartilage tissue engineering,” *J. Biomed. Mater. Res. Part A*, vol. 104, no. 11, pp. 2764–2774, Nov. 2016.

[162] A. Ranga, M. P. Lutolf, J. Hilborn, and D. A. Ossipov, “Hyaluronic Acid Hydrogels Formed in Situ by Transglutaminase-Catalyzed Reaction,” *Biomacromolecules*, vol. 17, no. 5, pp. 1553–1560, May 2016.

[163] J. Kundu, J.-H. Shim, J. Jang, S.-W. Kim, and D.-W. Cho, “An additive manufacturing-based PCL-alginate-chondrocyte bioprinted scaffold for cartilage tissue engineering,” *J. Tissue Eng. Regen. Med.*, vol. 9, no. 11, pp. 1286–1297, Nov. 2015.

[164] a. I. Pearce, R. G. Richards, S. Milz, E. Schneider, and S. G. Pearce, “Animal models for implant biomaterial research in bone: A review,” *Eur. Cells Mater.*, vol. 13, no. 0, pp. 1–10, 2007.

[165] P. V Turner, T. Brabb, C. Pekow, and M. A. Vasbinder, “Administration of substances to laboratory animals: routes of administration and factors to consider,” *J Am Assoc Lab Anim Sci*, vol. 50, no. 5, pp. 600–613, 2011.

[166] C. R. Chu, M. Szczodry, and S. Bruno, “Animal models for cartilage regeneration and repair.,” *Tissue Eng. Part B. Rev.*, vol. 16, no. 1, pp. 105–15, 2010.

[167] W. Dolores, R. Christian, N. Harald, P. Hildegunde, and W. Georg, “Cellular and molecular composition of fibrous capsules formed around silicone breast implants with special focus on local immune reactions,” *J. Autoimmun.*, vol. 23, no. 1, pp. 81–91, 2004.

[168] H. W. David Richard Schmidt and W. J. Kao, *Biological interactions on materials surfaces*. Springer, 2009.

[169] X. Hu, P. Cebe, A. S. Weiss, F. Omenetto, and D. L. Kaplan, “Protein-based composite Protein-based composite biomaterials have been actively pursued as they,” *Mater. Today*, vol. 15, no. 5, pp. 208–215, 2012.

[170] Y. I. Matveev, Y. Grinberg, I. V Sochava, and V. B. Tolstoguzov, “Glass transition temperature of proteins . Calculation based on the additive contribution method and experimental data,” *Food Hydrocoll.*, vol. 11, no. 2, pp. 125–133, 1997.

[171] H. Batzer and U. T. Kreibich, “Influence of water on thermal transition in natural

polymers and synthetic polyamides," *Polym. Bull. 5*, vol. 25, no. 2, pp. 585–590, Feb. 1981.

[172] R. Chapanian, M. Y. Tse, S. C. Pang, and B. G. Amsden, "The role of oxidation and enzymatic hydrolysis on the in vivo degradation of trimethylene carbonate based photocrosslinkable elastomers," *Biomaterials*, vol. 30, no. 3, pp. 295–306, 2009.

[173] D. P. Lovell, "Biological Importance and Statistical Significance," *J. Agric. Food Chem.*, vol. 61, no. 35, pp. 8340–8348, Sep. 2013.

[174] D. A. Müller, J. G. Snedeker, and D. C. Meyer, "Two-month longitudinal study of mechanical properties of absorbable sutures used in orthopedic surgery," *J. Orthop. Surg. Res.*, vol. 11, no. 1, p. 111, Dec. 2016.

[175] D. F. Williams, "On the mechanisms of biocompatibility," *Biomaterials*, vol. 29, no. 20, pp. 2941–2953, Jul. 2008.

[176] J. M. Anderson, "Biological Responses to Materials," *Annu. Rev. Mater. Res.*, vol. 31, no. 1, pp. 81–110, Aug. 2001.

[177] H. C. Bygd, K. D. Forsmark, and K. M. Bratlie, "The significance of macrophage phenotype in cancer and biomaterials," *Clin. Transl. Med.*, vol. 3, no. 1, p. 62, Dec. 2014.

[178] T. Yu, W. Wang, S. Nassiri, T. Kwan, C. Dang, W. Liu, and K. L. Spiller, "Temporal and spatial distribution of macrophage phenotype markers in the foreign body response to glutaraldehyde-crosslinked gelatin hydrogels," *J. Biomater. Sci. Polym. Ed.*, vol. 27, no. 8, pp. 721–742, May 2016.

[179] H. Wu, H. Wang, F. Cheng, F. Xu, and G. Cheng, "Synthesis and characterization of an enzyme-degradable zwitterionic dextran hydrogel," *RSC Adv.*, vol. 6, no. 37, pp. 30862–30866, 2016.

[180] R. Y. Tam, L. J. Smith, and M. S. Shoichet, "Engineering Cellular Microenvironments with Photo- and Enzymatically Responsive Hydrogels: Toward Biomimetic 3D Cell Culture Models," *Acc. Chem. Res.*, p. acs.accounts.6b00543, 2017.

[181] L. Klouda and A. G. Mikos, "Thermoresponsive hydrogels in biomedical applications," *Eur. J. Pharm. Biopharm.*, vol. 68, no. 1, pp. 34–45, Jan. 2008.

[182] S. Liu, K. T. Dicker, and X. Jia, "Modular and orthogonal synthesis of hybrid polymers and networks," *Chem. Commun.*, vol. 51, no. 25, pp. 5218–5237, 2015.

[183] Q. Q. Dou, S. S. Liow, E. Ye, R. Lakshminarayanan, and X. J. Loh, "Biodegradable thermogelling polymers: Working towards clinical applications," *Adv. Healthc. Mater.*, vol. 3, no. 7, pp. 977–988, 2014.

[184] Y. Lee, H. J. Chung, S. Yeo, C.-H. Ahn, H. Lee, P. B. Messersmith, and T. G. Park, "Thermo-sensitive, injectable, and tissue adhesive sol–gel transition hyaluronic acid/pluronic composite hydrogels prepared from bio-inspired catechol-thiol reaction," *Soft Matter*, vol. 6, no. 5, p. 977, 2010.

[185] E. A. Dimarzio and J. H. Gibbs, "Glass temperature of copolymers," *J. Polym. Sci.*, vol. 40, no. 136, pp. 121–131, 1959.

[186] H. M. L. Lambermont-Thijs, R. Hoogenboom, C.-A. Fustin, C. Bomal-D'Haese, J.-F. Gohy, and U. S. Schubert, "Solubility behavior of amphiphilic block and random copolymers based on 2-ethyl-2-oxazoline and 2-nonyl-2-oxazoline in binary water-ethanol mixtures," *J. Polym. Sci. Part A Polym. Chem.*, vol. 47, no. 2, pp. 515–522, Jan. 2009.

[187] G. Roudaut, D. Simatos, D. Champion, E. Contreras-Lopez, and M. Le Meste, "Molecular

mobility around the glass transition temperature: a mini review," *Innov. Food Sci. Emerg. Technol.*, vol. 5, no. 2, pp. 127–134, Jun. 2004.

[188] T. G. Fox and P. J. Flory, "The glass temperature and related properties of polystyrene. Influence of molecular weight," *J. Polym. Sci.*, vol. 14, no. 75, pp. 315–319, Sep. 1954.

[189] K. E. Smith, S. S. Parks, M. A. Hyjek, S. E. Downey, and K. Gall, "The effect of the glass transition temperature on the toughness of photopolymerizable (meth)acrylate networks under physiological conditions," *Polymer (Guildf).*, vol. 50, no. 21, pp. 5112–5123, Oct. 2009.

[190] L. Bromberg, "Temperature-responsive gels and thermogelling polymer matrices for protein and peptide delivery," *Adv. Drug Deliv. Rev.*, vol. 31, no. 3, pp. 197–221, May 1998.

[191] E. Mah and R. Ghosh, "Thermo-Responsive Hydrogels for Stimuli-Responsive Membranes," *Processes*, vol. 1, no. 3, pp. 238–262, Sep. 2013.

[192] S. A. Young, S. E. Sherman, T. T. Cooper, C. Brown, F. Anjum, D. A. Hess, L. E. Flynn, and B. G. Amsden, "Mechanically resilient injectable scaffolds for intramuscular stem cell delivery and cytokine release," *Biomaterials*, vol. 159, pp. 146–160, Mar. 2018.

[193] S. W. Kim, H. J. Kim, K. E. Lee, S. S. Han, Y. S. Sohn, and B. Jeong, "Reverse Thermal Gelling PEG-PTMC Diblock Copolymer Aqueous Solution," *Macromolecules*, vol. 40, no. Waters 515, pp. 5519–5525, 2007.

[194] A. Vidyasagar, S. H. Ku, M. Kim, M. Kim, H. S. Lee, T. R. Pearce, A. V. McCormick, F. S. Bates, and E. Kokkoli, "Design and Characterization of a PVLA-PEG-PVLA Thermosensitive and Biodegradable Hydrogel," *ACS Macro Lett.*, pp. 1134–1139, Sep. 2017.

[195] A. Navaei, D. Truong, J. Heffernan, J. Cutts, D. Brafman, R. W. Sirianni, B. Vernon, and M. Nikkhah, "PNIPAAm-based biohybrid injectable hydrogel for cardiac tissue engineering," *Acta Biomater.*, vol. 32, pp. 10–23, 2016.

[196] T. Ci, L. Chen, L. Yu, and J. Ding, "Tumor regression achieved by encapsulating a moderately soluble drug into a polymeric thermogel.," *Sci. Rep.*, vol. 4, p. 5473, 2014.

[197] H. Ajiro, Y. Takahashi, and M. Akashi, "Thermosensitive biodegradable homopolymer of trimethylene carbonate derivative at body temperature," *Macromolecules*, vol. 45, no. 6, pp. 2668–2674, 2012.

[198] M. E. Helgeson, S. E. Moran, H. Z. An, and P. S. Doyle, "Mesoporous organohydrogels from thermogelling photocrosslinkable nanoemulsions," *Nat. Mater.*, vol. 11, no. 4, pp. 344–352, 2012.

[199] F. Y. Hsieh, H. H. Lin, and S. hui Hsu, "3D bioprinting of neural stem cell-laden thermoresponsive biodegradable polyurethane hydrogel and potential in central nervous system repair," *Biomaterials*, vol. 71, pp. 48–57, 2015.

[200] A. A. Vdovchenko, A. V. Hubina, E. G. Vlakh, and T. B. Tennikova, "Self-assembled polymer particles based on thermoresponsive biodegradable copolymers of amino acids," *Mendeleev Commun.*, vol. 27, no. 2, pp. 153–154, Mar. 2017.

[201] J. Yang, R. van Lith, K. Baler, R. A. Hoshi, and G. A. Ameer, "A Thermoresponsive Biodegradable Polymer with Intrinsic Antioxidant Properties," *Biomacromolecules*, vol. 15, no. 11, pp. 3942–3952, Nov. 2014.

Appendix

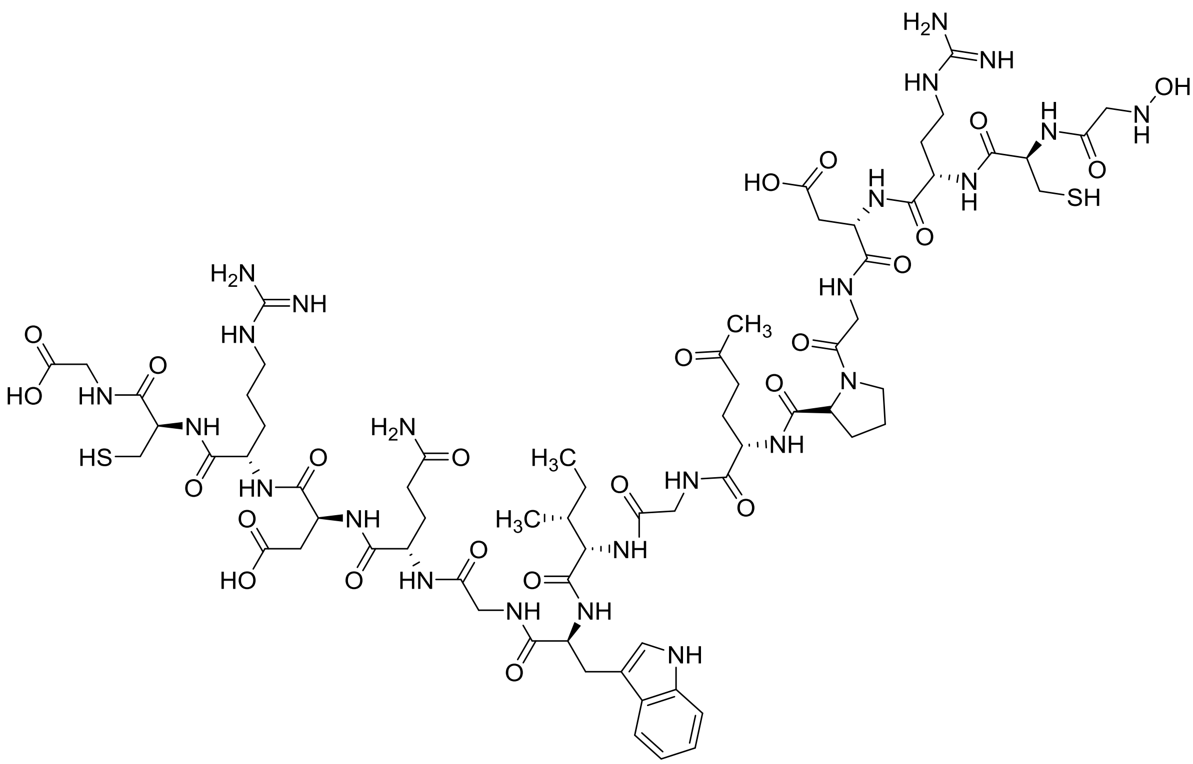

A. 1. Chemical structure of the MMP-sensitive peptide (GCRDGPQGIWGQDRCG).

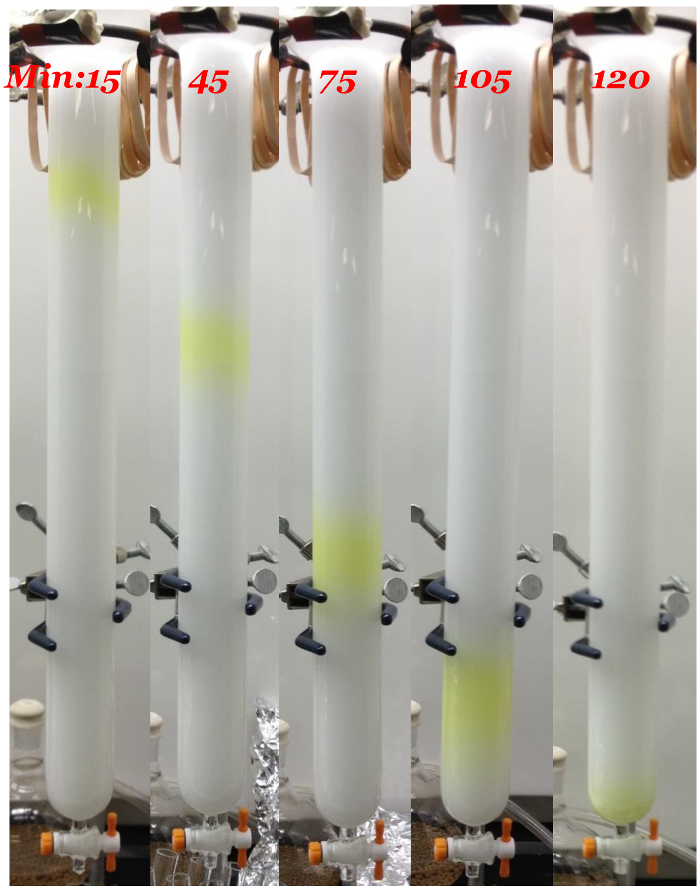

RESIN CHEMISTRY OF TOYOPEARL SEC RESINS
(HYDROXYLATED ACRYLIC)

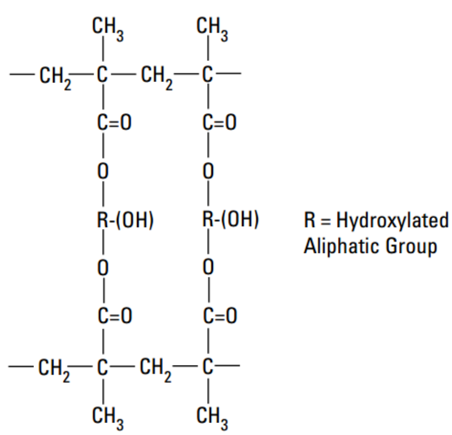

A. 2. Size exclusion chromatography of the PTMC-based polymers, time in min (top), chemical structure of the resin (bottom)

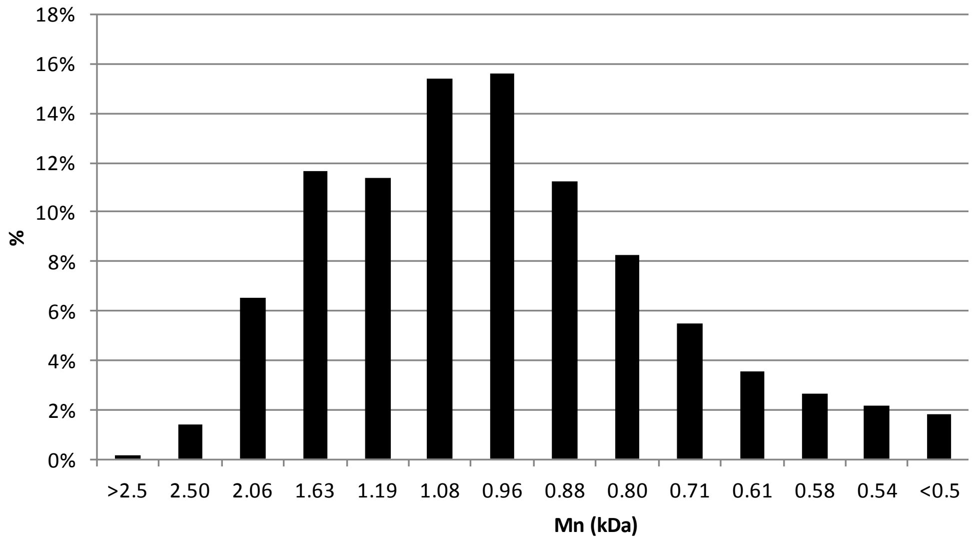

A. 3. M_n distribution of VS-PTMC-MA after fractionation by size exclusion chromatography

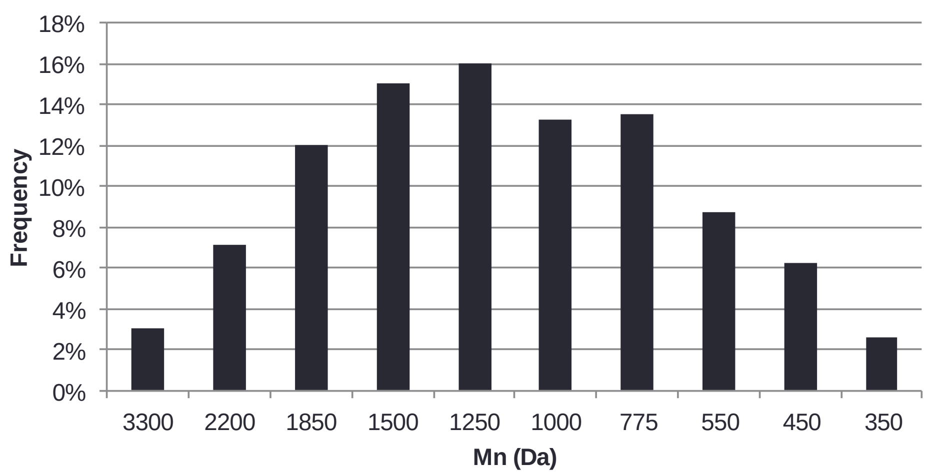

A. 4. M_n distribution of VS-PTMC-PEG-MA after fractionation by size exclusion chromatography

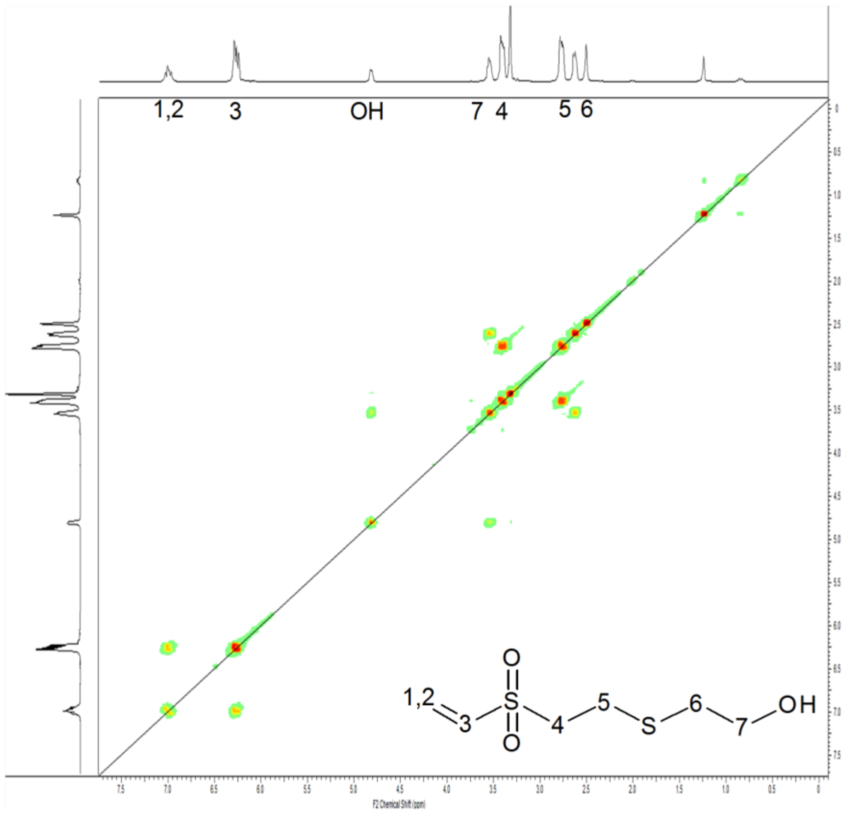

A. 5. Homonuclear correlation spectroscopy (COSY) NMR of 2-((2-vinylsulfonyl ethyl)thio)ethanol initiator

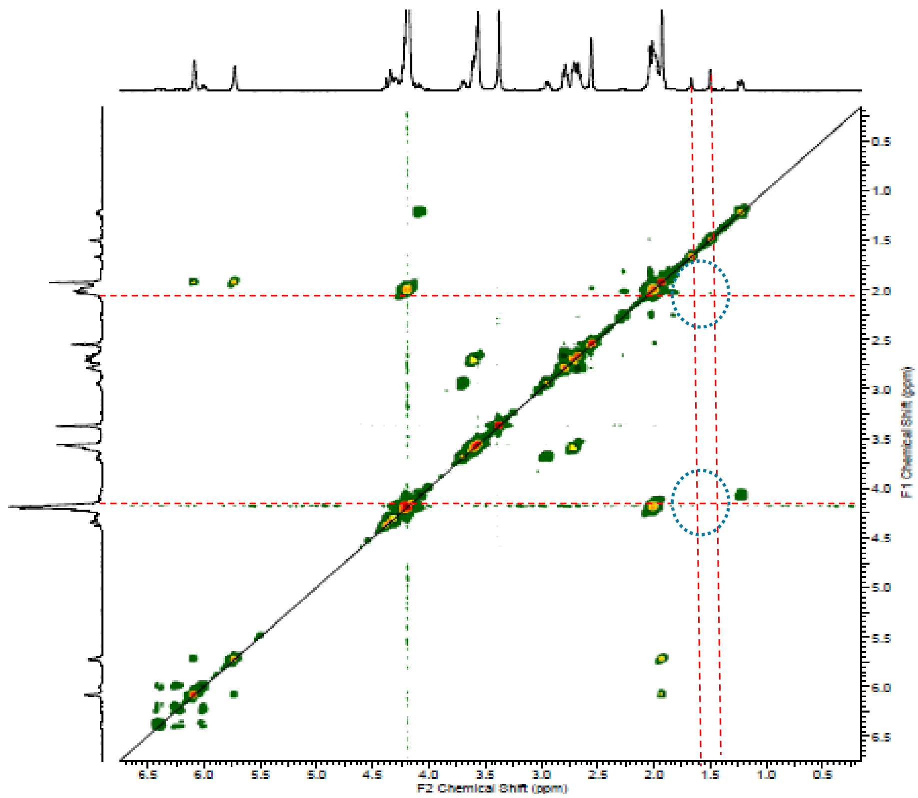

A. 6. Homonuclear correlation spectroscopy (COSY) NMR of MA-PEG-PTMC-VS

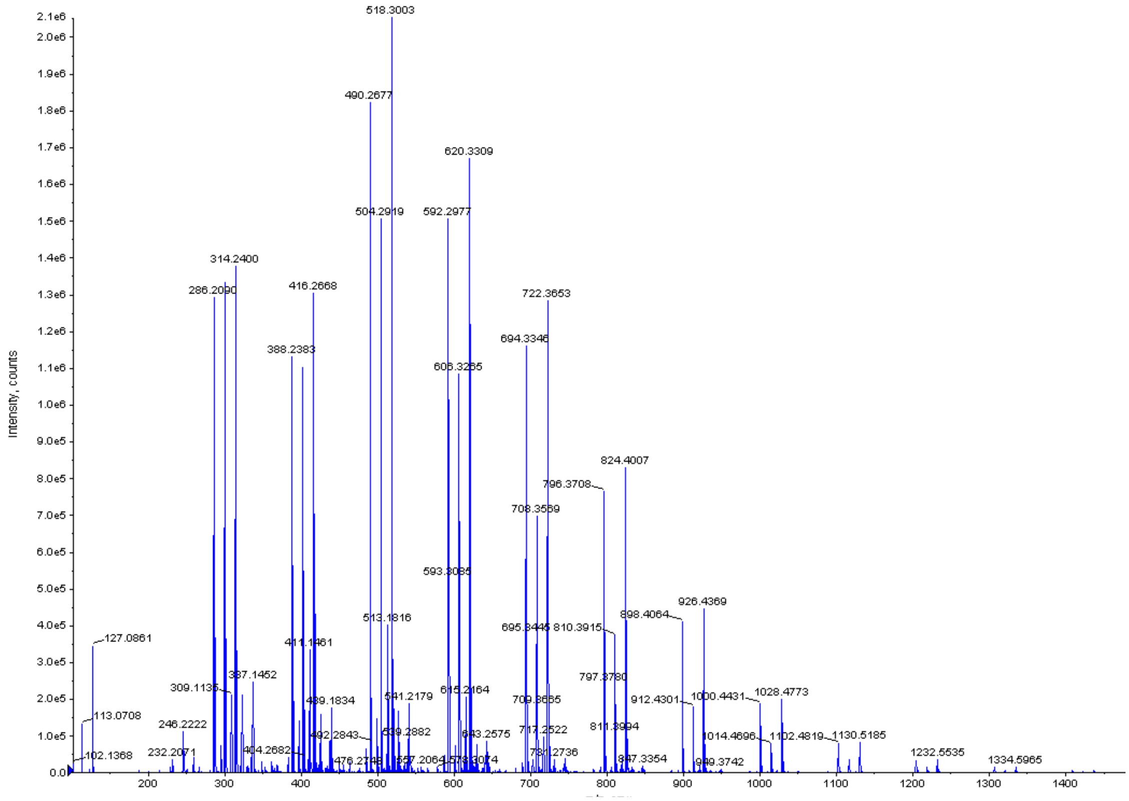

A. 7. Mass spectrometry of VS-PTMC-MA 800 Da.

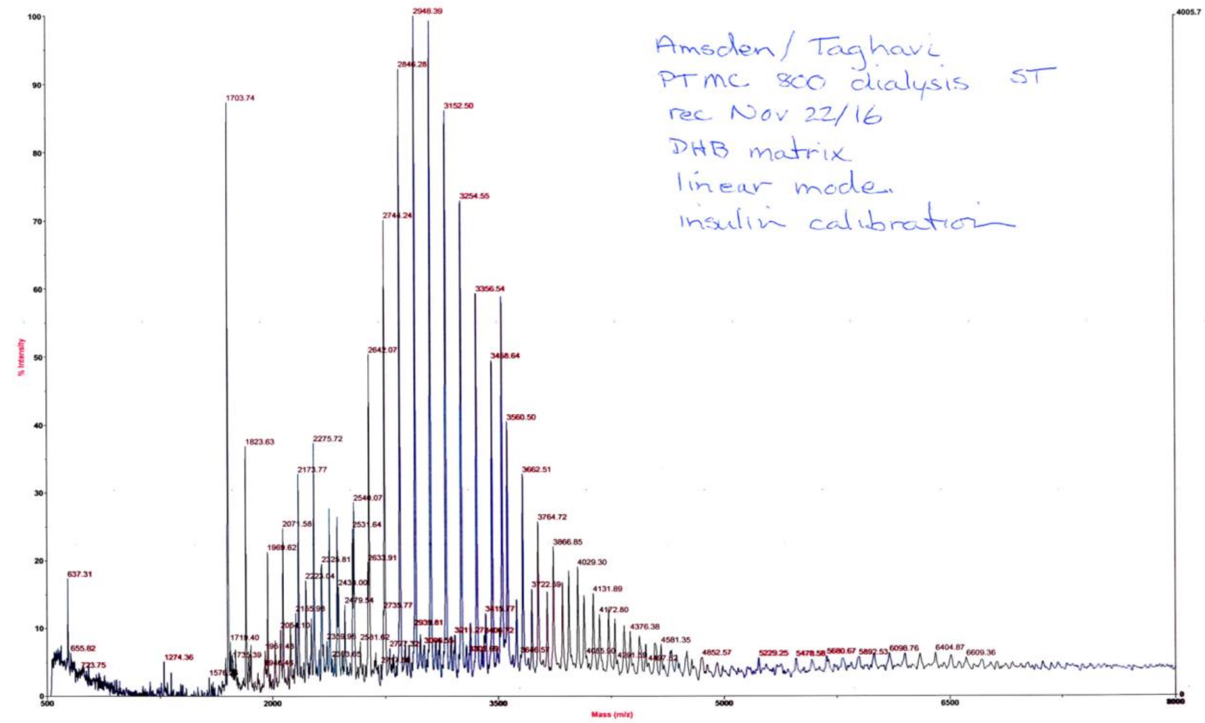

A. 8. Mass spectrometry of peptide-(PTMC-MA)*2* prepolymer prepared from PTMC-MA 800 Da

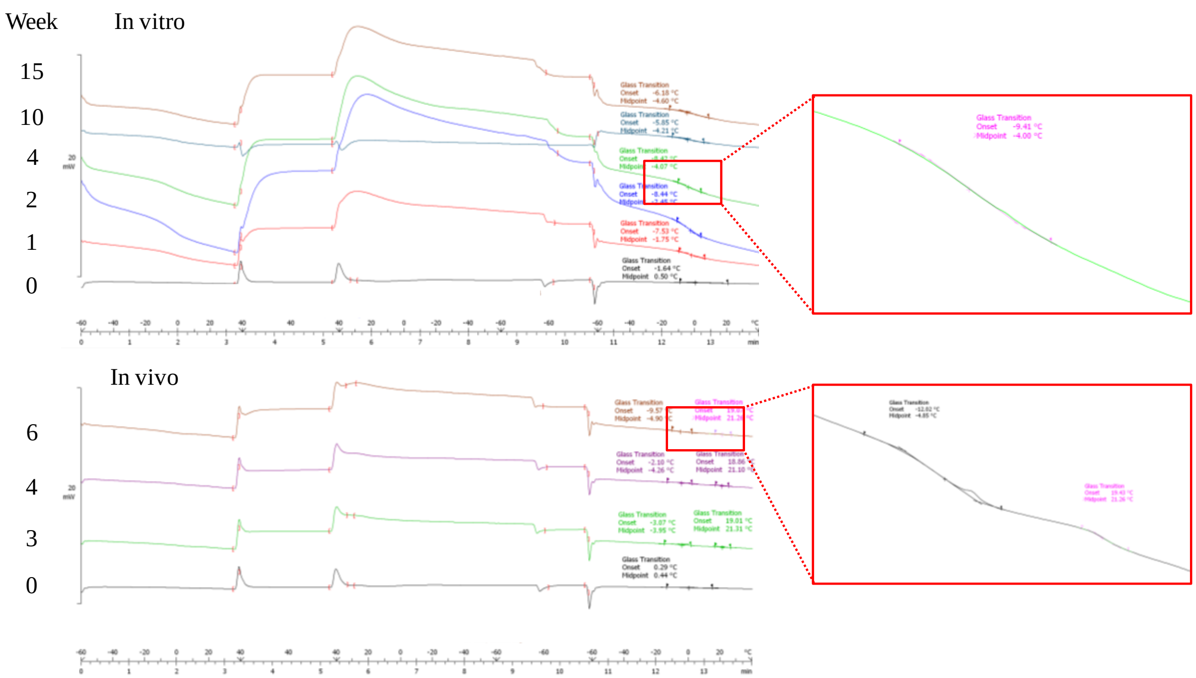

A. 9. Thermographs of peptide-(PTMC-MA)$_2$ degraded over 15 weeks *in vitro* and 6 weeks *in vivo*

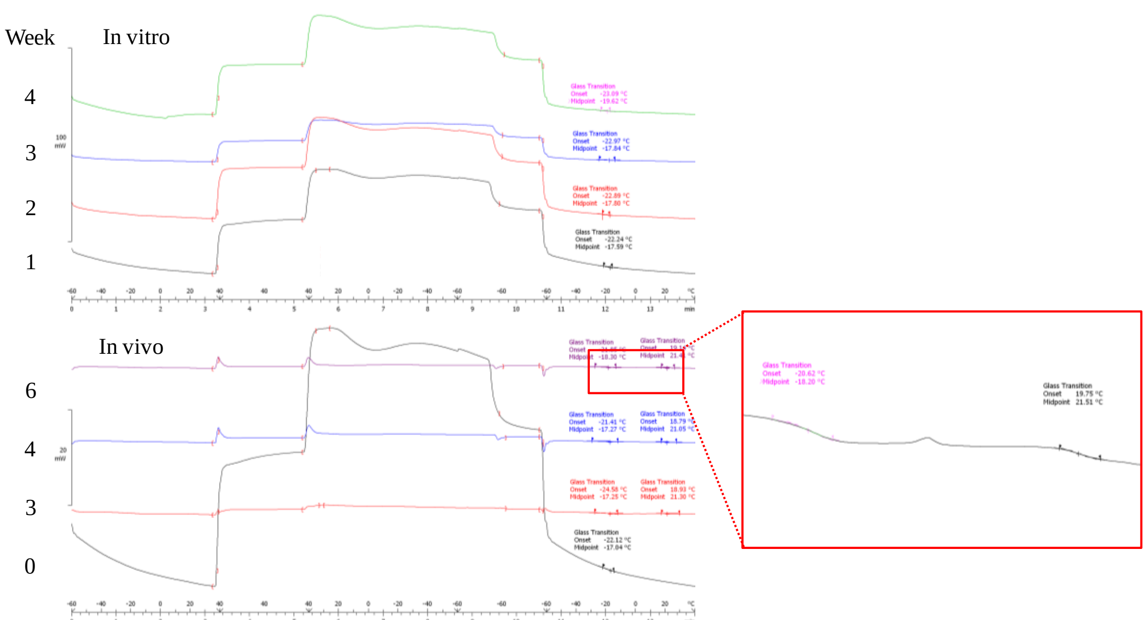

A. 10. Thermographs of peptide-(PTMC-PEG-MA)$_2$ degraded over 6 weeks *in vitro* and *in vivo*

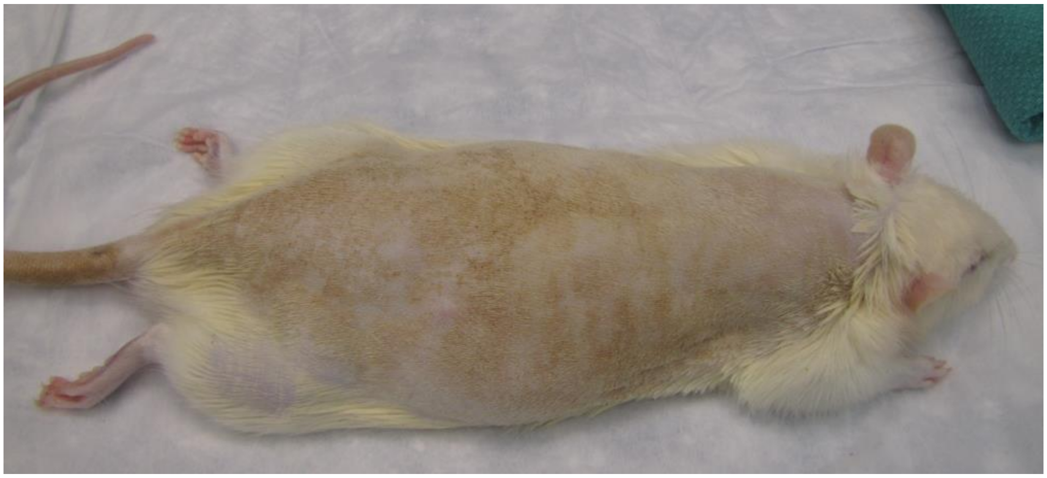

A. 11. Implantation site on the back of Wistar rat, 6 weeks post implantation

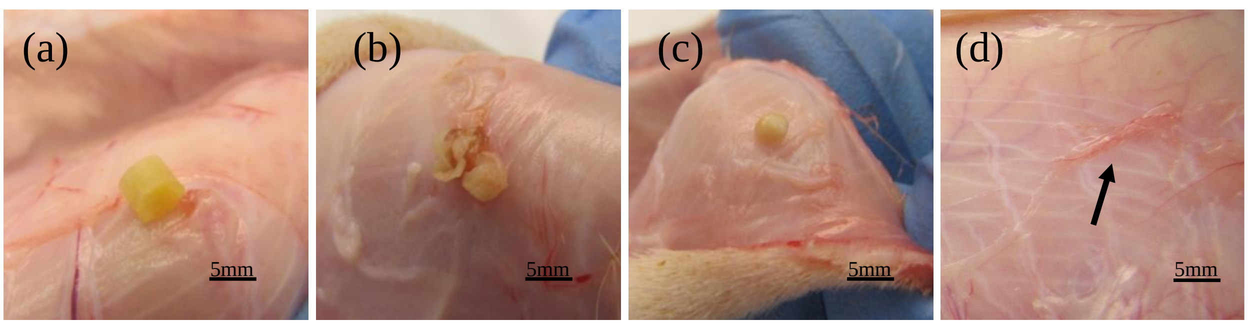

A. 12. Physical appearance of the tissue and implanted prepared from (a) PEG-(PTMC-MA)$_2$, (b) peptide-(PTMC-PEG-MA)$_2$, (c) peptide-(PTMC-MA)$_2$ and (d) Vicryl^{TM} suture, the implant area is shown by the arrow, after 6 weeks of implantation.

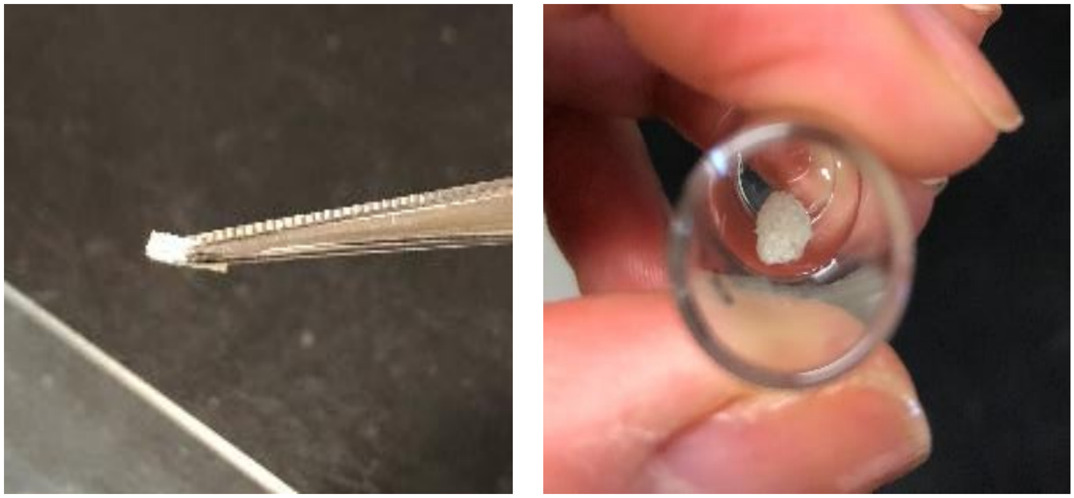

A. 13. Aqueous crosslinking of peptide-(PTMC-PEG-MA)$_2$ prepolymers